ORNL/CON-69

Contract No. W-7405-eng-26

Energy Division

LABORATORY EVALUATION OF THE HEATING CAPACITY AND EFFICIENCY OF A HIGH-EFFICIENCY, AIR-TO-AIR HEAT PUMP WITH EMPHASIS ON FROSTING/DEFROSTING OPERATION

W. A. Miller

Date Published: December 1982

Department of Energy
Office of Buildings Energy Research and Development

OAK RIDGE NATIONAL LABORATORY
Oak Ridge, Tennessee 37830
operated by
UNION CARBIDE CORPORATION
for the
DEPARTMENT OF ENERGY

CONTENTS

List of Figures v
List of Tables vii
Acknowledgments ix
Abstract 1
1. Introduction 1
2. Summary and Recommendations 3
  2.1 Heat Pump Performance Observed Using a Wet Evaporator Coil 3
  2.2 Performance Observed at 4.4°C (40°F) Ambient Temperature 3
  2.3 Frosting Performance for Ambient Temperatures Less Than 4.4°C (40°F) 4
  2.4 Frosting and Defrosting Losses 5
  2.5 Adequacy of Defrosting Controls 5
  2.6 Effect of Refrigerant Charge on System Performance 6
  2.7 Effect of Airflow on Frosting 7
3. Experimental Facility 8
  3.1 Experimental Setup 8
  3.2 Heat Pump 11
    3.2.1 Refrigerant Temperature and Pressure Measurements 12
    3.2.2 Alterations to Heat Pump Electrical Circuit 13
  3.3 Instrumentation 13
    3.3.1 Data Acquistion System 13
    3.3.2 Refrigerant Flow Measurements 13
    3.3.3 Temperature Measurements 13
    3.3.4 Pressure Measurements 16
    3.3.5 Electrical Power Consumption 16
    3.3.6 Humidity Measurements and Control 16
  3.4 Experimental Procedure 17
    3.4.1 Steady-State Tests 17
    3.4.2 Frosting Tests 17
    3.4.3 Defrosting Test Procedure 18
    3.4.4 Charging Tests 18
    3.4.5 Data Collection Procedure Using DAS 18
4. Data Reduction Calculations 19
  4.1 Air- and Refrigerant-Side Heat Balances 19
  4.2 Conductance Coefficients 19
    4.2.1 Sensible Conductance Coefficients 19
    4.2.2 Heat and Mass Transfer *UA* Coefficient 20
5. Experimental Results — Nonfrosting Operation 21
  5.1 Steady-State System Performance with a Dry Outdoor Coil 21
    5.1.1 Steady-State Compressor Performance 21
    5.1.2 Normalized Steady-State System Analysis 21
  5.2 The Effect of Relative Humidity on Heating-Mode Performance of a Wet Outdoor Heat Exchanger 26
    5.2.1 Influence of Mass Transfer 27
    5.2.2 Thermal Conductance for a Wet Evaporator Coil 29
6. Experimental Results — Frosting Conditions at 4.4°C Ambient Temperature 30
  6.1 Performance Observed at 4.4°C (40°F) with Relative Humidities Less Than 70% 30
  6.2 Performance Measured at 4.4°C (40°F) with Relative Humidities of 70% and Greater 32
  6.3 Influence of Frost on System Operation at 4.4°C (40°F) 34

7. Experimental Results for Ambient Temperatures Less Than 4.4°C (40°F) 36
7.1 Performance as a Function of Temperature 36
7.1.1 Performance at 1.7°C (35°F) Ambient Temperature 36
7.1.2 Performance at −1.1°C (30°F) Ambient Temperature 37
7.1.3 Performance at −6.7°C (20°F) Ambient Temperature 39
7.2 Effect of Frost on Evaporator Tube Wall Temperature and Compressor Suction Pressure 39
7.3 Compressor Performance 40
8. Cumulative Losses Due to Frosting of the Outdoor Heat Exchanger 44
8.1 Introduction and Definition of Cumulative Frosting Losses 44
8.2 Correlation of Steady-State Performance as a Function of Temperature and Relative Humidity 45
8.3 Cumulative Frosting Losses as a Function of Time, Temperature, and Relative Humidity 47
9. Defrosting Operation 49
9.1 Transient Operation During the Defrosting Cycle 49
9.2 Adequacy of Defrosting Termination 53
9.3 Energy Consumption of Defrosting Operation 53
10. Alternative Defrosting Logics for an Outdoor Heat Exchanger of Spine Fin Configuration 55
10.1 Time and Temperature 55
10.2 Demand Defrosting Sensors 56
10.2.1 Static Pressure Sensor 56
10.2.2 Fan Power Consumption 56
10.2.3 Temperature Difference Across the Frost Layer 57
11. Charge Sensitivity Test 59
11.1 Performance as a Function of Refrigerant Charge 59
11.2 Sensitivity of System Pressures and Temperatures to Amount of Charge 60
11.3 Thermostatic Expansion Valve Instability 62
References 64
Appendix A. Experimental Data 66
Appendix B. Computer Program for the Data Acquisition System 72
Appendix C. Performance at −8.3°C (17°F) 84

LIST OF FIGURES

1. Indoor unit air loop 8
2. Outdoor unit air loop 8
3. Indoor unit 9
4. Outdoor unit 10
5. Heat pump refrigerant sensor locations 12
6. Heat pump electrical circuit 14
7. Data acquisition system 15
8. Humidity control instrumentation 17
9. Steady-state system performance 22
10. Steady-state performance traits 23
11. Refrigerant properties across the compressor 24
12. Normalized system analysis 25
13. COP for a wet outdoor heat exchanger 26
14. Heating capacity for a wet outdoor heat exchanger 27
15. Evaporator capacity for a wet outdoor heat exchanger 28
16. Evaporator tube wall temperature over the entire two-phase region for a wet coil 28
17. Sensible *UA* coefficients over the two-phase region of the outdoor heat exchanger 29
18. COP measured at 4.4°C (40°F) 30
19. Heating capacity measured at 4.4°C (40°F) 31
20. Evaporator capacity measured at 4.4°C (40°F) 31
21. Tube wall temperature over the entire two-phase region of the outdoor heat exchanger 32
22. Absolute refrigerant pressure at the compressor inlet 33
23. Outdoor airflow measured at 4.4°C (40°F) 33
24. Parametric study of heat pump performance observed at various outdoor relative humidity levels for an ambient temperature of 4.4°C (40°F) 35
25. COP measured at 1.7°C (35°F) 36
26. Heating capacity measured at 1.7°C (35°F) 37
27. COP measured at −1.1°C (30°F) 38
28. Heating capacity measured at −1.1°C (30°F) 38
29. COP measured at −6.7°C (20°F) 39
30. Heating capacity measured at −6.7°C (20°F) 40
31. Evaporator tube wall temperature observed for a −1.1°C (30°F) ambient temperature 41
32. Compressor suction pressure observed for a −1.1°C (30°F) ambient temperature 41
33. Parametric study of heat pump performance observed at various outdoor relative humidity levels for an ambient temperature of −1.1°C (30°F) 42
34. Compressor efficiency observed at −1.1°C (30°F) 43
35. Example of cumulative frosting loss 44
36. COP frosting loss coefficients calculated for a 1.7°C (35°F) ambient temperature 48
37. Heating capacity frosting loss coefficients calculated for a 1.7°C (35°F) ambient temperature 48
38. Defrosting cycle observed following a −1.1°C (30°F), 70% relative humidity test 50
39. Defrosting cycle observed after −1.1°C (30°F), 80% relative humidity test 51
40. Defrosting cycle observed after −1.1°C (30°F), 90% relative humidity test 52
41. COP observed at 80% relative humidity 55
42. COP observed at 90% relative humidity 56
43. Outdoor fan power measured at 1.7°C (35°F) 57

44. Temperature difference between the ambient air and the evaporator tube wall observed at 1.7°C (35°F) 58
45. Temperature difference between the ambient air and the evaporator tube wall observed at −1.1°C (30°F) 58
46. Refrigerant flow rate at refrigerant charge of 5.24 kg (11 lb 9 oz) 59
47. Influence of refrigerant charge on system performance observed at an ambient temperature of 8.3°C (47°F) 60
48. Refrigerant pressures as influenced by charge variation observed at an ambient temperature of 8.3°C (47°F) 61
49. Refrigerant temperatures as influenced by charge variation observed at an ambient temperature of 8.3°C (47°F) 62
50. Thermostatic expansion valve stability as influenced by charge variation observed at 8.3°C (47°F) and 55% relative humidity outdoor ambient conditions 63
C.1. COP measured at −8.3°C (17°F) 84
C.2. Heating capacity measured for an ambient temperature of −8.3°C (17°F) 85
C.3. Outdoor heat exchanger capacity measured for an ambient temperature of −8.3°C (17°F) 85
C.4. Parametric study of heat pump performance traits observed at various outdoor relative humidity levels for an ambient temperature of −8.3°C (17°F) 86
C.5. Outdoor airflow measured while the heat pump operated at −8.3°C (17°F) 87

LIST OF TABLES

1. Observed steady-state performance compared with Air-Conditioning and Refrigeration Institute ratings 3
2. Performance observed at 4.4°C (40°F) 4
3. Degradation of system performance due to frosting of the outdoor heat exchanger 4
4. Degradation of performance due to frosting and defrosting for an ambient temperature of −1.1°C (30°F) 5
5. Frosting losses incurred as a function of defrosting sensor scheme 6
6. Features of tested heat pump 11
7. Temperature and pressure sensors, refrigerant circuit 12
8. Frosting test ambient conditions 18
9. Loss of quasi-steady-state COP due to frosting 45
10. Loss of quasi-steady-state capacity output due to frosting 46
11. Percentage drop in performance due to frosting/defrosting 54

ACKNOWLEDGMENTS

My sincere appreciation is given to all those members of the Efficiency and Renewables Research Section of ORNL's Energy Division who assisted in the completion and publication of this report. Special thanks must be given to S. J. Ball, Bill Jackson, Steve Fischer, Jean Bledsoe, Gene Holt, John Farmer, and the late J. N. Summers for their unselfish assistance during the duration of the project.

LABORATORY EVALUATION OF THE HEATING CAPACITY AND EFFICIENCY OF A HIGH-EFFICIENCY, AIR-TO-AIR HEAT PUMP WITH EMPHASIS ON FROSTING/DEFROSTING OPERATION

W. A. Miller

ABSTRACT

A high-efficiency, air-to-air split-system residential heat pump of nominal 3-ton capacity was instrumented and tested in the heating mode under laboratory conditions. Performance of the system was measured during steady-state, dehumidifying, and frosting-defrosting conditions, with major emphasis placed on the dynamic frosting operation of the system. The study encompassed an evaluation of system and component performance for ambient temperature levels between 8.3 and −8.3°C (47 and 17°F respectively) and for discrete humidity levels ranging from 50 to 90%.

The heat pump coefficient of performance (COP) and capacity, measured at 4.4°C (40°F) as a function of time after system start-up, decreased with time because of frost accumulation on the outdoor heat exchanger but increased with increasing ambient relative humidity. At ambient temperatures less than 4.4°C (40°F), the COP and capacity degradations caused by frost formation increased with increasing relative humidity because of greater frost accumulation of the outdoor heat exchanger.

Experimental results revealed that both unnecessary and late defrosting operations occur when a time-and-temperature defrosting control is used. Concepts of advanced defrosting controls that could feasibly reduce both frosting and defrosting losses were developed from experimental data. Frosting caused greater degradation of heating capacity than defrosting did. Cumulative frosting loss coefficients were calculated as a function of time, temperature, and relative humidity and are applicable to modeling of frosting losses calculated in a seasonal performance program.

1. INTRODUCTION

This report presents the results of dynamic frosting performance tests of a high-efficiency, air-to-air heat pump. The work is the third experiment in a planned program of heat pump studies which will be used in a combined experimental and analytical approach to improving heat pump performance. The objectives of this experimental study, similar to those of two previous studies,[1,2] are

1. to determine the base-case performance of the selected heat pump and the characteristics of some of its components under both steady-state and frosting-defrosting conditions,
2. to measure experimentally the degradation of heat pump performance due to frost formation on the outdoor heat exchanger, and
3. to measure the sensitivity of the performance parameters to variations in the refrigerant charge.

The major emphasis of this third experiment is on operating the system under frosting conditions. Both frosting of the outdoor heat exchanger and subsequent defrosting operations reduce the efficiency and capacity of a heat pump; however, in past studies the frosting losses have received much less attention than the defrosting losses. The accumulation of frost on the outdoor heat exchanger increases the resistance to heat flow because of (1) the reduced airflow across the coil and (2) the insulating effect of the frost. The accumulation of frost lowers the capacity of the outdoor heat exchanger, thus lowering system coefficient of performance (COP) and heating capacity.

This report presents an analysis of frosting as a function of air temperature and relative humidity. The results provide a data base for formulation and validation of analytical models of seasonal performance. The models can then be used to evaluate recommendations for candidate improvements in heat pump design.

Previous work has been conducted on "low-first-cost" and "middle-of-the-line" heat pumps.[1,2] This third series of tests was conducted on a high-efficiency, split-system air-to-air heat pump.[3] As in previous tests, air loops were constructed for both indoor and outdoor units. In the outdoor loop improvements were made in both temperature and humidity control.

2. SUMMARY AND RECOMMENDATIONS

The heat pump tested in these experiments yielded heating-mode performance data that agreed well with the rated values published by the Air-Conditioning and Refrigeration Institute (ARI). The ARI ratings and observed COP of the unit are shown in Table 1. The observed values are from tests in which 0.6 m^3/s (1273 cfm) of air was supplied to the indoor unit at 21.1°C (70°F) during both high- and low-temperature tests. The outdoor air was conditioned to 8.3°C (47°F) during the high-temperature tests and to −8.3°C (17°F) during the low-temperature tests. The outdoor air relative humidity was maintained at 70% for both tests.

Under dry-coil conditions, the overall efficiency of the compressor and motor increased from 46% at −8.3°C (17°F) to 53.5% at 8.3°C (47°F). See Appendix A for a detailed display of steady-state system peformance.

Table 1. Observed steady-state performance compared with Air-Conditioning and Refrigeration Institute ratings

	Observed	Rated
Coefficient of performance[a]	2.95	3.1
Coefficient of performance[b]	2.15[c]	2.1
Heating capacity,[a] kW (Btu/h)	9.6 (32,750)	9.96 (34,000)
Heating capacity,[b] kW (Btu/h)	5.3 (18,146)	5.27 (18,000)

[a]At 8.3°C (47°F).
[b]At −8.3°C (17°F).
[c]Averaged over an 80-min frosting cycle; does not include losses due to defrosting.

2.1 Heat Pump Performance Observed Using a Wet Evaporator Coil

Under nonfrosting dehumidifying conditions at the outdoor coil, a small improvement in heat pump COP was observed as the moisture content of the outdoor air was increased. The time-averaged COP, which was approximately 2.9 for the 8.3°C (47°F), 60% relative humidity condition, increased to 2.95 and 3.0 as the relative humidity was increased to 70 and 80% for subsequent test runs. The corresponding heating capacities improved from 9083 W (31,000 Btu/h) to 9596 W (32,750 Btu/h) to 9962 W (34,000 Btu/h) as the relative humidity was increased from 60 to 70 to 80%. Increasing the ambient relative humidity yielded higher rates of mass transfer of moisture and thus higher latent heat contributions to the outdoor coil, which produced the improvement in COP and heating capacity.

2.2 Performance Observed at 4.4°C (40°F) Ambient Temperature

The heat pump COP and heating capacity, measured at 4.4°C (40°F) as a function of time after system start-up, decreased with time due to frost accumulation on the outdoor heat exchanger. However, the heat pump COP and capacity both improved by increasing the ambient relative humidity above 70%. The COP improved from 2.75, observed at 60% relative humidity, to values above 2.9 as the relative humidity was increased for subsequent test runs (Table 2). Similar trends were also observed in the heating capacity.

Table 2. Performance observed at 4.4°C (40°F)

Relative humidity (%)	COP	Heating capacity [kW (Btu/h)]	Initial evaporator wall temperature [°C (°F)]	Onset of frosting[a] (min)
50	2.75	8.2 (27,846)	−1.72 (28.9)	nonfrosting
70	2.82	8.5 (29,200)	−2.22 (28.0)	34
80	2.86	9.0 (30,808)	−0.33 (31.4)	87
90	2.92	9.1 (31,168)	0.88 (36.6)	155

[a]Onset of frosting was observed for a wall temperature of approximately −2.7°C (27°F) for the 4.4°C (40°F) test runs.

The increase in mass transfer, due to higher moisture content of the air, yielded greater latent heat contributions to the outdoor heat exchanger. The latent heat gain increased the total heat transfer to the outdoor heat exchanger and produced the observed improvement in system performance. The higher latent heat contribution also caused the evaporator tube wall temperature to increase, which delayed the onset of frosting (Table 2).

2.3 Frosting Performance for Ambient Temperatures Less Than 4.4°C (40°F)

System performance did not improve when the relative humidity was increased for test runs conducted at ambient temperatures less than 4.4°C (40°F). Increasing the relative humidity resulted in higher rates of frost accumulation and therefore increased the rate of COP and capacity degradation for relative humidities of 70% and greater (Table 3). Reductions of COP and heating capacity were on the order of 15 and 20%, respectively, for the −1.1 and 1.7°C (30 and 35°F) tests conducted at 80 and 90% relative humidity.

Frosting of the outdoor heat exchanger was observed at 70% relative humidity for ambient temperatures ranging from 4 to −1°C (40 to 30°F). For relative humidities greater than 80%, frosting of the outdoor heat exchanger was observed for all temperatures investigated.

Typical frosting data and system performance observed for the 1.7°C (35°F) tests are tabulated in Appendix A as a function of run time.

Table 3. Degradation of system performance due to frosting of the outdoor heat exchanger

Ambient temperature [°C (°F)]	Relative humidity (%)	COP		Heating capacity (Btu/h)		Duration of test (min)
		Initial	Final	Initial	Final	
1.67 (35)	70	2.73	2.13	27,740	19,000	140
1.67 (35)	80	2.76	2.18	28,977	19,900	65
1.67 (35)	90	2.61	2.15	27,782	19,900	55
−1.11 (30)	70	2.54	2.16	23,800	19,500	163
−1.11 (30)	80	2.75	2.11	27,502	19,300	54
−1.11 (30)	90	2.63	2.04	26,138	18,000	54
−6.67 (20)	70	2.23	2.15	20,399	19,500	158
−6.67 (20)	80	2.19	2.17	20,954	18,800	91
−6.67 (20)	90	2.32	1.81	21,672	15,000	84

2.4 Frosting and Defrosting Losses

The frosting and defrosting losses were insignificant for all ambient conditions having relative humidities less than 70%. The frosting losses, however, did increase significantly for ambient temperatures less than 4.4°C (40°F) that had relative humidities greater than 70%. Also, the frosting losses yielded greater reductions in heating capacity than did the defrosting losses, as typified by results of the −1.1°C (30°F) frosting tests listed in Table 4. Frosting of the outdoor heat exchanger produced a 16% degradation* in heating capacity for tests conducted at −1.1°C (30°F) with relative humidities of 80 and 90% respectively. Chilling of the indoor air stream during defrosting further degraded the capacity output by an additional 8%. Slightly larger degradations in COP vs heating capacity (Table 4), due to defrosting, were caused by usage of auxiliary heat to temper the chilled indoor air stream.

The results of all frosting tests revealed that frosting of the outdoor heat exchanger caused significant degradation of heating capacity and COP. Also, the use of auxiliary heat during defrosting periods caused significant degradation of COP. A seasonal performance analysis needs to be done for the magnitude of frosting and defrosting losses; this analysis could suggest the need for future research directed toward reduction of these losses in heat pump operation.

Table 4. Degradation of performance due to frosting and defrosting for an ambient temperature of −1.1°C (30°F)

Relative humidity (%)	Test duration (min)	COP			ΔCOP[c]		ΔQH[c]	
		quasi steady state	fr[a]	fr/def[b]	fr (%)	def[d] (%)	fr (%)	def (%)
70	163	2.54	2.35	2.24	7.50	4.33	6.33	2.00
80	54	2.75	2.43	2.00	11.73	15.41	15.52	8.06
90	54	2.63	2.32	1.87	11.88	17.20	16.76	9.15

[a]fr — Performance measured over duration of respective test, not including defrosting operation.

[b]fr/def — Performance measured over duration of respective test, including defrosting operation.

[c]Δ(COP, QH) — Percentage breakdown of frosting and defrosting based on quasi-steady-state COP and QH as determined from each temperature and relative humidity test run.

[d]def — Performance during defrosting period including chilling of indoor air, 5-kW auxiliary level.

2.5 Adequacy of Defrosting Controls

The time-and-temperature defrosting control is used by the majority of heat pump manufacturers. A timing cam can be set to operate on a 30-, 45-, or 90-min cycle and will initiate a defrosting cycle 10 min prior to completion of a given cycle provided the refrigerant temperature at the inlet to the evaporator is less than −2.2°C (28°F) for this particular heat pump.

Experimental results show that the 90-min cycle allows defrosting operations too infrequently for proper control of frost accumulations. The outdoor heat exchanger was observed to be 90%

*Degradations in COP and heating capacity as caused by frosting were calculated using, as a base, COP and heating capacity values that were extrapolated to the commencement of each frosting test.

blocked by frost within 50 min of frosting operation for relative humidities greater than 70% and ambient temperatures between −1.1 and 1.67°C (30 and 35°F). Reducing the period of the cycle would alleviate severe frost buildups, but shorter cycles would increase the number of needless, or false, defrosting operations. An unnecessary defrosting operation at 4.4°C (40°F) yielded a 2.5% reduction of steady-state COP and a 1.2% reduction in heating capacity. Although these losses are minimal, repetitive defrosting operations could possibly be more detrimental to performance than severe frosting of the outdoor heat exchanger. Either situation would increase wear on the compressor.

A demand defrosting device sensing the temperature difference between ambient air and the evaporator tube wall or refrigerant temperature would eliminate needless defrosting operations. The demand sensor would also control heavy frost accumulations on the outdoor heat exchanger better than the time-and-temperature defrosting sensor does. A comparative analysis of frosting losses, listed in Table 5, was made using experimental data and simulating both demand defrosting logic and time-and-temperature defrosting logic. The demand defrosting logic was based on an experimentally observed 8.3 C° (15 F°) temperature difference between ambient air and evaporator tube wall temperature, and the time-and-temperature logic was based on a 90-min cycle with previously mentioned temperature initiation and termination points.

Comparison of defrosting logics reveals that frosting losses are nominally 30% less for the demand scheme than for the time-and-temperature scheme. Using the demand defrosting logic obviously offers potential improvement in seasonal performance, but a seasonal performance analysis is needed for complete evaluation of the superiority of defrosting logics.

Table 5. Frosting losses incurred as a function of defrosting sensor scheme

Ambient temperature [°C (°F)]	Relative humidity (%)	Loss (%) in average COP		Loss (%) in cumulative heat output		Elapsed time (min) prior to defrosting	
		Demand	Time and temperature	Demand	Time and temperature	Demand	Time and temperature[a]
1.67 (35)	70	1.89	4.66	4.13	7.80	~55	80
1.67 (35)	80	7.48	10.87	11.15	16.30	44	Blocked[b]
1.67 (35)	90	5.06	8.28	8.16	13.90	32	Blocked
−1.11 (30)	70	5.43	4.32	2.93	0.81	~118	80
−1.11 (30)	80	9.32	11.73	12.23	15.52	42	Blocked
−1.11 (30)	90	7.06	11.88	9.53	16.76	30	Blocked

[a]90-min cycle.
[b]Approximately 90% of the outdoor coil was blocked with frost; however, air was able to pass over the top of the coil.

2.6 Effect of Refrigerant Charge on System Performance

Heating-mode refrigerant charge tests were performed while the system operated under an 8.3°C (47°F) ambient temperature and 55% relative humidity. The addition of 0.45 kg (1 lb) of refrigerant charge over the design charge of 4.73 kg (10 lb 7 oz) yielded a slight improvement in system performance. The COP, heating capacity, and outdoor heat exchanger capacity all increased by approximately 2% over their performances at design charge level.

The variation of the refrigerant charge from 0.23 kg (0.5 lb)* less than the design charge to 0.68 kg (1.5 lb) more than the design charge had little effect on refrigerant conditions or system performance. This insensitivity is due to an observed backup of refrigerant in the indoor heat exchanger caused by the throttling action of the thermostatic expansion valve in the outdoor unit. The addition of charge above 5.4 kg (12 lb) would eventually result in reductions of heating capacity yielding a loss in COP.

2.7 Effect of Airflow on Frosting

In a study conducted for the Edison Electric Institute, Sepsy and Winchell observed a reduction of frost accumulation on a plate and fin heat exchanger as the airflow was increased.[4] Their tests were conducted at 4.4°C (40°F) and 90% relative humidity, conditions identical to those of tests in which the onset of frosting was delayed on the spine fin heat exchanger. The similarity of results suggests the possibility of retarding frost formation by increasing the air velocity across the outdoor coil for ambient temperatures at 4.4°C (40°F). There is an excellent chance of eliminating frosting at the 4.4°C (40°F) temperature level by increasing the airflow across the outdoor heat exchanger, thus narrowing the frosting range and improving the performance of the system at this temperature level. However, further experimentation is needed to observe the effect of increased airflow on system performance under more severe frosting conditions and under steady-state conditions.

*This amount of charge still allowed a liquid seal at the inlet to the thermostatic expansion valve and also enabled refrigerant-side heat balances to be performed.

3. EXPERIMENTAL FACILITY

3.1 Experimental Setup

The split-system heat pump used in the experimental study was installed in two separate air loops, one loop housing the indoor unit and the other housing the outdoor unit. Figures 1 through 4 show the individual loops.

Each loop was constructed of glass-fiber duct board backed by aluminum for structural strength, and sharp-edged orifice plates were installed to measure the airflow across each unit. Thermocouple grids were used to measure the average air temperature entering and exiting each individual unit. Moisture content was varied in the outdoor unit air loop by injecting steam into the loop airstream

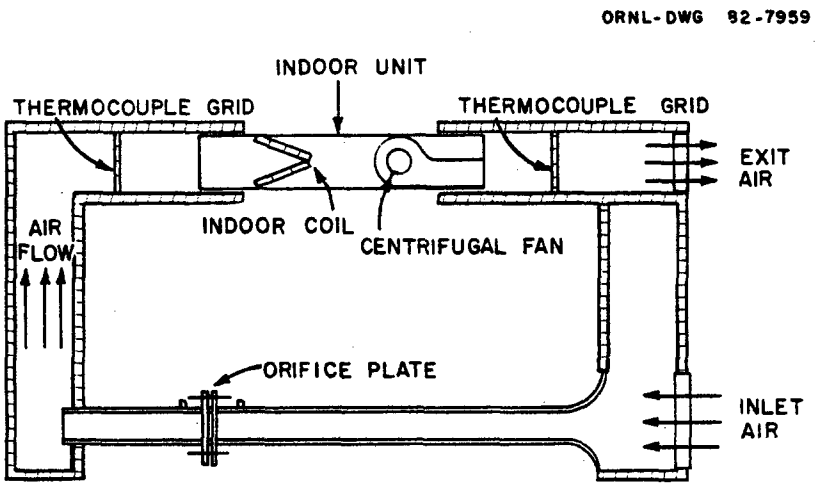

Fig. 1. Indoor unit air loop.

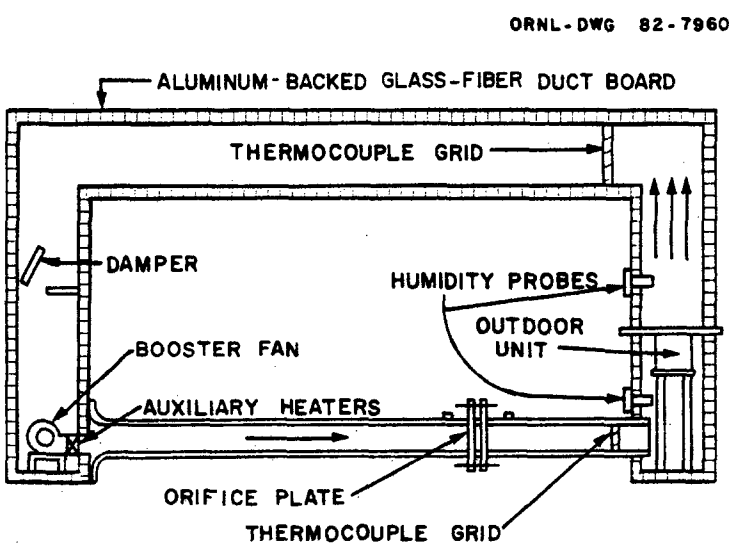

Fig. 2. Outdoor unit air loop.

ORNL-PHOTO 7703-79

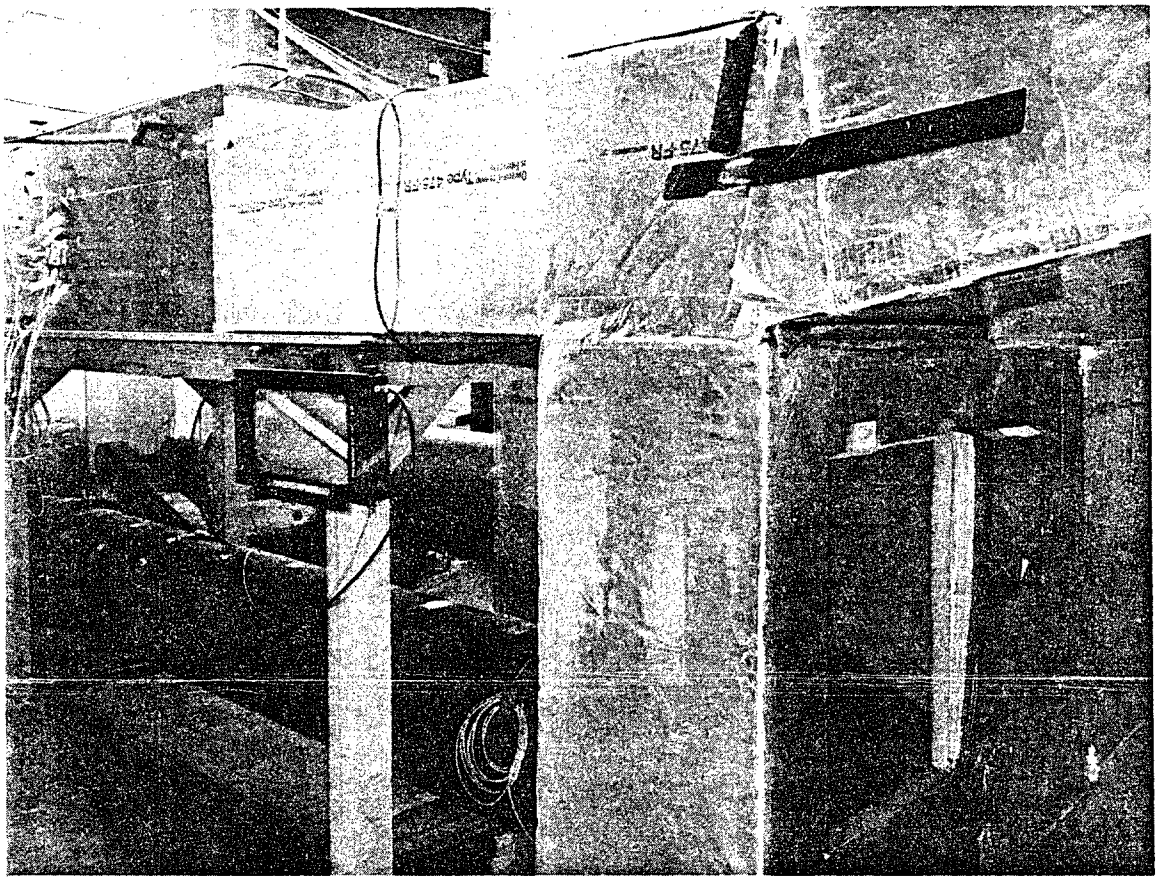

Fig. 3. Indoor unit.

ORNL-PHOTO 7267-79

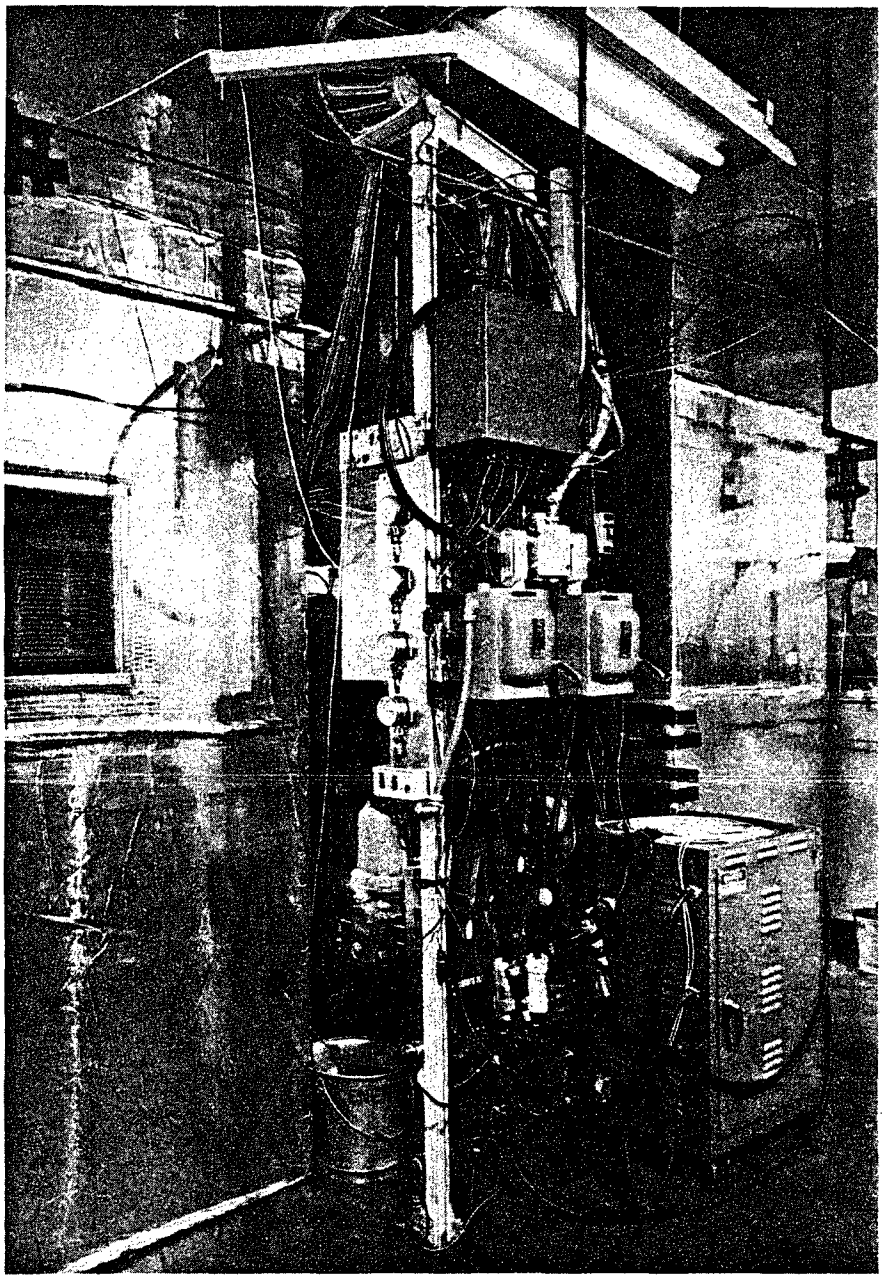

Fig. 4. Outdoor unit.

and by using instrument air (dry air) to lower the moisture content for low-humidity test runs. Relative humidity was measured by two hygrosensors: one sensor used for humidity control was positioned at the entrance of the outdoor unit, and another sensor was placed just downstream of the outdoor unit. A centrifugal fan, driven by a variable-speed motor, was placed in series with the fan of the outdoor unit to maintain a zero static pressure drop across the outdoor unit and thus simulate free-flow conditions. Air temperature within the outdoor loop was tempered by using auxiliary heaters powered by a variable voltage transformer, and the outdoor air was cooled by the outdoor unit.

3.2 Heat Pump

The heat pump selected for this study has one of the highest efficiency ratings commercially available. The one-row spine fin outdoor heat exchanger has two parallel refrigerant circuits. The indoor coil is of the more common tube-and-plate fin construction. Liquid refrigerant is throttled in the heating mode by a thermostatic expansion valve and distributor tubes. The control bulb for the expansion valve is attached to the suction line of the compressor, and the external equalizer is located at the evaporator exit. This design increases the capacity of the outdoor coil by allowing a greater refrigerant flow through the heat exchanger, as compared to the conventional control bulb placement at the external equalizer. The placement of the bulb also protects it during cooling-mode operation, when superheated refrigerant flows through the outdoor coil.

The heat pump has no suction-line accumulator, and the automatic defrosting control is based on the inlet evaporator refrigerant temperature and an elapsed time control. The salient features of this heat pump are listed in Table 6. The efficiencies of both indoor and outdoor fans were calculated from experimental data and are listed below.

Ambient temperature	Indoor fan efficiency	Outdoor fan efficiency
8.3°C (47°F)	17.8%	8%
−8.3°C (17°F)	19.8%	7.9%

Table 6. Features of tested heat pump

Feature	Description
Refrigerant	R-22 (chlorodifluoromethane)
Compressor	Capacity, 10.4 kW (35,500 Btu/h)[a] Displacement, 60.6 cm^3 (3.7 $in.^3$) Hermetically sealed
Outdoor heat exchanger	Aluminum spine fin, 20 fins/in., with 1/2-in. inner diameter aluminum tubing Two parallel refrigerant circuits 1.63-m^2 (17.5-ft^2) face area
Outdoor fan	Three-blade propeller 0.56-m (22-in.) diameter, 1/6-hp motor Direct drive Nominal m^3/s = 1.32 (cfm = 2800)
Indoor heat exchanger	Aluminum plate fin, 13 fins/in., with 1/2-in. inner diameter copper tubing Three rows deep with two parallel refrigerant circuits 0.32-m^2 (3.44-ft^2) face area
Indoor fan	Centrifugal, 0.25-m (10-in.) diameter by 0.2-m (8-in.) width Direct drive Three speeds 1/3-hp motor
Controls	Combination of expansion valve and capillary tubes for heating Expansion valve for cooling Time/temperature defrosting control Four-way reversing valve

[a]Rated at 48.8°C (120°F), condenser; 7.2°C (45°F), evaporator; 21.1°C (70°F), suction; and 8.3°C (15°F), subcooling.

3.2.1 Refrigerant Temperature and Pressure Measurements

The heat pump was instrumented at various locations for the measurement of refrigerant temperatures and pressures. Figure 5 illustrates the location of all refrigerant loop temperature and pressure sensors. The description of each measurement, correlated to Fig. 5, is listed in Table 7.

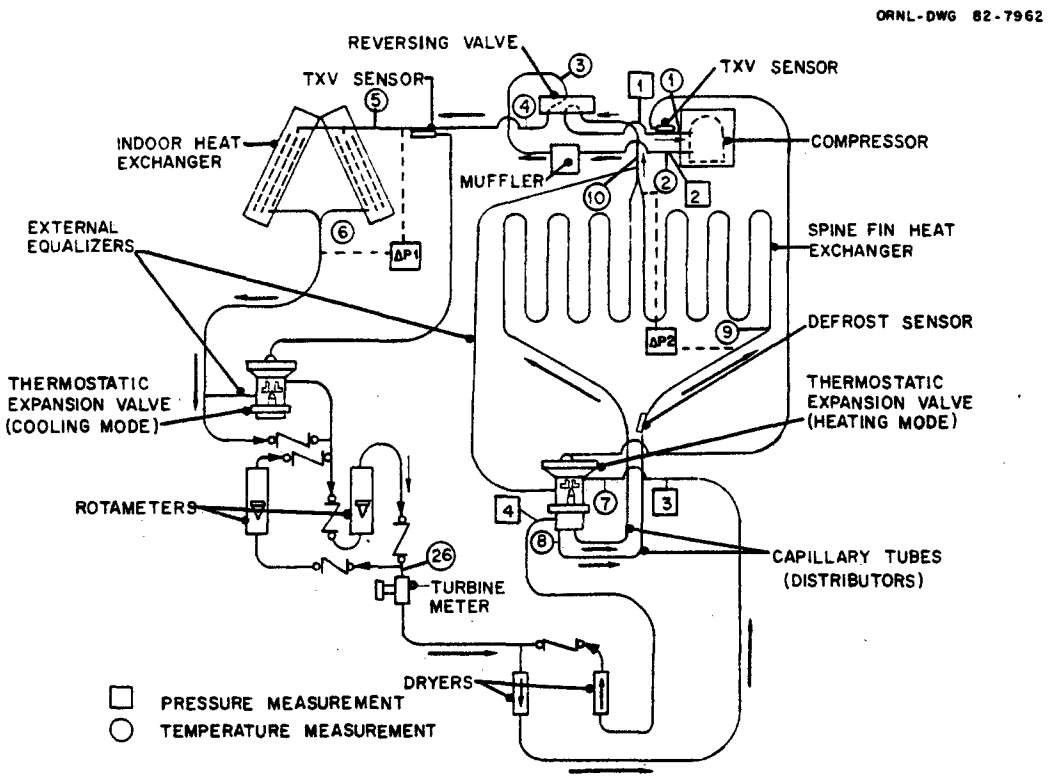

Fig. 5. Heat pump refrigerant sensor locations.

Table 7. Temperature and pressure sensors, refrigerant circuit

Sensor	Description of data taken
Temperature 1	Suction inlet to compressor shell
Temperature 2	Discharge line exit from compressor shell
Temperature 3	Entering reversing valve (discharge line)
Temperature 4	Exit of reversing valve (discharge line)
Temperature 5	Inlet to indoor coil
Temperature 6	Outlet to indoor coil
Temperature 7	Inlet to thermostatic expansion valve
Temperature 8	Outlet of thermostatic expansion valve
Temperature 9	Inlet to outdoor coil (exit of capillaries)
Temperature 10	Outlet to outdoor coil
Temperature 26	Inlet to turbine meter
Pressure 1	Inlet to compressor shell (between compressor and reversing valve)
Pressure 2	Compressor shell outlet
Pressure 3	Inlet to thermostatic expansion valve
Pressure 4	Outlet from thermostatic expansion valve
Pressure ΔP1	Pressure drop across indoor coil
Pressure ΔP2	Pressure drop across outdoor coil

3.2.2 Alterations to Heat Pump Electrical Circuit

The heat pump electrical circuit was altered to allow manual control of the compressor, outdoor fan, and indoor fan, as shown by the encircled numbers in Fig. 6. Manual switch 1, connected across terminals Y and R, will energize the motor contactor relay, which in turn closes the motor contacts MS-1 and MS-2 and allows the flow of electrical power to the compressor run and start windings. A high-pressure cutoff switch (point 2) is connected in series with the compressor manual switch for the protection of the compressor in case of accident or human error. To defrost the heat pump, the reverse cycle switch (point 3) between terminals O and R is energized and the outdoor fan switch (point 4) is opened. The defrosting cycle is terminated by reversing the above procedure, opening the reverse cycle switch, and closing the outdoor fan switch.

3.3 Instrumentation

3.3.1 Data Acquistion System

The data acquistion system (DAS), shown in Fig. 7, consists of a Digital Equipment Corporation (DEC) PDP-8E digital computer with an 8K word memory, a Vidar integrating digital voltmeter with an ohms converter, and a reed relay scanner. The programs used by the computer were written in a version of the FOCAL language modified locally to facilitate data acquisition. The computer displays instantaneous heat pump status and performance, allowing the observation of any drifts in performance and/or heat pump system malfunctions. For these experiments, the DAS scans all performance parameters and computes averages on a predetermined number of refrigerant flow rate cycles.* The averaged values are then printed and punched on tape for later use in data reduction.

3.3.2 Refrigerant Flow Measurements

Two variable-area flowmeters (rotameters) were used for visual observation of the refrigerant flow rate during cooling- and heating-mode operation. Spring-loaded check valves were installed at the entrance and exit of each rotameter to ensure operation of one rotameter during the heating mode and the other during the cooling mode. The check valves produce a pressure loss of about 6.9 kPa (1 psi) per valve, which has a negligible effect on refrigerant subcooling and accounts for only 2% of the refrigerant throttling between condenser and evaporator.

A turbine meter was used to measure and record refrigerant flow rates during heating-mode operation. The meter was selected to operate in its linear range for a flow rate varying from 0.75 to 3 L/min (0.2 to 0.8 gal/min) during heating-mode operation. The meter is linear to within $\pm 0.5\%$ of the reading for the above range in flow rate. Operating at full capacity, the maximum pressure drop of 20.7 kPa (3 psi) observed through the meter accounts for only 3% of refrigerant throttling.

3.3.3 Temperature Measurements

Copper-Constantan and Chromel-Alumel thermocouples were used for refrigerant and air temperature measurements. Floating reference junctions, previously described by Domingorena,[1,2] were used to measure all system temperatures. The voltage output of each thermocouple circuit is converted to engineering units of temperature by the DAS (Sect. 3.3.1) using simple algorithms.

---

*The refrigerant flow cycles are further discussed in Sect. 11.3.

ORNL–DWG 82–7958

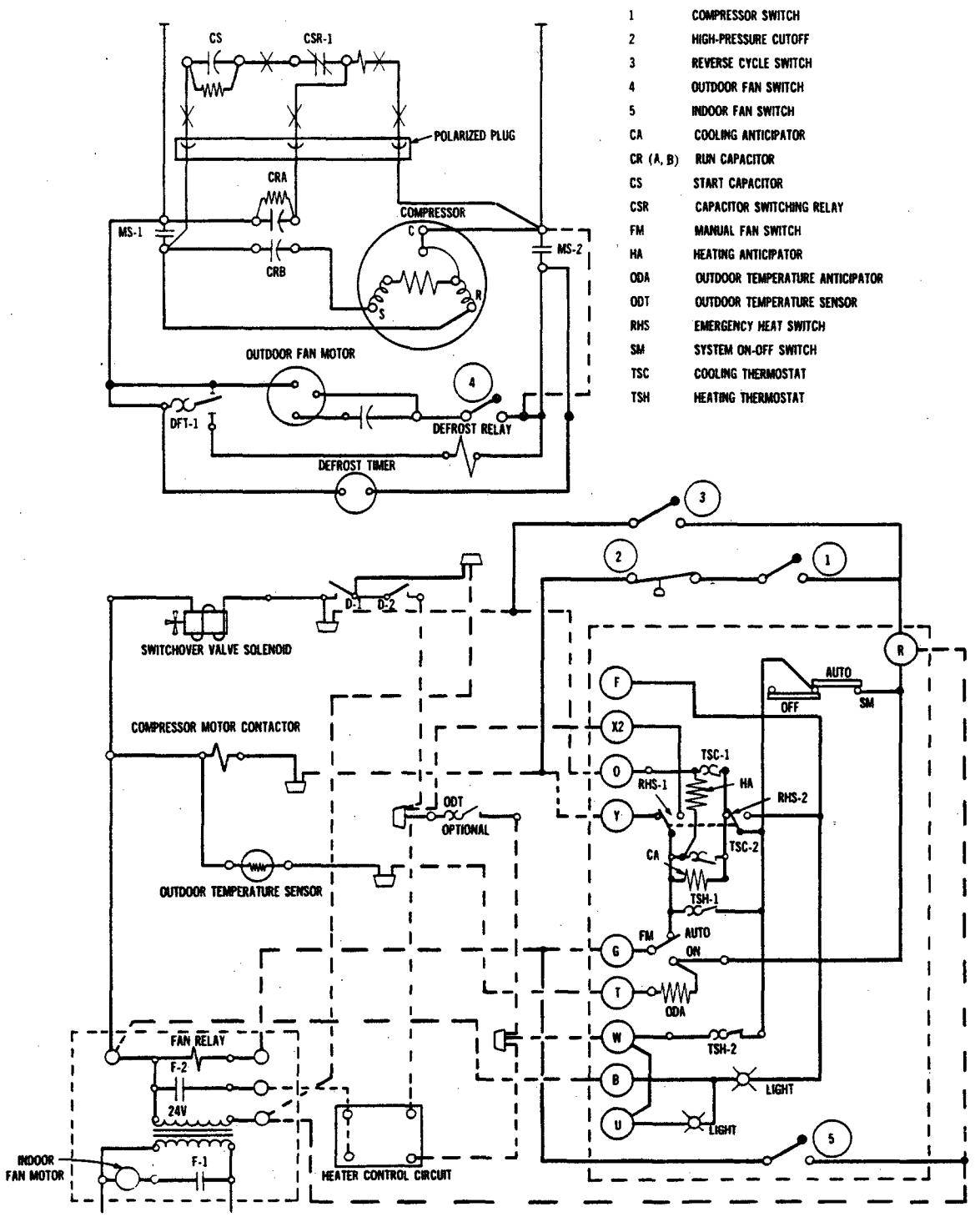

Fig. 6. Heat pump electrical circuit.

ORNL-PHOTO 6967-77

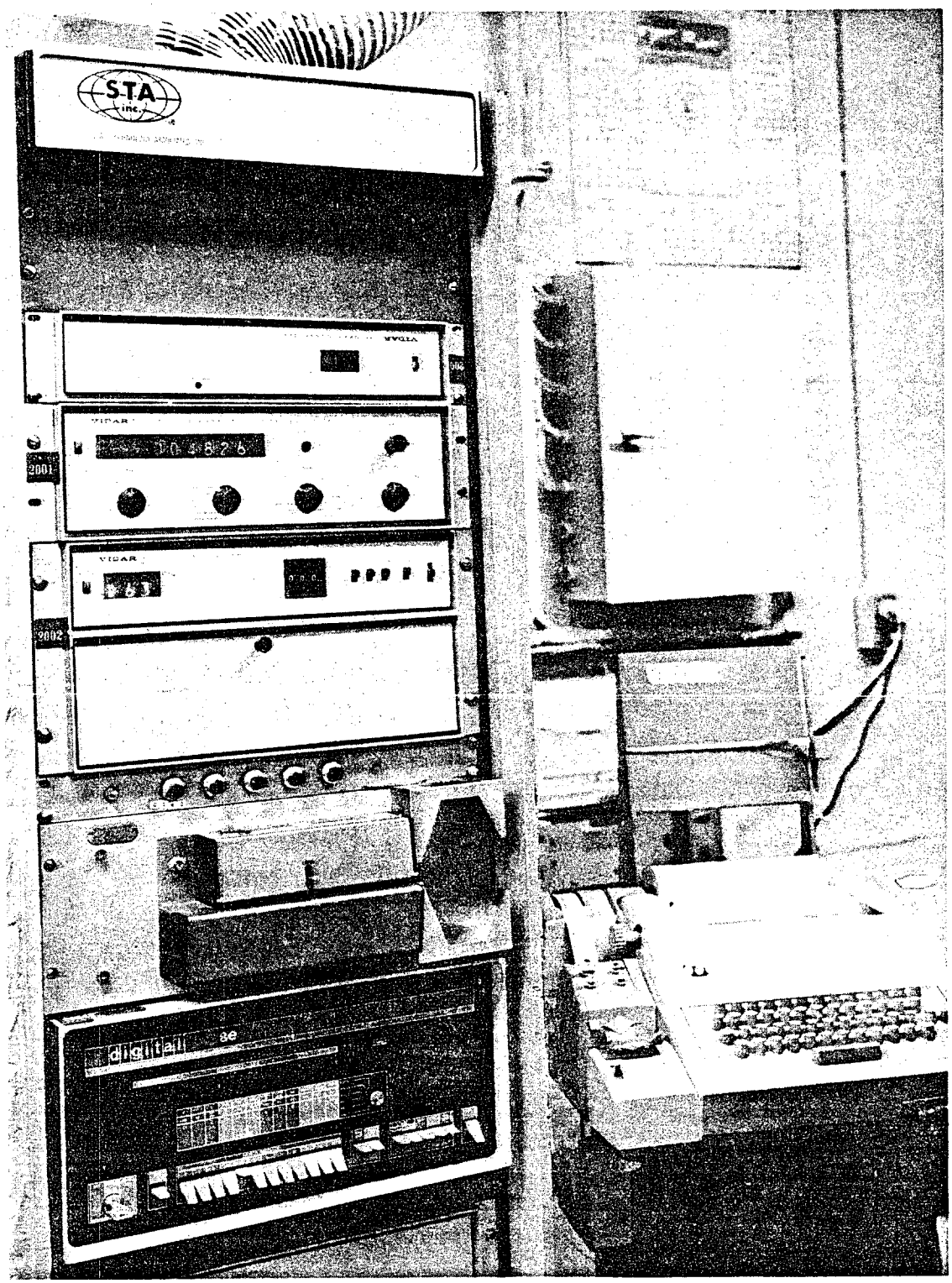

Fig. 7. Data acquisition system.

Thermocouples sensing refrigerant temperatures were clamped to refrigerant lines and covered with foamed elastomer insulation. Air temperatures were measured by grids of evenly spaced thermocouples electrically connected in parallel. Care was taken to make the lead wires of all the thermocouples of equal length to avoid error in air temperature measurement. This arrangement allowed the measurement of average air temperature at the duct cross section.

3.3.4 Pressure Measurements

Refrigerant pressures were measured by dynamic-response pressure transducers powered by an external, constant voltage source. The output of each cell was monitored by the DAS and converted to absolute pressure values by the following general expression:

$$P = G \quad V + B ,$$

where

V = transducer output, mV;
G = gain, or slope of pressure vs mV calibration curve;
B = bias, or reference datum for P_{abs}.

Bourdon gages were used periodically to check the accuracy of the pressure transducers.

Pressure drops across the heat exchangers were monitored by differential pressure transducers. These transducers produce a 10- to 50-mA DC signal that is proportional to the differential pressure. A 200-Ω precision resistor is placed in series with the current output; the voltage drop across this resistor is then monitored by the DAS for conversion to pressure measurement.

3.3.5 Electrical Power Consumption

Thermal-watt converters were used to measure the power consumption of the compressor, outdoor fan, and indoor fan. These thermal converters contain an electrical circuit in which the difference of power dissipated in two heaters is proportional to the power measured. The voltage output of the converter, monitored by the DAS, is a linear function of power from which values of instantaneous power consumption can be obtained.

3.3.6 Humidity Measurements and Control

The hygrosensors used to measure relative humidity within the outdoor air loop were compared to humidity measurements observed using a sling psychrometer. Both sensors measured relative humidity levels to within a tolerance of 2% of sling psychrometer measurements for an ambient temperature of 21°C (70°F).

The humidity sensor just upstream from the outdoor unit (Fig. 2) was used in a feedback control system, shown in Fig. 8, to maintain a constant relative humidity level within the outdoor air loop. The humidity measurement of the sensor is compared to a set point value of relative humidity by the DAS, which calculates the required compensation signal output and energizes either contact 1 or contact 2. The DAS then monitors the output of the operational amplifier and opens the energized set of contacts once the calculated voltage output has been obtained. A voltage-to-current converter and a current-to-pressure converter transfer the signal output to an air pressure signal. The 2- to 90-kPa (3- to 13-psi) signal actuates a control valve, which regulates the injection rate of steam to the air loop.

ORNL-DWG 82-7963

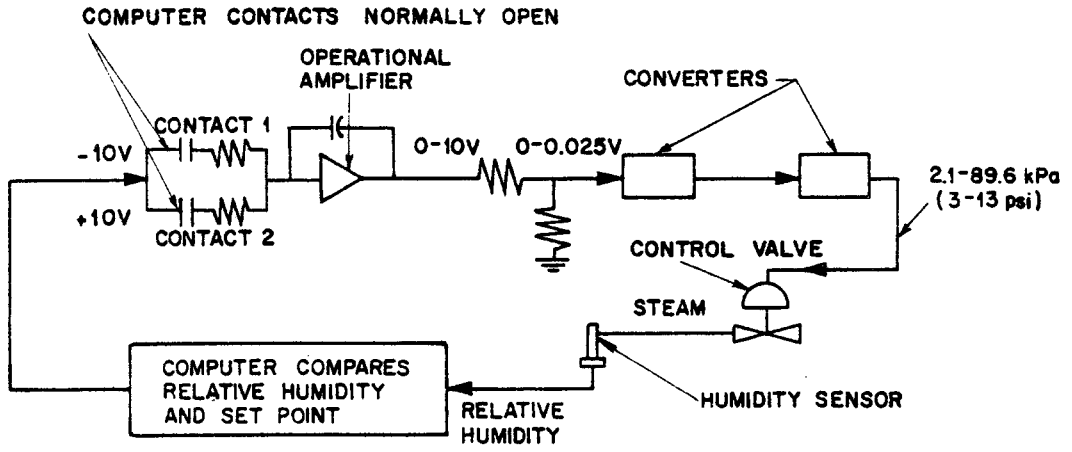

Fig. 8. Humidity control instrumentation.

3.4 Experimental Procedure

3.4.1 Steady-State Tests

Steady-state testing commenced once the heat pump had achieved proper indoor and outdoor ambient conditions. The DAS was then enabled to monitor and record all performance parameters listed in Table 7 plus power consumptions and refrigerant mass flow rates. For outdoor temperatures of 2 and −1°C (35 and 30°F) and relative humidities greater than 70%, frosting of the outdoor heat exchanger had begun prior to data collection. Thus, direct measurement of steady-state performance at these temperature and humidity levels was unobtainable. The steady-state performance was extrapolated to the start of each test from the slope of the curves representing reduced test data per respective temperature and relative humidity test run.

3.4.2 Frosting Tests

Frosting tests (Table 8) were performed to observe the effect of relative humidity and temperature on heat pump COP and capacity. The time of frost initiation and the duration of each frosting test were noted for each test run. The DAS was again used to monitor and record performance parameters identical to those monitored and recorded in steady-state tests. The airflow across the outdoor unit was also recorded and used as the criterion for defrosting of the heat exchanger in the outdoor unit. If the airflow was reduced by at least 50% of its nominal value [1.32 m^3/s (2800 ft^3/min)] by frost buildup, the defrosting cycle was manually initiated. (The automatic defrosting control installed in this heat pump was bypassed in order to observe the effects of severe frost accumulations on the heat exchanger of the outdoor unit.)

Table 8. Frosting test ambient conditions

Outdoor air temperature[a] [°C (°F)]		Outdoor air loop relative humidity (%)				
8.3	(47)	50		70		90
4.4	(40)	50	60	70	80	90
1.67	(35)	50	60	70	80	90
−1.11	(30)	50	60	70	80	90
−6.67	(20)		60	70	80	90
−8.33	(17)		60	70	80	90

[a]Indoor air temperature held at 21.1°C (70°F).

3.4.3 Defrosting Test Procedure

Defrosting tests commenced at the termination of each frosting test. The time required for defrosting was noted, and instantaneous values of compressor power consumption, compressor high- and low-side pressures and temperatures, and the refrigerant temperature leaving the outdoor heat exchanger were monitored and recorded at 8-s intervals by the DAS. Upon completion of the defrosting cycle, the heat pump was manually restored to heating-mode operation.

3.4.4 Charging Tests

The charge variation tests specifically dealt with the influence on system performance of refrigerant charges other than the nameplate charge 4.73 kg (10 lb 7 oz) and were performed while the system operated at a 8.3°C (47°F) ambient air temperature and 55% ambient relative humidity. The indoor return air was maintained at 21°C (70°F). The refrigerant charge was varied from 4.3 kg (9.5 lb), the minimum amount required for elimination of two-phase flow at the condenser exit, to 5.4 kg (12 lb). Performance data were recorded after each 0.1-kg (4.0-oz) addition of refrigerant.

3.4.5 Data Collection Procedure Using DAS

The DAS data-reduction program was designed to monitor all heat pump performance parameters over a prescribed number of cycles of the refrigerant flow rate. All performance parameters, listed in Table 7, were monitored every 7 s to obtain representative time-averaged values of system performance. Special data acquisition procedures monitoring data over an integral number of oscillations of refrigerant flow rate were necessary because the hunting behavior of the thermostatic expansion valve (Sect. 11.3) caused a somewhat regular cyclic variation in refrigerant flow rate. In Appendix B, the block diagram of the data reduction program displays the method used in monitoring, averaging, and reducing all data during operation of the system.

The data reduction program incorporated in the DAS was also designed to monitor outdoor coil wall temperatures. The program was modified by feeding an encoded tape to the DAS which changes the data indices as required to monitor outdoor coil temperatures. These data points are scanned every 8 s, and averaged outdoor coil temperatures are recorded on the teletypewriter and encoded on punched paper tape at the end of an integral number of refrigerant flow cycles.

4. DATA REDUCTION CALCULATIONS

The recorded experimental data were transferred to a DEC PDP-10 computer for use in a more extensive data reduction program.

4.1 Air- and Refrigerant-Side Heat Balances

Calculations of air- and refrigerant-side heat balances performed around the indoor heat exchanger were in good agreement. The air-side heat flows were lower than those for the refrigerant side by approximately 5% of the refrigerant heat balance. The error is probably due to nonuniform airflow and air-temperature stratification within the air duct. Air- and refrigerant-side COP calculations were made by dividing the corresponding heating capacity by the total power consumption of the heat pump. The refrigerant-side heating capacity used here is defined as heat rejected by the refrigerant in the indoor heat exchanger plus heat from the blower motor.

4.2 Conductance Coefficients

Overall thermal conductance coefficients *(UA)* were calculated for both dry and wet evaporator coils. Under wet-coil conditions, the net heat exchange to the outdoor heat exchanger is due to both heat and mass transfer. Experimental results for a wet outdoor heat exchanger have shown that mass transfer directly affects heat transfer. The change in magnitude that mass transfer causes in heat transfer can be observed by comparing the sensible and effective *UA* coefficients calculated for a wet spine fin heat exchanger.

4.2.1 Sensible Conductance Coefficients

The sensible conductance *UA* coefficients from air to tube wall and from air to refrigerant were calculated on the basis of logarithmic mean temperature difference (LMTD). The outdoor heat exchanger is of a cross-flow arrangement in which the refrigerant fluid is mixed and the air is unmixed. The refrigerant specific heat varies from inlet to outlet of the outdoor heat exchanger, and the refrigerant remains a saturated mixture through approximately 90% of the total heat exchanger. Since there is no noticeable change in refrigerant temperature within the two-phase region of the outdoor heat exchanger, the LMTD is suitable for calculation of the *UA* coefficient for the two-phase region of the outdoor cross-flow heat exchanger.

These *UA* coefficients for sensible heat transfer from air to tube wall and from air to refrigerant are calculated as follows:

$$UA_{A-W} = \frac{Q_S/(T_{A_1} - T_{A_2})}{\ln\,[(T_{A_1} - T_W)/(T_{A_2} - T_W)]} ,$$

$$UA_{A-R} = \frac{Q_S/(T_{A_1} - T_{A_2})}{\ln\,[(T_{A_1} - T_R)/(T_{A_2} - T_R)]} ,$$

where

UA_{A-W} = sensible conductance coefficient from air to tube wall,
UA_{A-R} = sensible conductance coefficient from air to refrigerant,
T_{A_1} = inlet air temperature to outdoor unit,
T_{A_2} = outlet air temperature to outdoor unit,
T_W = average wall temperature over two-phase region of outdoor coil,
T_R = bulk refrigerant temperature in two-phase region of outdoor coil.

4.2.2 Heat and Mass Transfer *UA* Coefficient

Under dehumidifying conditions, the heat flow to the outdoor heat exchanger is due to both heat and mass transfer. Under these conditions the driving potential for heat flow is no longer a temperature difference; rather, it is a moist air enthalpy difference. The overall effective *UA* coefficient from air to tube wall is therefore calculated through use of a logarithmic mean enthalpy difference (LMHD). The LMHD is identical in form to the LMTD:

$$\text{LMHD} = \frac{H_{A_1} - H_{A_2}}{\ln\left[(H_{A_1} - H_{W,F,SAT})/(H_{A_2} - H_{W,F,SAT})\right]} ,$$

where

$H_{W,F,SAT}$ = a fictitious saturated moist air enthalpy calculated at the evaporator wall temperature,
H_{A_1} = inlet moist air enthalpy,
H_{A_2} = outlet moist air enthalpy.

The effective *UA* coefficient is then calculated using the following equation:

$$UA_{eff} = Q_R/\text{LMHD} \cdot C_{P_{AIR}} ,$$

where $C_{P_{AIR}}$ = moist air specific heat.

The effective *UA* coefficient is defined here as a product of the moist air specific heat and the quotient of Q_R/LMHD. This definition yields similarity of units for comparison of trends in sensible and effective *UA* coefficients.

5. EXPERIMENTAL RESULTS — NONFROSTING OPERATION

The heating-mode performance of a heat pump is usually characterized by the COP and the heating capacity. These quantities are functions of the outdoor heat exchanger capacity, which is, in turn, dependent on the driving potentials of ambient temperature and humidity levels. System performance will be examined in terms of these driving potentials for ambient conditions that allow for a dry evaporator surface, those that produce a wet surface, and, finally, those that produce frosting on the coil. The results of these analyses for dry and wet coils will be combined to seek an understanding of the transient operation under frosting conditions.

5.1 Steady-State System Performance with a Dry Outdoor Coil

The COP, heating capacity, and outdoor heat exchanger capacity increased linearly with increasing ambient temperature under dry-coil conditions, as characterized in Fig. 9. The system COP increased from 2.12 at −8.3°C (17°F) to 2.9 at 8.3°C (47°F); the heating capacity increased from 5.51 kW (18,800 Btu/h) at −8.3°C (17°F) to 9.14 kW (31,190 Btu/h) at 8.3°C (47°F). The steady-state data used in calculating this system performance are tabulated in Appendix A.

5.1.1 Steady-State Compressor Performance

The divergence of heating capacity and outdoor heat exchanger capacity increased linearly with increasing ambient temperatures. Augmenting the outdoor ambient temperature resulted in larger air-side-temperature driving potentials, which then led to increased evaporator refrigerant temperature and pressure and thus increased refrigerant density at the compressor inlet (Figs. 10 and 11). Because the compressor is essentially a constant volume pump, the increase in inlet refrigerant density led to an increase in both refrigerant flow rate and compressor power consumption, as shown in Fig. 10. The rate of increase in refrigerant mass flow rate is greater than the rate of increase in compressor power consumption and is reflected in the higher COP and compressor efficiencies at the higher ambient temperatures. Figure 10 shows that the compressor efficiency* improved from 46% at −8.3°C (17°F) to 53.5% at 8.3°C (47°F).

5.1.2 Normalized Steady-State System Analysis

The compressor power, refrigerant mass flow rate, and refrigerant conditions at the compressor inlet are directly related to the outdoor ambient temperature displayed by the normalized plots in Fig. 12. This analysis, utilizing observed system performance at 8.3°C (47°F) as characteristic values, reveals the direct relationship of evaporator heat gain to the overall system performance.

These normalized plots will be helpful in explaining the observed trends in system performance under wet-coil, nonfrosting conditions and under dynamic frosting conditions. The slopes of refrigerant mass flow rate and compressor power consumption (Fig. 12) indicate that the rate of work per unit of mass flow rate increases as the ambient temperature decreases. The increase of work per unit of mass flow rate for decreasing ambient temperature results in an inverse relationship between

*Compressor efficiency is defined here as the ratio of isentropic compressor output (measured at the shell outlet) to the measured power input.

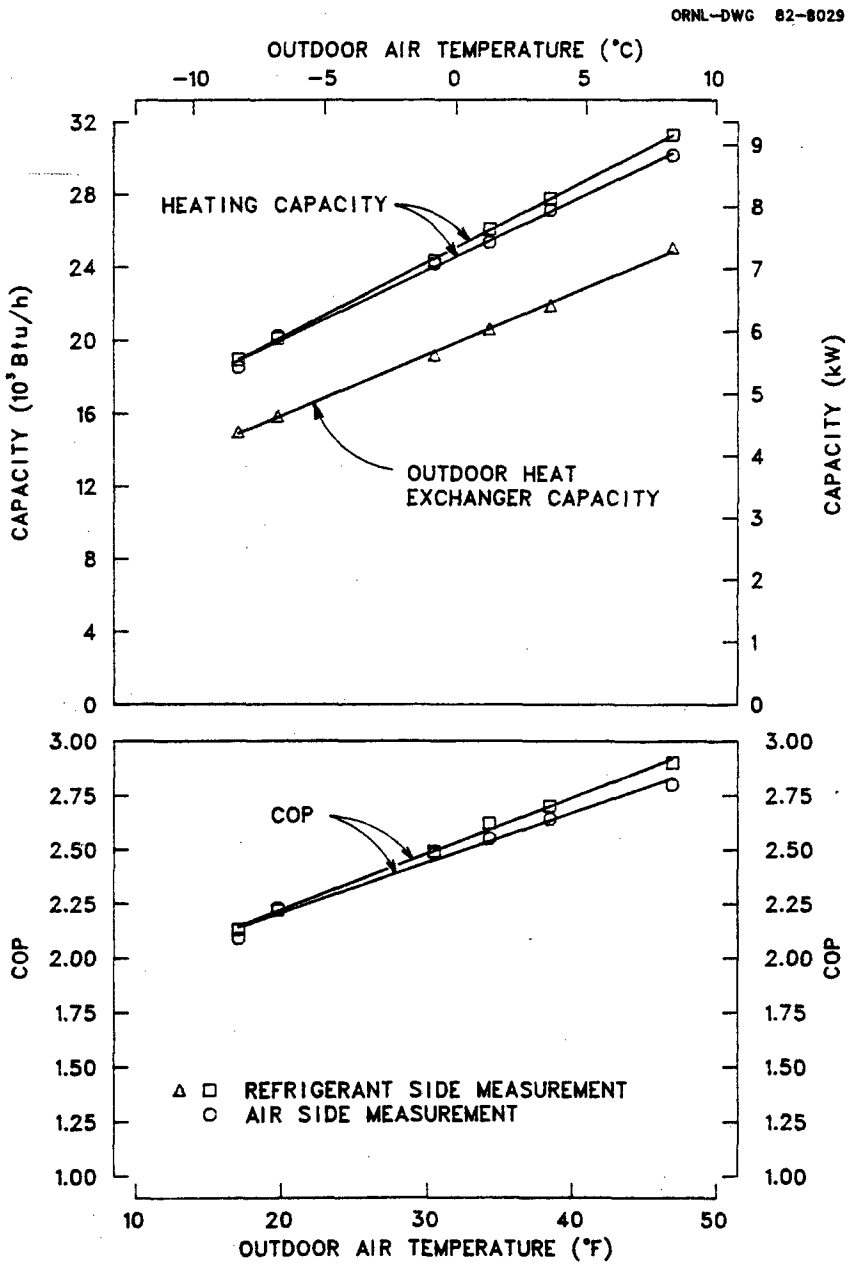

Fig. 9. Steady-state system performance.

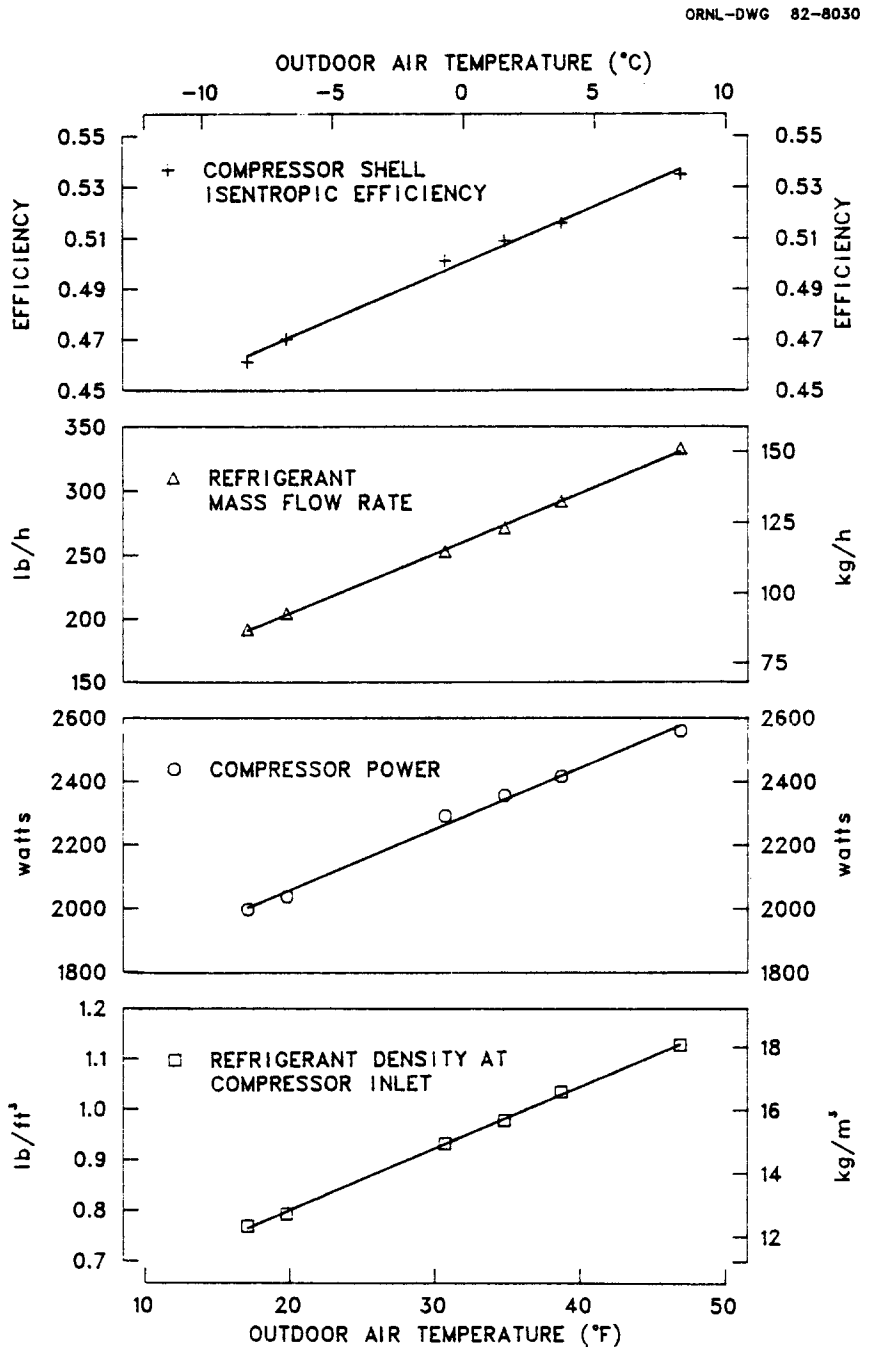

Fig. 10. Steady-state performance traits.

ORNL-DWG 82-8031

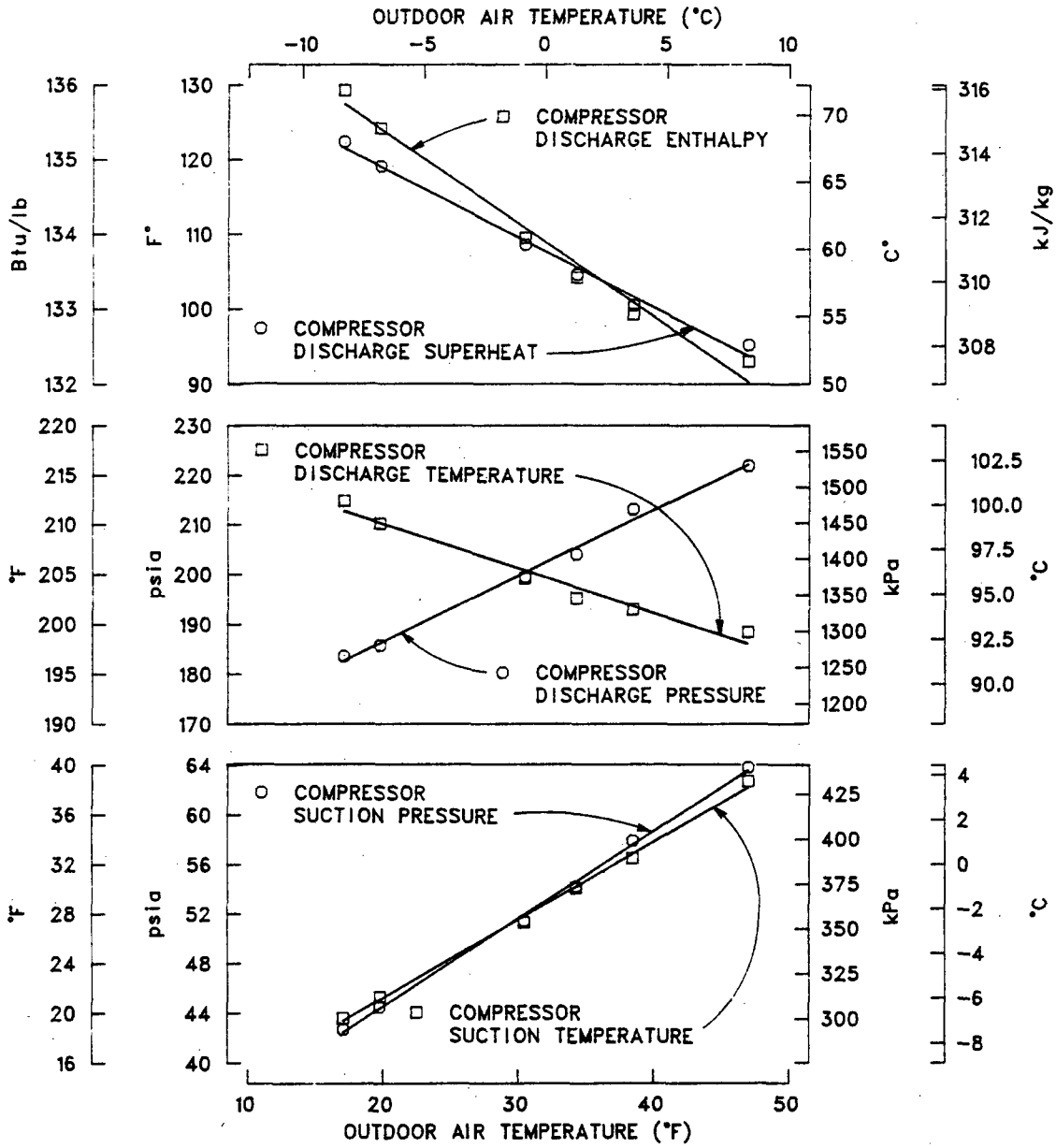

Fig. 11. Refrigerant properties across the compressor.

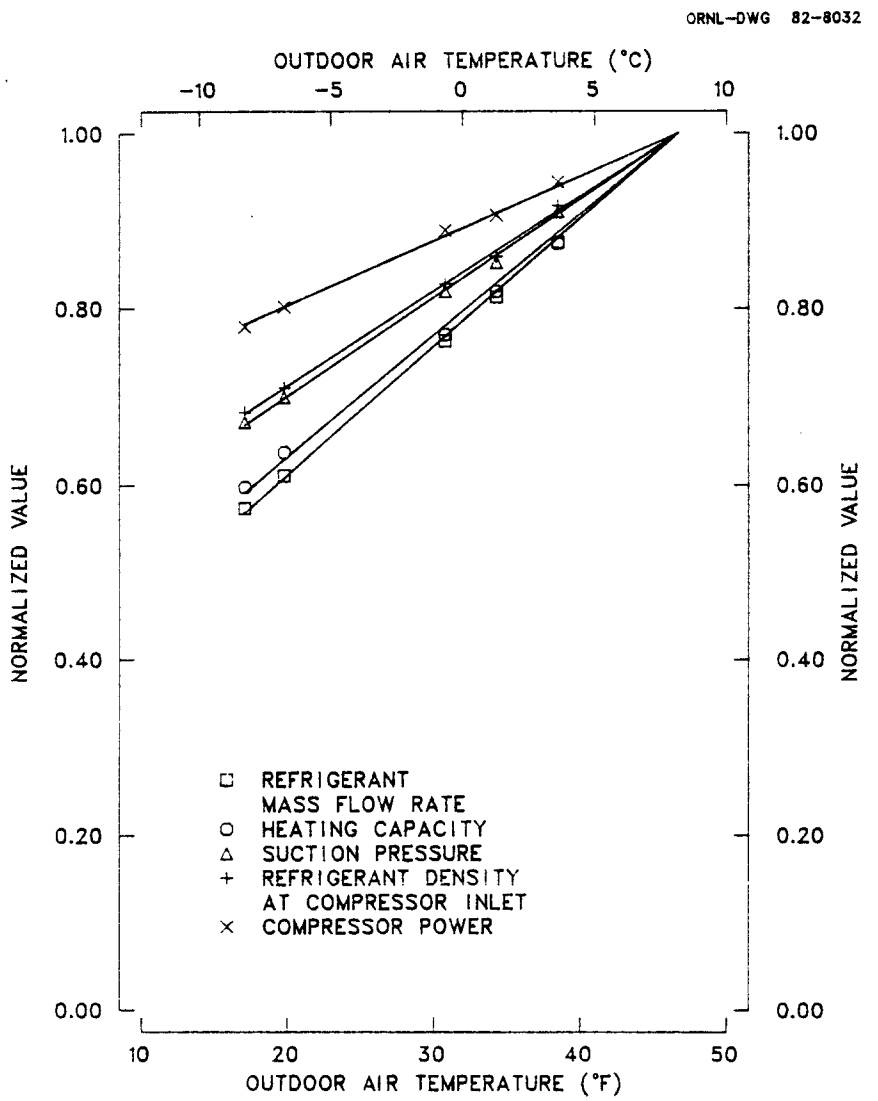

Fig. 12. Normalized system analysis.

refrigerant temperature and pressure at the compressor exit port (Fig. 11). As the ambient temperature lowers, the discharge refrigerant temperature increases because of a greater work input to the refrigerant. However, lowering the ambient temperature yields a decrease in refrigerant pressure and density at the compressor inlet. Lower refrigerant flow rates then result, producing a decrease in discharge pressure. This inverse relationship between temperature and pressure at the compressor exit port yields a decrease in both discharge superheat and refrigerant enthalpy as the ambient temperature increases over the temperature ranges shown in Fig. 11.

5.2 The Effect of Relative Humidity on Heating-Mode Performance of a Wet Outdoor Heat Exchanger

System COP and heating capacity improved slightly under conditions of high humidity in the nonfrosting range. With an 8.3°C (47°F) ambient air temperature and a relative humidity of 60% or more, the outdoor coil surface temperature is below the dew point of the air but above the freezing point of water. Thus, the coil is wet but not frosted. As shown in Fig. 13, the average COP at this temperature was observed to increase from 2.9 to 2.95 and 3.05 as the relative humidity was increased by increments of ten percentage points from 60 to 80%. The corresponding heating capacities were 9.14, 9.64, and 10.0 kW (31,200, 32,900, and 34,200 Btu/h); see Fig. 14.

These test results reveal the effect of moisture content of the outdoor air on heating-mode steady-state performance. Hence, the basis of comparison for frosting losses will be made using steady-state data per respective temperature and relative humidity test level.

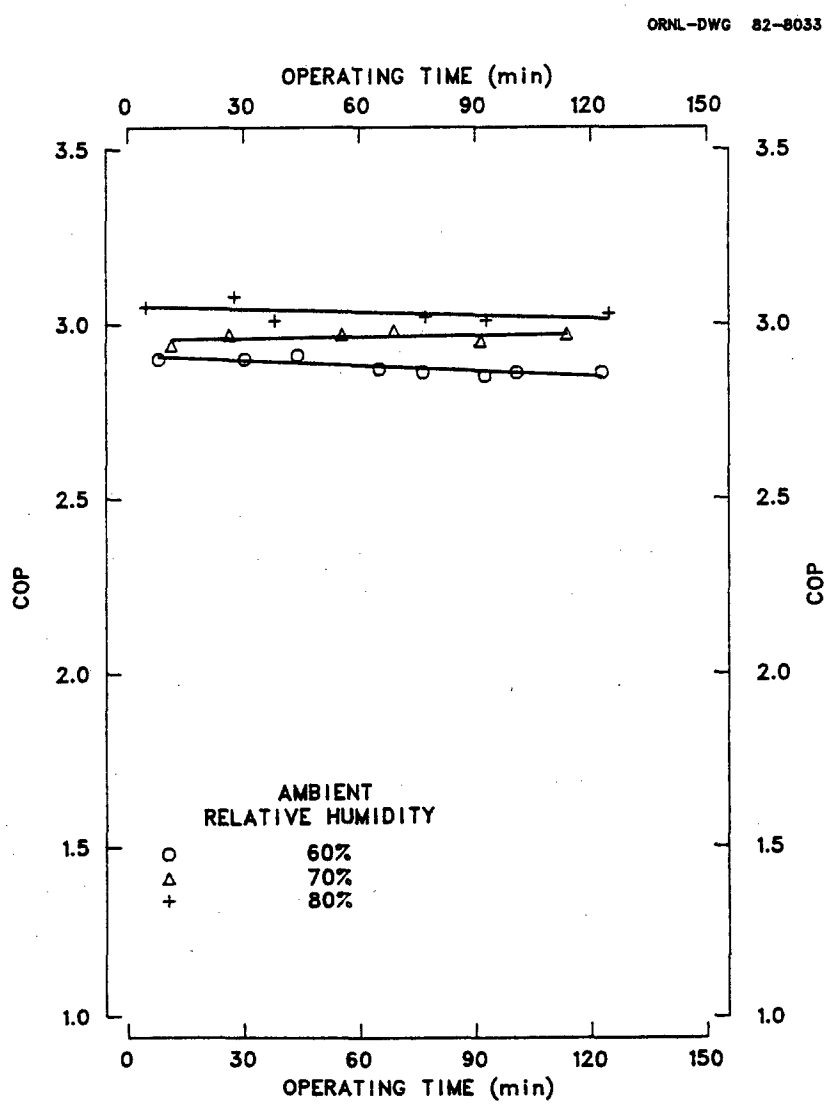

Fig. 13. COP for a wet outdoor heat exchanger.

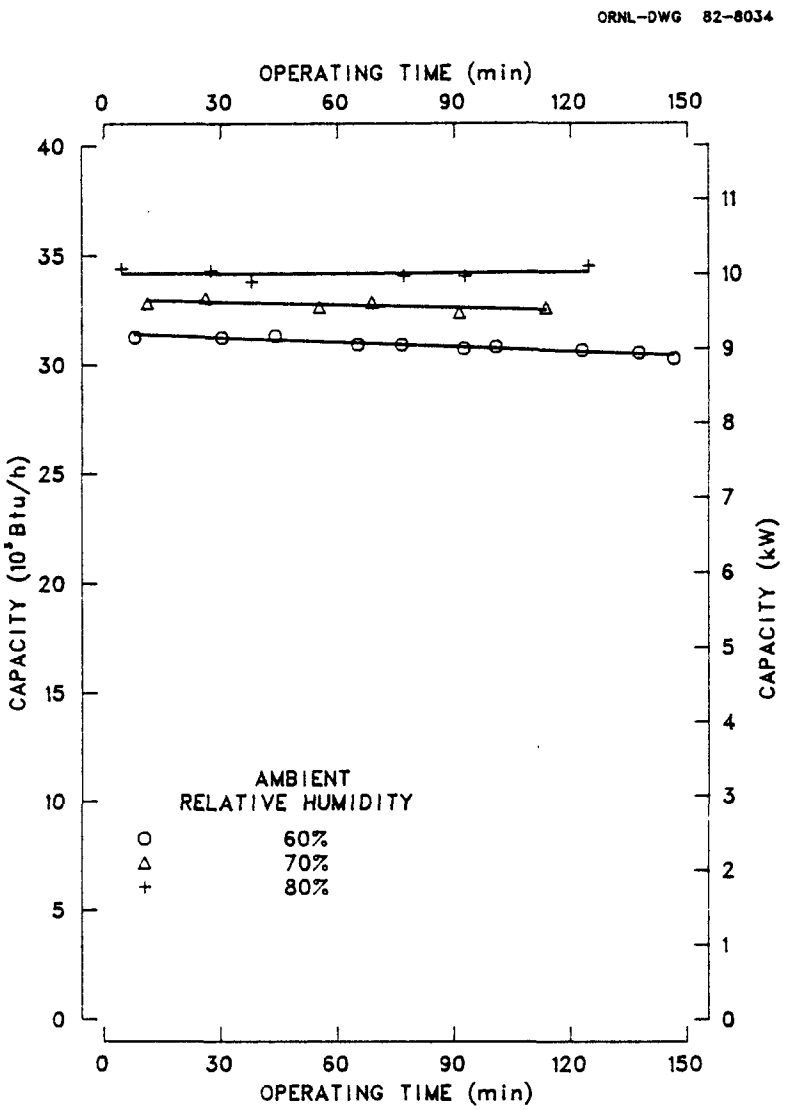

Fig. 14. Heating capacity for a wet outdoor heat exchanger.

5.2.1 Influence of Mass Transfer

The improvements in COP and heating capacity are the result of an increased outdoor heat exchanger capacity (Fig. 15). For a constant dry-bulb temperature, an increase in the relative humidity yields higher rates of mass transfer and an increased latent heat contribution to the outdoor heat exchanger. At the completion of the 60% relative humidity test run, 1.33 L (0.35 gal) of condensate were collected, and 3.19 and 11.48 L (0.84 and 3.03 gal) of condensate were collected after the 70 and 80% humidity tests respectively. The increased amount of collected condensate therefore verifies the increase of mass transfer to the outdoor heat exchanger, which produced the increased wall temperature shown in Fig. 16.

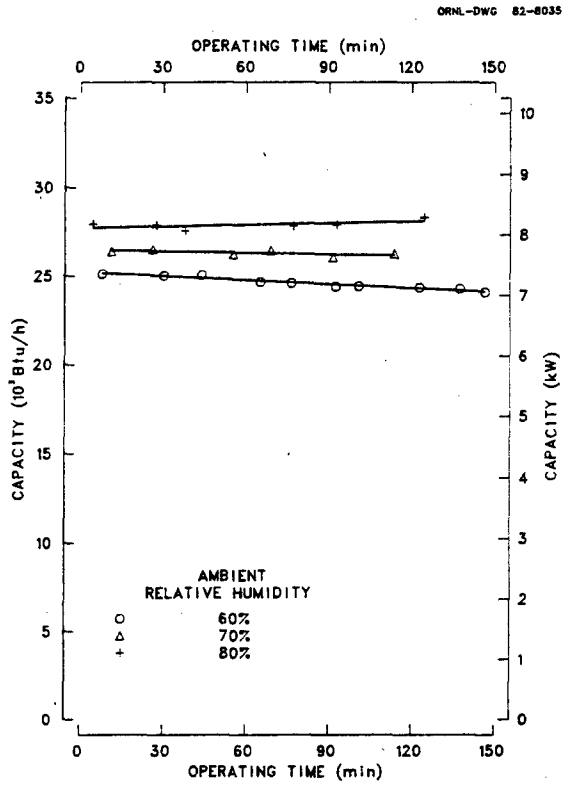

Fig. 15. Evaporator capacity for a wet outdoor heat exchanger.

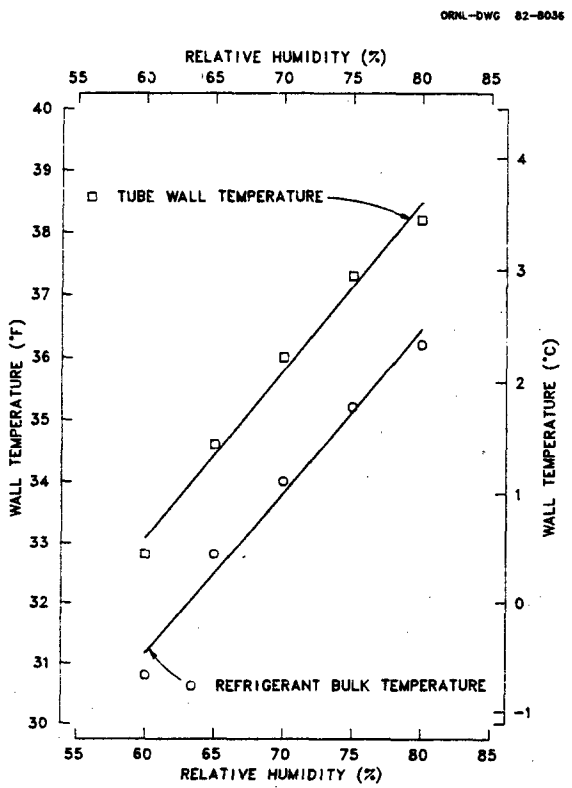

Fig. 16. Evaporator tube wall temperature over the entire two-phase region for a wet coil.

5.2.2 Thermal Conductance for a Wet Evaporator Coil

Under nonfrosting wet-coil conditions observed at 8.3°C (47°F), the sensible and effective *UA* coefficients increased for relative humidities greater than 70% (Fig. 17). The sharp increase in the effective *UA* is due to the increased mass transfer for ambient conditions greater than 60% relative humidity. During the 70 and 80% relative humidity tests, droplets of water were observed adhering to the spine fins of the outdoor heat exchanger. These water droplets may have a roughness effect, as suggested by McQuiston,[5] which would induce a mixing or turbulence of the air stream traversing the free-flow area of the outdoor heat exchanger. The increased turbulence would produce larger air-side convection coefficients yielding the increase in the sensible *UA* coefficients.

For the 8.3°C (47°F) wet-coil tests, the outdoor volumetric airflow decreased from a nominal value of 1.19 m^3/s (2515 ft^3/min) at 60% relative humidity to values of 1.17 m^3/s (2475 $ft^3/$ min) and 1.15 m^3/s (2440 ft^3/min) for the 70 and 80% humidity tests. The slight reduction of airflow coupled with a decrease in the free-flow area for a wet-coil could result in an increase in the linear velocity and Reynolds number of the air traversing the coil. An increase in the air velocity traversing the coil would then yield higher air-side convection coefficients.

It is also plausible, as suggested by Yamakawa, Takahashi, and Ohtani,[6] that the condensation of water vapor onto the outdoor heat exchanger would heat the thermal boundary layer. The latent heat contribution heating the thermal boundary layer would then cause the layer to become thin, thus increasing the heat transfer coefficients.

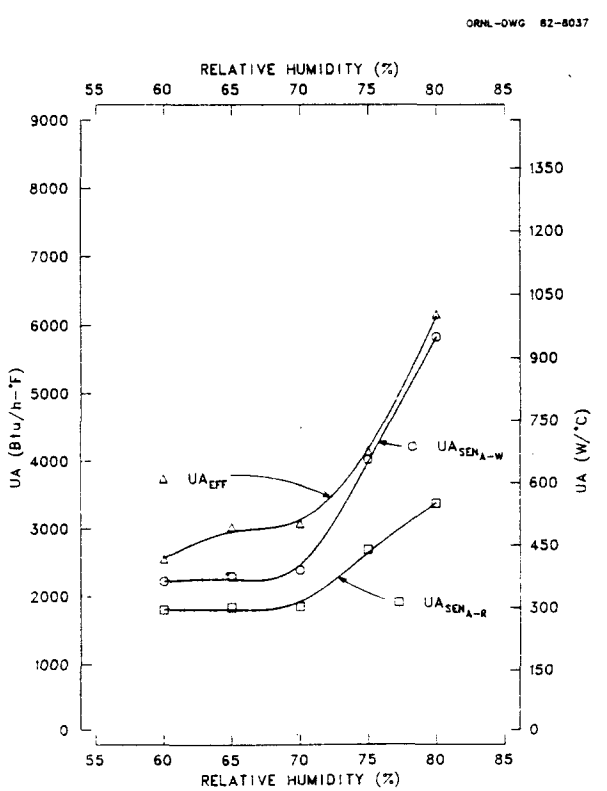

Fig. 17. Sensible *UA* coefficients over the two-phase region of the outdoor heat exchanger.

6. EXPERIMENTAL RESULTS — FROSTING CONDITIONS AT 4.4°C AMBIENT TEMPERATURE

6.1 Performance Observed at 4.4°C (40°F) with Relative Humidities Less than 70%

The dry-coil COP observed at 4.4°C (40°F) and 50% relative humidity was approximately 2.75, and the heating capacity at this condition was nominally 8.1 kW (27,750 Btu/h). System performance remained constant with time since the evaporator tube wall temperature was greater than the inlet-air-dew-point temperature and neither dehumidification nor frosting could occur. Increasing the relative humidity to 60% allowed light dehumidification and frosting to begin on the outdoor heat exchanger. The frosting produced a gradual reduction in the outdoor heat exchanger capacity and thus system COP and capacity as compared to the nonfrosting steady-state COP and capacity obtained at 50% relative humidity. At termination of this test run, no appreciable amounts of defrosting water were collected.

Incrementing the inlet air relative humidity from 50 to 70% produced an increased rate of frost accumulation on the outdoor heat exchanger. The COP observed during the 70% humidity test dropped from 2.82 to 2.24 within 140 min of heating-mode operation (Fig. 18). Similarly, the heating and outdoor heat exchanger capacities were both reduced by approximately 27% of their initial values (Figs. 19 and 20).

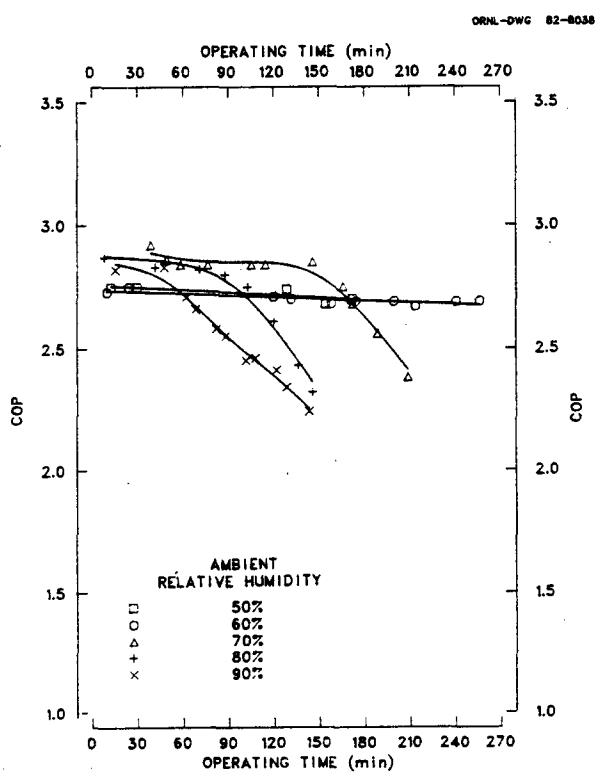

Fig. 18. COP measured at 4.4°C (40°F).

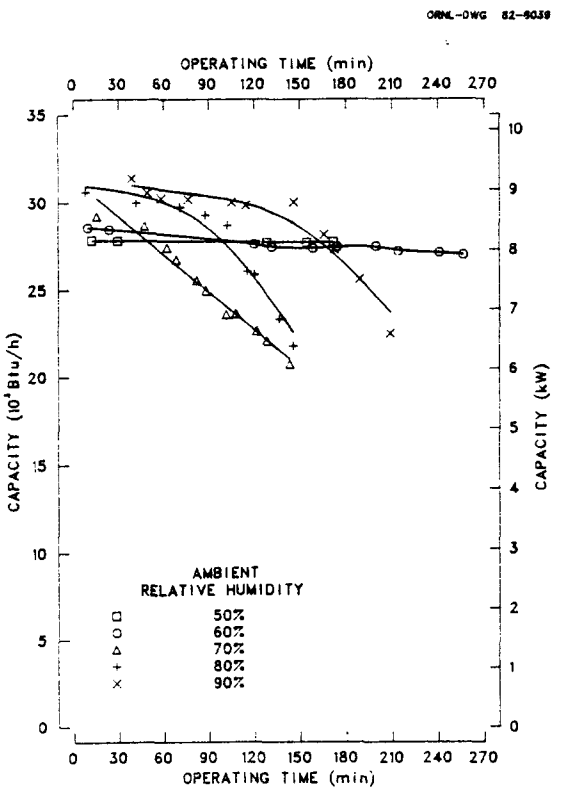

Fig. 19. Heating capacity measured at 4.4°C (40°F).

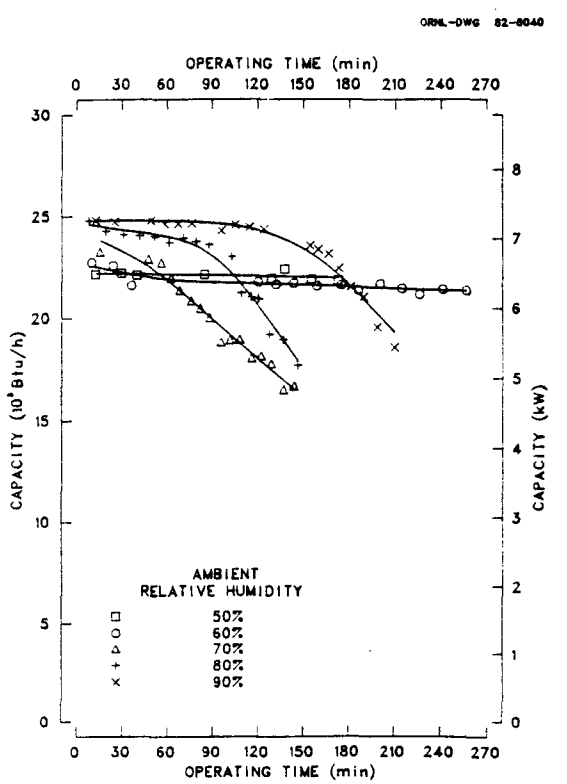

Fig. 20. Evaporator capacity measured at 4.4°C (40°F).

6.2 Performance Measured at 4.4°C (40°F) with Relative Humidities of 70% and Greater

Parken, Beausoliel, and Kelly observed, in frosting studies conducted on a 5-ton heat pump, 5.5°C (42°F) ambient temperature as the boundary at which frosting occurred on the outdoor heat exchanger.[7] Intuitively, it would seem that the increase in ambient relative humidity under frosting conditions should increase the rate of frosting. However, test results at 4.4°C (40°F) for relative humidities greater than 70% revealed an initial improvement in system performance, as shown in Figs. 18, 19, and 20. The COP increased from 2.75 (base case performance) to values of 2.82, 2.85, and 2.92 as the respective relative humidity was increased from 70 to 90%. Similarly, the heating capacity increased from 8.1 kW (27,750 Btu/h) to values of 8.5, 8.9, and 9.23 kW (29,200, 30,400, and 31,500 Btu/h) as the relative humidity was increased from 70 to 90%. The increase in system performance is due to the increased mass transfer rate as the moisture content of the air is enhanced above moisture levels preset at 60% humidity. The augmented mass transfer increased both the evaporator tube wall temperature and compressor inlet pressure (Figs. 21 and 22). This increase in the tube wall temperature over the two-phase region of the outdoor heat exchanger resulted in a delay in the onset of frosting as the relative humidity was increased. Frosting commenced 35 min into the 70% test run, and at 80 and 90% relative humidities frosting did not begin until 85 min and 160 min, respectively, of run time had elapsed. The plots of outdoor airflow in Fig. 23 reveal this delay in frost formation for relative humidities greater than 70%. These plots also reveal the discrepancy between the onset of frosting and the start of a defrosting operation that would have occurred with a time-and-temperature defrosting control set for a 90-min cycle.

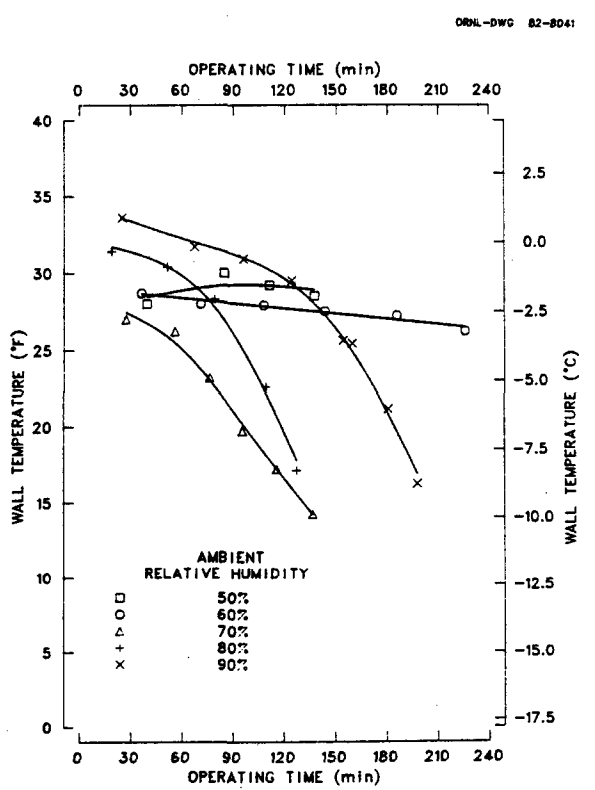

Fig. 21. Tube wall temperature over the entire two-phase region of the outdoor heat exchanger.

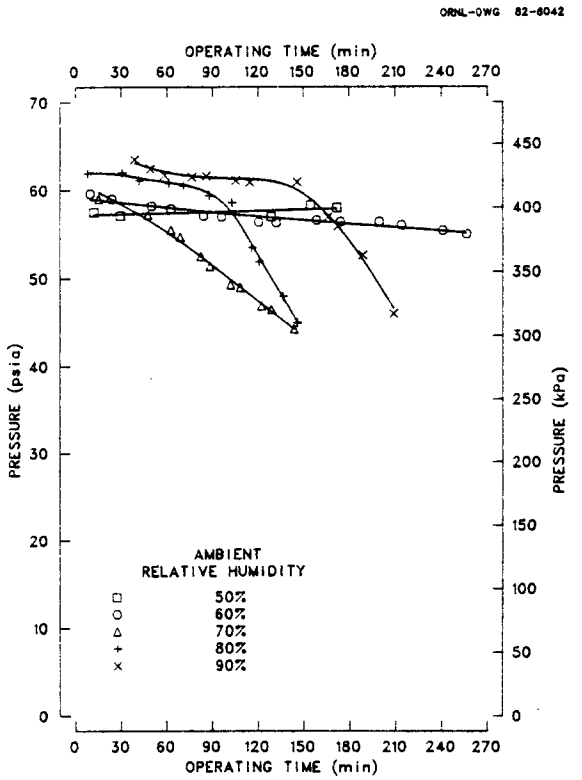

Fig. 22. Absolute refrigerant pressure at the compressor inlet.

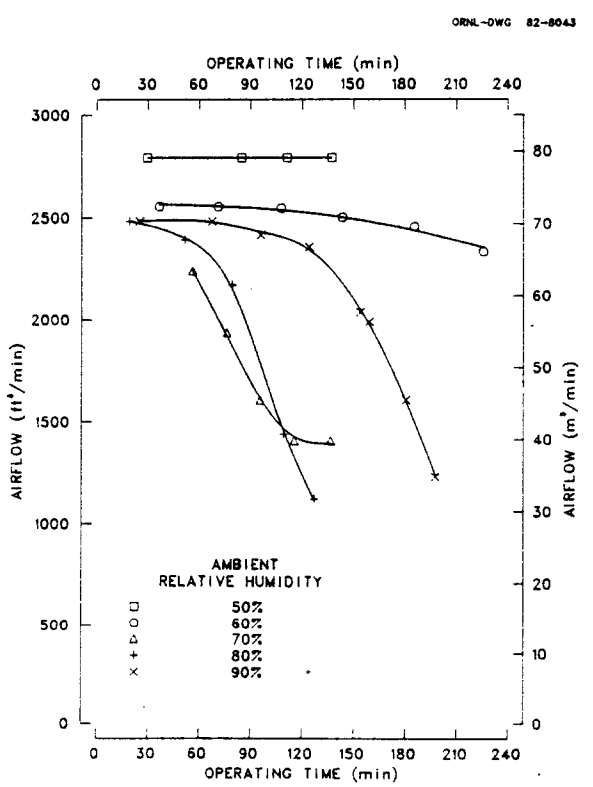

Fig. 23. Outdoor airflow measured at 4.4°C (40°F).

At the onset of the 80 and 90% test runs conducted at 4.4°C (40°F), the outdoor coil was initially saturated with water, and a flow of condensate from the coil was observed until frosting began. The accumulation of water on the outdoor heat exchanger gradually increased the resistance to heat flow and thus lowered the tube wall temperature to a point favorable for frosting operation, as seen in Fig. 21. Once frosting commenced, the higher relative humidities, reflecting an increase in the moisture content of the air, enhanced the rate of frost accumulation, resulting in greater rates of performance degradation. Figures 18, 19, and 20 show the increase in slope for relative humidities greater than 70%.

6.3 Influence of Frost on System Operation at 4.4°C (40°F)

The initial increase in the outdoor heat exchanger capacity due to increased mass transfer of moisture for relative humidities greater than 70% resulted in an increase in refrigerant density at the compressor inlet. The constant volume pumping action of the compressor led to higher refrigerant mass flow rates and higher rates of compressor power consumption, as shown in Fig. 24. Once frosting commenced, the reduction in the outdoor heat exchanger capacity lowered the refrigerant temperature yielding a decrease in the refrigerant density at the compressor inlet, which then yielded a reduction in both refrigerant mass flow rate and compressor power consumption. The reduction of refrigerant flow rate decreased the heating capacity of the heat pump, since its heat output is directly related to the refrigerant mass flow rate. The COP also decreases due to the reduction of heating capacity and the decreased ratio of refrigerant mass flow rate to compressor power consumption as revealed by the preceding normalized analysis (Sect. 5.1.2).

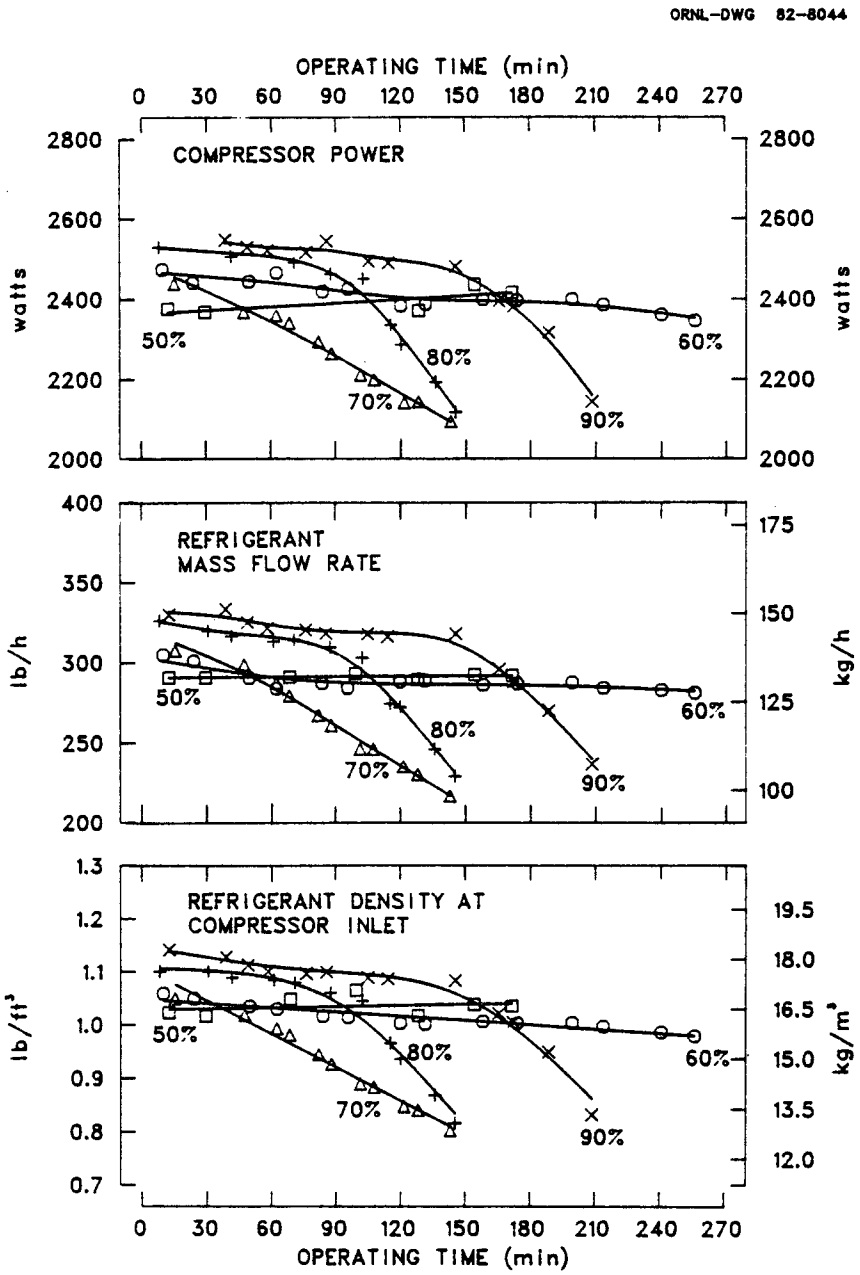

Fig. 24. Parametric study of heat pump performance observed at various outdoor relative humidity levels for an ambient temperature of 4.4°C (40°F).

7. EXPERIMENTAL RESULTS FOR AMBIENT TEMPERATURES LESS THAN 4.4°C (40°F)

The trends in system performance present at 4.4°C (40°F) were not observed at lower ambient temperatures. For tests conducted at ambient temperatures of 1.7, −1.1, −6.7, and −8.3°C (35, 30, 20, and 17°F), increasing the relative humidity increased the rate of frost accumulation on the outdoor heat exchanger. The threshold of frosting was observed at 60% relative humidity for the 1.7 and −1.1°C (35 and 30°F) ambient conditions, but at the lower ambient temperatures of −6.7 and −8.3°C (20 and 17°F) the threshold of frosting was observed to occur at 70% relative humidity.

7.1 Performance as a Function of Temperature

7.1.1 Performance at 1.7°C (35°F) Ambient Temperature

At an ambient temperature of 1.7°C (35°F), conditions favorable to frosting, the system COP and capacity decreased for relative humidity levels greater than 60%. The increased moisture content in the air increased the rate of performance degradation (Figs. 25 and 26) due to the increased frosting rates on the outdoor heat exchanger.

The COP at 70% relative humidity reduced from an initial value of 2.58 to 2.18, a 15% reduction within 80 min of operation. At the higher humidity of 80%, the COP reduced from 2.63 to 2.15, an 18% reduction, within 60 min of operation. Incrementing the humidity to 90% did not increase the extent of peformance degradation; however, the time of degradation was decreased to 50 min. The heating capacity observed during 70, 80, and 90% relative humidity tests decreased by

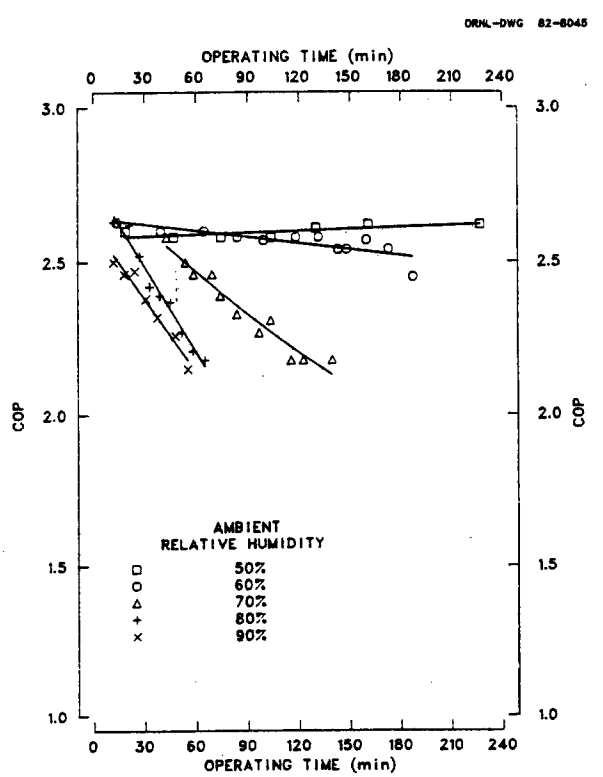

Fig. 25. COP measured at 1.7°C (35°F).

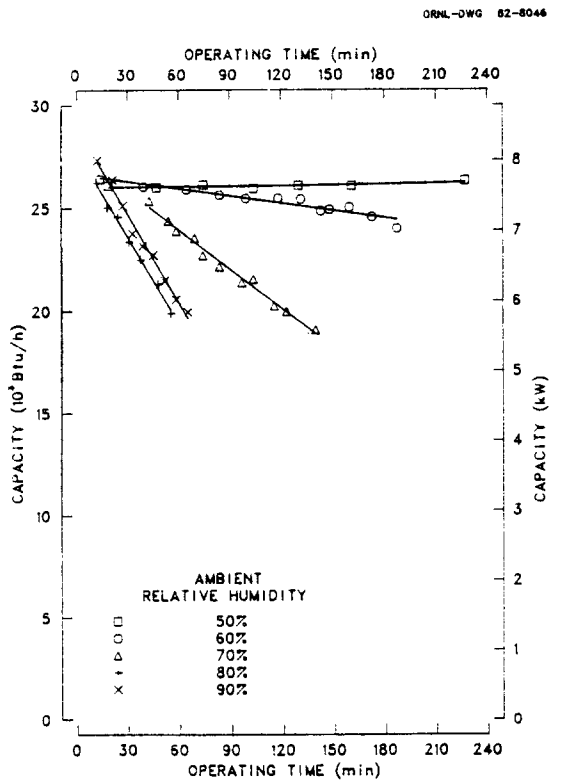

Fig. 26. Heating capacity measured at 1.7°C (35°F).

24% of the initial values; however, the time required for the 24% degradation reduced from 100 to 55 and 45 min respectively (Fig. 26).

Frosting data observed at 1.7°C (35°F) are tabulated in Appendix A for detailed analysis of typical system operation during frosting operation.

7.1.2 Performance at −1.1°C (30°F) Ambient Temperature

Frosting was light during the 60% relative humidity test conducted at −1.1°C (30°F), and no noticeable reduction in system performance was observed (Figs. 27 and 28). Incrementing the relative humidity to 70% produced a noticeable frost accumulation on the outdoor heat exchanger; however, it was only moderately frosted at termination of the experiment. The COP during the 70% humidity test reduced from an initial value of 2.45 to 2.15 within 160 min of operation, while the corresponding heating capacity dropped from 6.93 kW (23,650 Btu/h) to 5.71 kW (19,500 Btu/h). The increase of relative humidity above 70% augmented the rate of frost accumulation on the outdoor heat exchanger to a point at which 90% of the coil was blocked with frost after 50 min of operation. The COP dropped from approximately 2.5 to values of 2.1 and 2.0, respectively, for the 80 and 90% humidity tests (Fig. 27). The heating capacity dropped from nominally 7.3 kW (25,000 Btu/h) to values of 5.4 kW (19,250 Btu/h) and 5.27 kW (18,000 Btu/h), respectively, for the 80 and 90% humidity tests (Fig. 28).

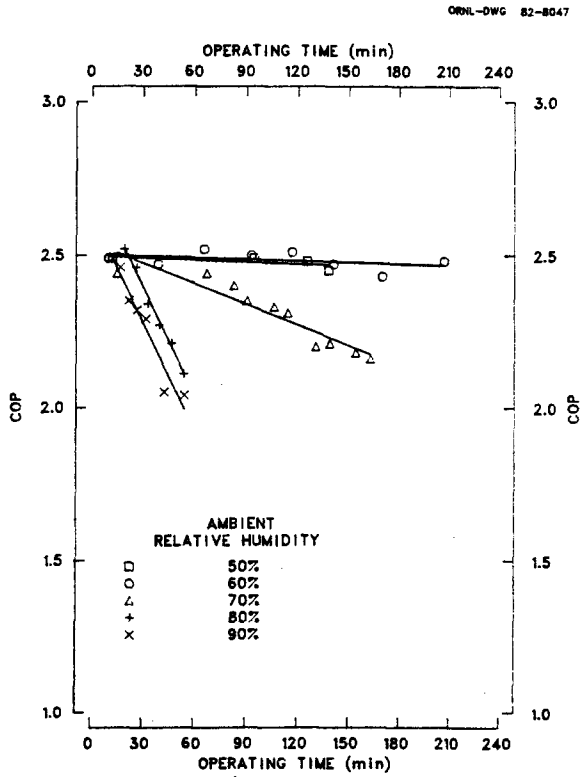

Fig. 27. COP measured at −1.1°C (30°F).

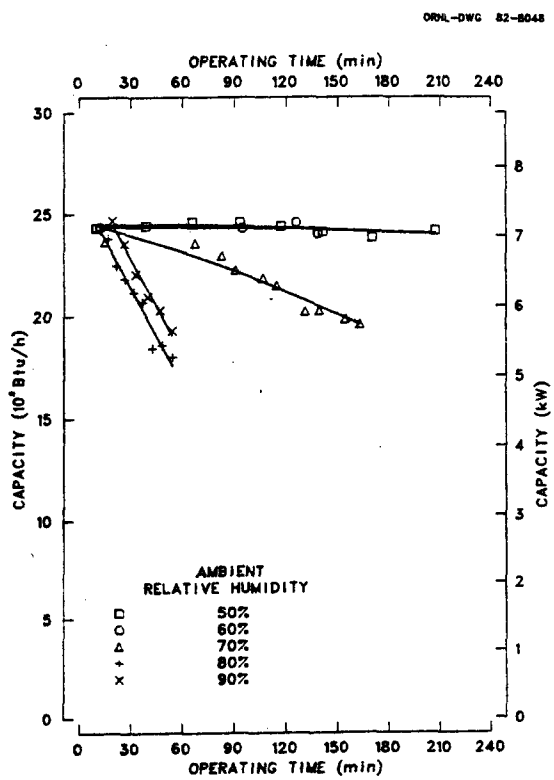

Fig. 28. Heating capacity measured at −1.1°C (30°F).

7.1.3 Performance at −6.7°C (20°F) Ambient Temperature

No new trends in system performance were observed for this set of test runs at −6.7°C (20°F). Lowering the ambient temperature for a given relative humidity lowers the moisture content of the air and necessitates higher relative humidities for the accumulation of frost on the outdoor heat exchanger of a given heat pump. Figures 29 and 30 portray the near steady-state performance for relative humidities less than 80%. The outdoor heat exchanger was moderately frosted at 80% humidity causing only a slight reduction in system COP and capacity (Figs. 29 and 30). However, at 90% relative humidity, the COP dropped from 2.2 to 1.83 and the heating capacity dropped from 5.86 kW (20,000 Btu/h) to 4.83 kW (16,500 Btu/h) within 70 min of operation due to the accumulation of frost. Once again, at the termination of this 90% humidity test run, approximately 90% of the free-flow area of the outdoor heat exchanger was observed to be blocked with frost.

The performance of the system was also observed at −8.3°C (17°F), and results are nearly identical to those seen at −6.7°C (20°F). The plots of system performance and outdoor volumetric airflow are presented in Appendix C but will not be discussed within the text.

7.2 Effect of Frost on Evaporator Tube Wall Temperature and Compressor Suction Pressure

The frost accumulation on the outdoor heat exchanger increased the resistance to heat flow and thus reduced both evaporator tube wall temperature and refrigerant suction pressure at the inlet to the compressor. Using the −1.1°C (30°F) test runs as typical results, the tube wall temperature,

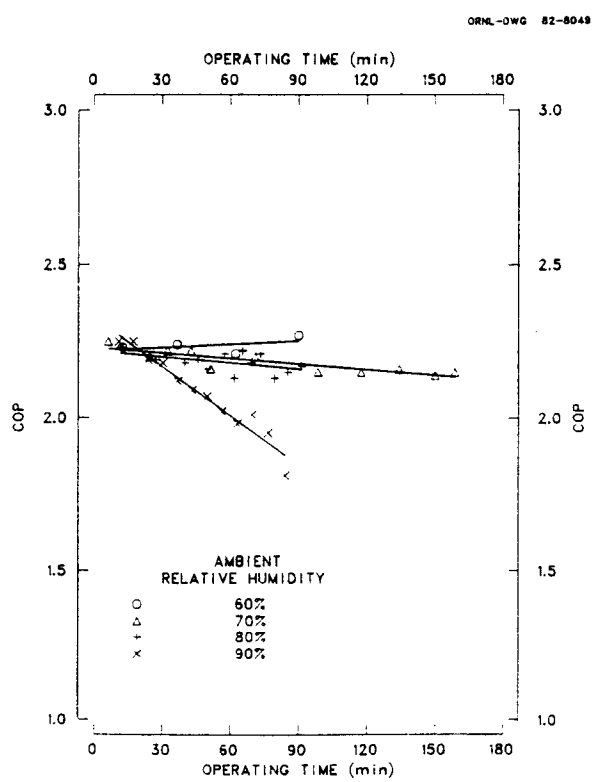

Fig. 29. COP measured at −6.7°C (20°F).

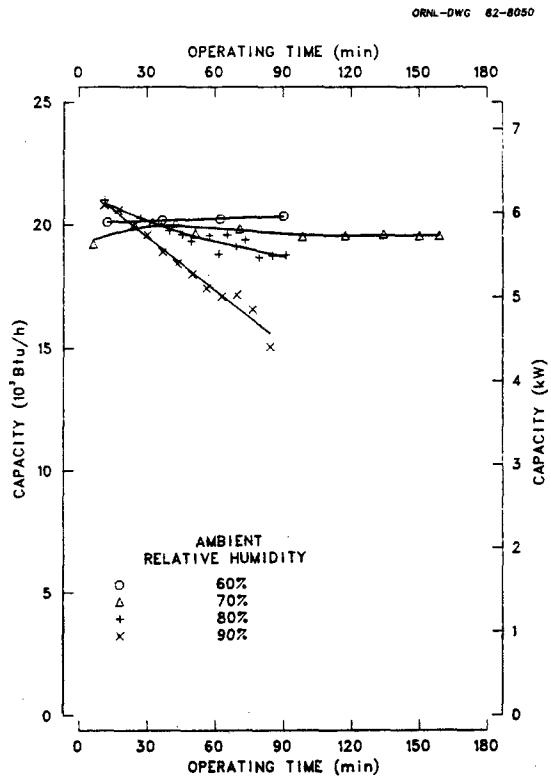

Fig. 30. Heating capacity measured at −6.7°C (20°F).

characterized in Fig. 31, was nominally −5.55°C (22°F) for the low-humidity test runs of 50 and 60%. The spine fins, having an average temperature below 0°C (32°F), immediately began to frost for the −1.1°C (30°F) test having humidity levels of 70% and greater. The wall temperature decreased from −6.7°C (20°F) to −14°C (6°F) within 50 min during the 90% relative humidity test (Fig. 31). The suction pressure at the inlet to the compressor, plotted in Fig. 32, shows nearly identical trends to those of the tube wall temperature because the saturation temperature in the two-phase region of the outdoor heat exchanger directly affects refrigerant pressure to the compressor.

7.3 Compressor Performance

The reduction of suction pressure yielded corresponding reductions in compressor inlet refrigerant density, which in turn yielded corresponding reductions in both refrigerant mass flow rate and compressor power consumption. Again using typical results observed at −1.1°C (30°F), the reduction of refrigerant density, characterized in Fig. 33, caused the refrigerant mass flow rate to decrease from 118 kg/h (260 lbm/h) to approximately 86.4 kg/h (190 lbm/h) for the 90% relative humidity test. The corresponding power consumption reduced from 2250 to approximately 1950 W. The 26% reduction in mass flow rate as compared to the 15% reduction in compressor power lowers the overall efficiency of the compressor and motor, as seen by the slope of the 80 and 90% humidity test curves of compressor efficiency in Fig. 34. The compressor efficiency for the 90% humidity condition dropped from 51.5 to 46% within 30 min of operating time.

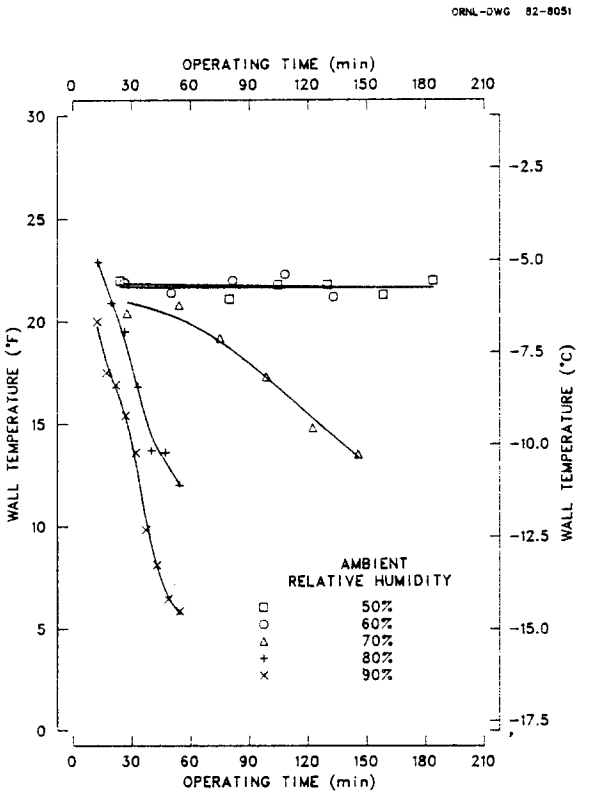

Fig. 31. Evaporator tube wall temperature observed for a −1.1°C (30°F) ambient temperature.

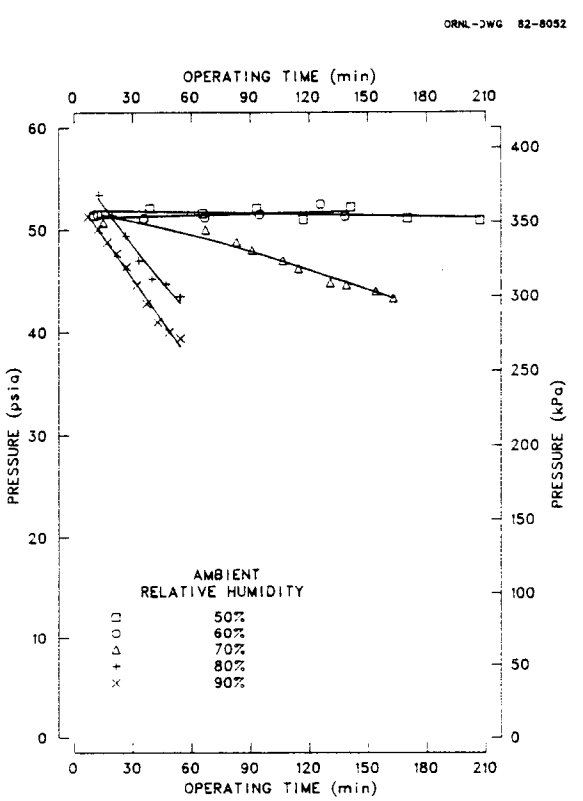

Fig. 32. Compressor suction pressure observed for a −1.1°C (30°F) ambient temperature.

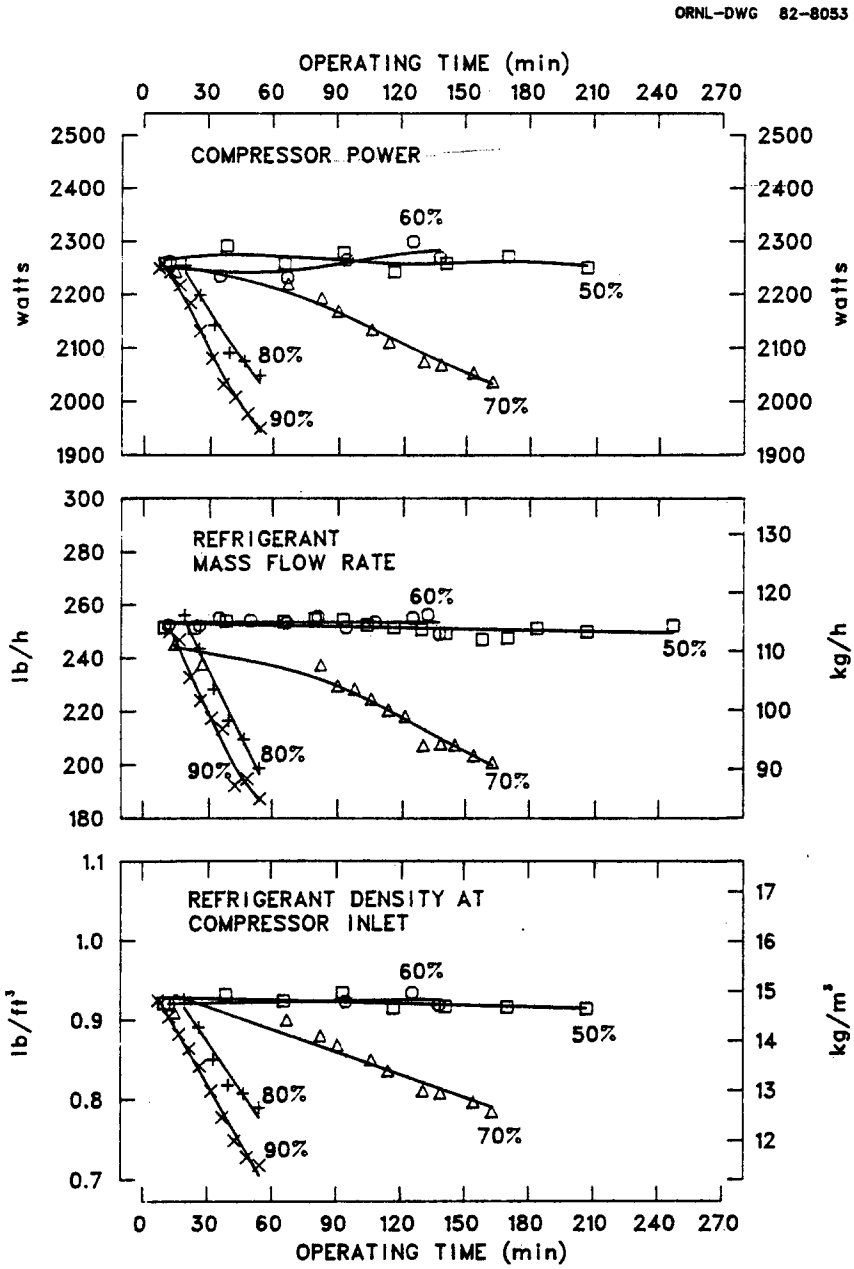

Fig. 33. Parametric study of heat pump performance observed at various outdoor relative humidity levels for an ambient temperature of −1.1°C (30°F).

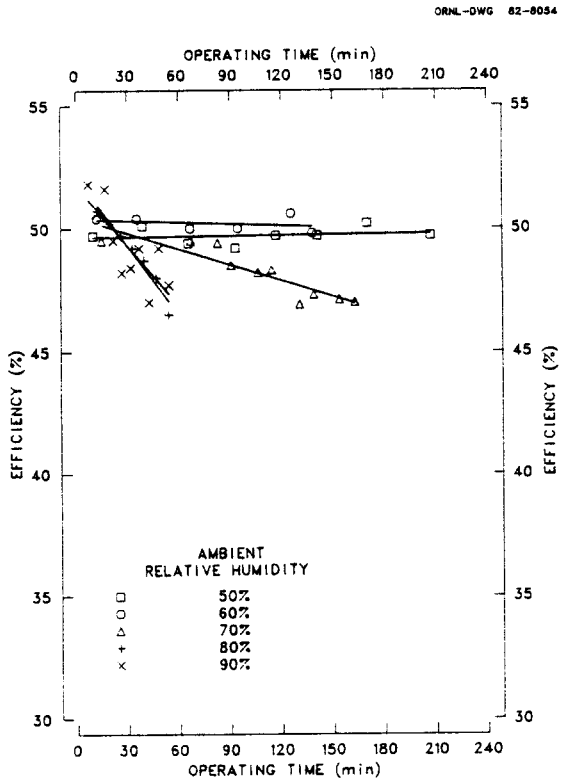

Fig. 34. Compressor efficiency observed at −1.1°C (30°F).

8. CUMULATIVE LOSSES DUE TO FROSTING OF THE OUTDOOR HEAT EXCHANGER

8.1 Introduction and Definition of Cumulative Frosting Losses

Cycling and defrosting losses are usually considered the major losses to efficient heat pump operation. However, few heat pump studies have investigated the losses incurred while frost is forming on the outdoor heat exchanger. These frosting losses, as discussed in Sects. 6 and 7, produce significant reductions in both COP and heating capacity. This reduction of performance from steady-state operation results in cumulative frosting losses, as represented by the shaded area in Fig. 35.

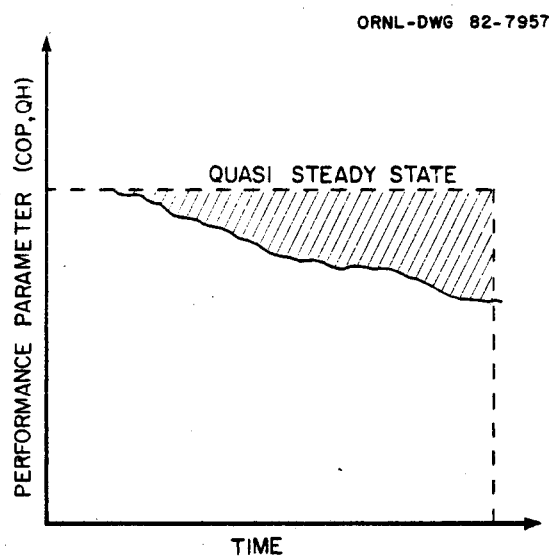

Fig. 35. Example of cumulative frosting loss.

Frosting loss coefficients, expressing the percentage loss in cumulative quasi-steady-state heat output and COP, were derived from experimental data for determination of the frosting loss as a function of temperature, relative humidity, and heat pump operating time. The loss coefficients can be used to determine the dynamic frosting performance of heat pumps having an outdoor heat exchanger of spine fin configuration. The heating output and COP under frosting conditions can be calculated using the following equations:

$$QH_{FROST} = \sum_{i=1}^{N} \dot{Q}H_{F_i}\tau_i = \dot{Q}H_{SS}(\tau)(1 - m_1/100) \ , \quad \text{in Btu} \ ,$$

$$\mathrm{COP}_{AVG} = \frac{\sum_{i=1}^{N}(\dot{Q}H_{F_i})\tau_i}{\sum_{i=1}^{N}(\dot{W}_{F_i})\tau_i} = \mathrm{COP}_{SS}(1 - m_2/100) \ ,$$

where

QH_{FROST} = cumulative heat output over given frosting period;
COP_{AVG} = average COP calculated over given frosting period;
$\dot{Q}H_{F_i}$ = average heating capacity under frosting conditions for time τ_i;
$\dot{W}_{F_i}$ = average power usage of heat pump under frosting conditions for time τ_i;
$\dot{Q}H_{SS}$ = steady-state heating capacity;
COP_{SS} = steady-state COP;

$\tau = \sum_{i=1}^{N} \tau_i$, in hours;

N = integral number of time increments;
m_1 = coefficient expressing the percentage loss in cumulative steady-state heat output;
m_2 = coefficient expressing the percentage loss in steady-state COP.

8.2 Correlation of Steady-State Performance as a Function of Temperature and Relative Humidity

Under low-temperature and high-humidity conditions, frosting usually commenced prior to data collection; therefore, quasi-steady-state performance had to be extrapolated to the start of each frosting test using the slope of the respective curves of observed COP and heating capacity test data. Steady-state, dry-coil performance could not be used as a base case for determination of frosting losses observed at a given temperature and relative humidity level because the increase of relative humidity slightly improved the steady-state performance of the unit.

The quasi-steady-state performance as a function of ambient temperature and relative humidity condition can be calculated using the following biquadratic equation:

$$F(T, \phi) = aT^2 + bT + c\phi^2 + d\phi + eT\phi + f ,$$

where

$F(T, \phi)$ = steady-state COP or heating capacity;
T = ambient dry-bulb temperature;
ϕ = ambient relative humidity.

The coefficients a through f, determined by two-dimensional, least squares fits to the data, are given by the following tabulation:

Coefficient	COP constants	Heating capacity constants
a	-4.5149×10^{-4}	-2.1996
b	5.2557×10^{-2}	4.3766×10^{2}
c	-2.129×10^{-4}	-1.7199
d	3.4162×10^{-2}	2.6156×10^{2}
e	3.42225×10^{-5}	2.0640
f	5.1365×10^{-5}	3.3736×10^{-5}

8.3 Cumulative Frosting Losses as a Function of Time, Temperature, and Relative Humidity

The losses in average COP and cumulative heat output are listed for 15-min intervals of heat pump run time in Tables 9 and 10. These losses yielded nominal 3 to 15% reductions in both heat output and COP over a 90-min interval for all ambient temperatures having relative humidities greater than 70%. The frosting losses are thus of the same order of magnitude as the cycling losses. Frosting losses were largest for tests conducted at 1.7 and −1.1°C (35 and 30°F), with relative humidities greater than 70% as listed in Tables 9 and 10.

Frosting losses of approximately 10% were observed in both COP and heating capacity for the 1.7°C (35°F), 80 and 90% tests (Figs. 36 and 37). Increasing the moisture content of the air augmented frost accumulations that yielded increased rates of performance degradation as depicted by the slopes of the 80 and 90% test curves plotted in Figs. 36 and 37. The observed nominal 10% reduction of both COP and heating capacity for the 80 and 90% humidity tests occurred within 60 min and was observed when the outdoor heat exchanger was 90% blocked with frost. Similar results were also observed at −6.7°C (20°F) when relative humidities were greater than 80%. With the outdoor coil nearly blocked with frost, a 10% loss in steady-state performance was observed within 75 min of operation.

Table 9. Loss of quasi-steady-state COP due to frosting

m_2, the percentage of quasi-steady-state COP degradation at time. See Sect. 8.1

Relative humidity (%)	Time (min)					
	15	30	45	60	75	90
Temperature = 4.4°C (40°F)						
60	0.00	0.00	0.20	1.19	2.10	2.31
70	0.05	0.21	0.53	1.08	1.93	3.02
80	0.38	1.56	1.77	2.04	2.15	2.17
90	0.00	0.00	0.80	0.41	0.73	0.88
Temperature = 1.7°C (35°F)						
60	0.37	0.70	0.96	1.13	1.28	1.47
70	0.00	0.00	0.62	2.52	4.07	5.78
80	3.30	4.97	7.62	10.09		
90	3.17	4.78	6.86			
Temperature = −1.1°C (30°F)						
60	0.12	0.23	0.35	0.45	0.52	0.56
70	2.39	3.76	4.30	4.37	4.30	4.53
80	3.76	6.67	9.93			
90	3.98	7.06	10.11			
Temperature = −6.7°C (20°F)						
70	0.00	0.31	0.35	1.03	1.03	1.33
80	0.00	0.39	0.93	1.04	1.14	1.45
90	2.61	3.90	5.49	7.12	8.54	
Temperature = −8.3° (17°F)						
70	0.00	0.13	0.21	0.83	1.41	1.69
90	2.44	3.38	5.13	7.04		

Table 10. Loss of quasi-steady-state capacity output due to frosting

m_1, the percentage of quasi-steady-state capacity degradation. See Sect. 8.1

Relative humidity (%)	Time (min)					
	15	30	45	60	75	90
Temperature = 4.4°C (40°F)						
60	0.00	0.00	0.46	1.39	2.23	2.57
70	0.11	0.38	0.87	1.71	2.98	4.63
80	0.69	1.43	1.84	2.33	2.61	2.92
90	0.03	0.14	0.42	0.92	1.38	1.67
Temperature = 1.7°C (35°F)						
60	0.50	0.97	1.39	1.69	1.95	2.25
70	0.00	0.69	2.59	4.93	7.03	9.23
80	3.87	7.27	11.38	15.12		
90	3.58	7.61	11.44			
Temperature = −1.1°C (30°F)						
60	0.10	0.26	0.46	0.66	0.80	0.83
70	0.37	0.55	0.59	0.60	0.71	1.23
80	4.23	8.39	13.10			
90	5.09	9.53	14.21			
Temperature = −6.7° (20°F)						
70	0.31	1.10	1.23	1.82	2.08	2.25
80	0.65	1.61	2.86	3.92	4.77	5.71
90	3.00	5.18	7.78	10.40	12.57	
Temperature = −8.3°C (17°F)						
70	0.00	0.22	0.33	0.93	1.51	1.82
90	2.96	4.35	6.68	9.16		

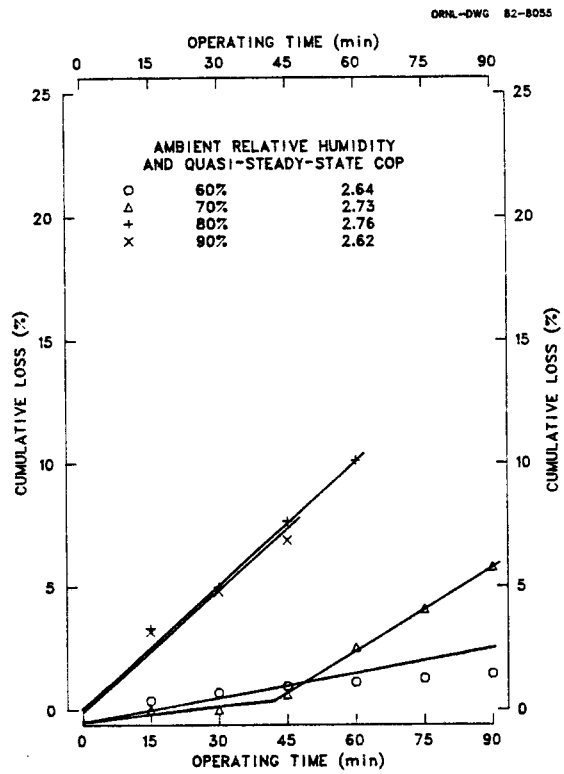

Fig. 36. COP frosting loss coefficients calculated for a 1.7°C (35°F) ambient temperature.

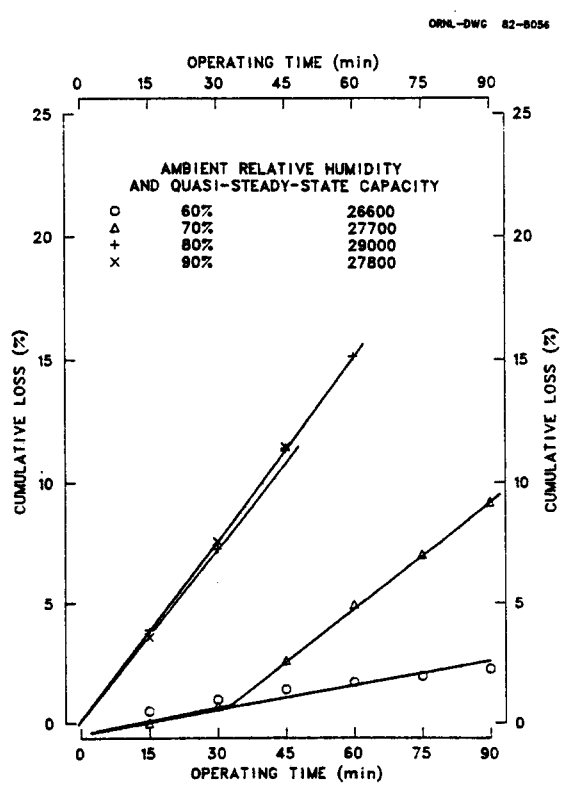

Fig. 37. Heating capacity frosting loss coefficients calculated for a 1.7°C (35°F) ambient temperature.

9. DEFROSTING OPERATION

Defrosting tests were conducted at the completion of each frosting test. Scans of compressor power and refrigerant temperatures and pressures were recorded every 8 s during the defrosting period. Refrigerant temperatures and pressures were measured at the inlet and outlet of the compressor shell, and refrigerant temperatures were measured at the defrosting initiation sensor. Typical defrosting tests for an ambient temperature of −1.1°C (30°F) and relative humidities of 70 through 90% are presented in Figs. 38 through 40.

9.1 Transient Operation During the Defrosting Cycle

The accumulation of frost on the outdoor heat exchanger lowers both the evaporator heat gain and the refrigerant superheat at the inlet to the compressor. The thermostatic expansion valve in the outdoor unit is designed to counteract this drop in refrigerant superheat at the inlet to the compressor by increasing the severity of the throttling process. The increased throttling action results in a continued backup of liquid refrigerant within the indoor heat exchanger until the commencement of the defrosting cycle. At the initiation of the defrosting cycle, the reversing valve is energized to cooling-mode operation. This process connects the compressor suction line directly to the two-phase mixture within the indoor heat exchanger. During this period, observations revealed a noticeable amount of two-phase refrigerant flowing back through the condenser hot gas line to the compressor. However, rapid scans of suction temperature and pressure at the compressor inlet revealed the observed two-phase flow to have flashed to gas before entering the compressor housing. The flashing of the refrigerant mixture is caused by the large drop in pressure from the indoor heat exchanger to the compressor inlet.

Using the defrosting cycle observed at −1.1°C (30°F) and 70% relative humidity (Fig. 38), a brief description of the defrosting cycle will be presented. Energizing the four-way reversing valve at the start of the defrosting operation results in an initial drop in head pressure and an initial jump in suction pressure due to the switching of refrigerant lines within the reversing valve. Within 32 s, the discharge pressure dropped from 1.3 to 0.81 MPa (188.5 to 117 psia) and the suction pressure increased from 314 to 721 KPa (45.6 to 104.7 psia). After these initial pertubations, both suction and head pressure decreased for a period of 50 s. Within this period, the refrigerant accumulated in the outdoor heat exchanger and the indoor heat exchanger became nearly evacuated of refrigerant. The head pressure then started to increase, allowing throttling within the indoor heat exchanger to begin. After 80 s of defrosting, there was a steady increase in suction pressure, head pressure, and also compressor power. This increase persisted until termination of the defrosting cycle, which, under normal conditions, would occur after the outlet outdoor heat exchanger temperature reached 13°C (55°F). At termination of the defrosting cycle, the compressor power and high- and low-side pressures again followed trends observed at the start of the cycle. However, a two-phase mixture of refrigerant was observed entering the compressor housing immediately following the defrosting cycle. The amount of liquid entering the compressor could not be determined and is assumed to be small because of the short interval over which it was observed.

The defrosting tests, following the frosting tests at −1.1°C (30°F) and 80 and 90% relative humidity, were for a longer period due to the increased amount of frost on the outdoor heat exchanger. The trends of compressor power and refrigerant temperature and pressure are nearly identical for the 70 through 90% defrosting runs plotted in Figs. 38, 39, and 40. The plot of

ORNL-DWG 82-8059

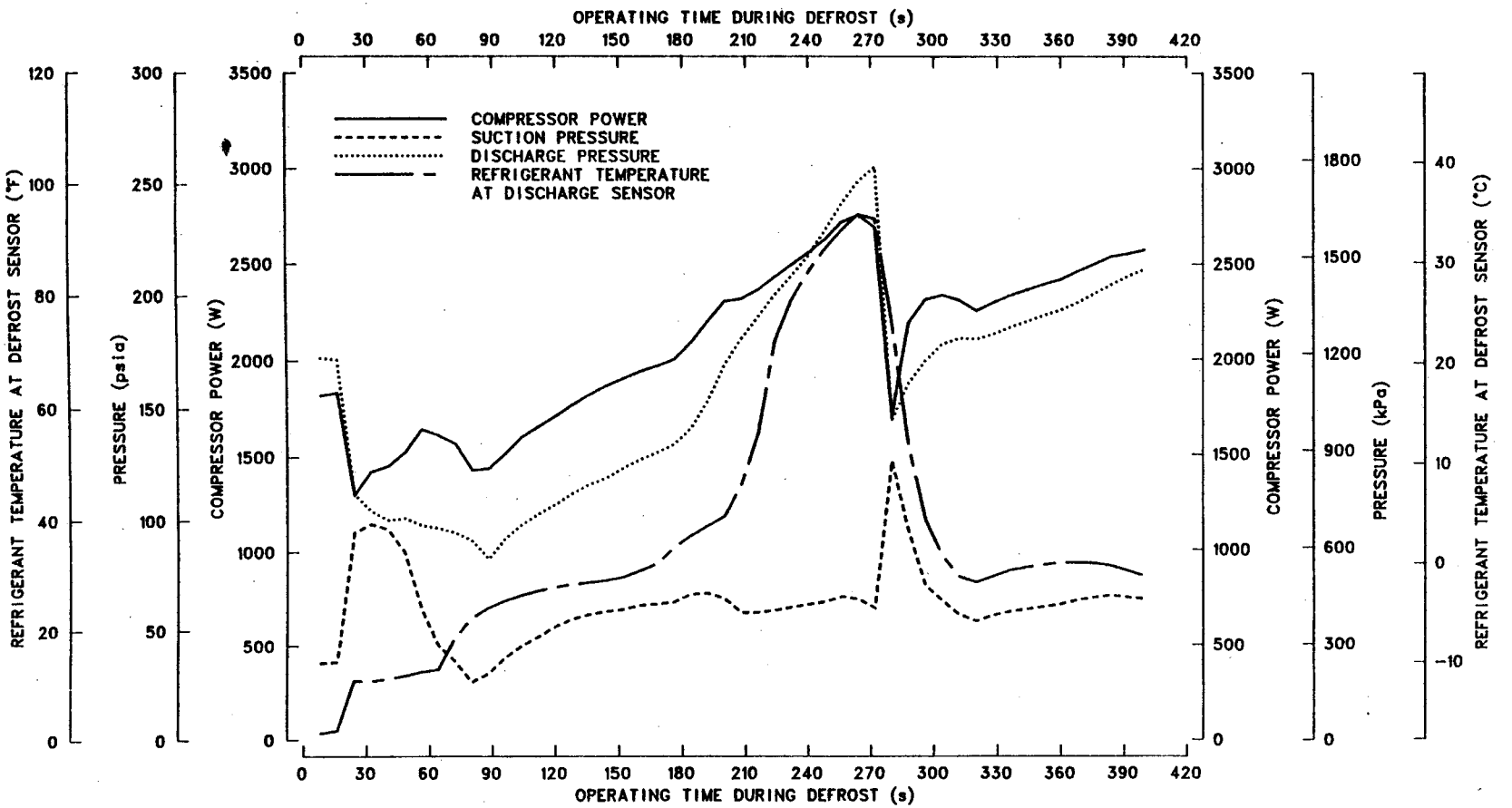

Fig. 38. Defrosting cycle observed following a −1.1°C (30°F), 70% relative humidity test.

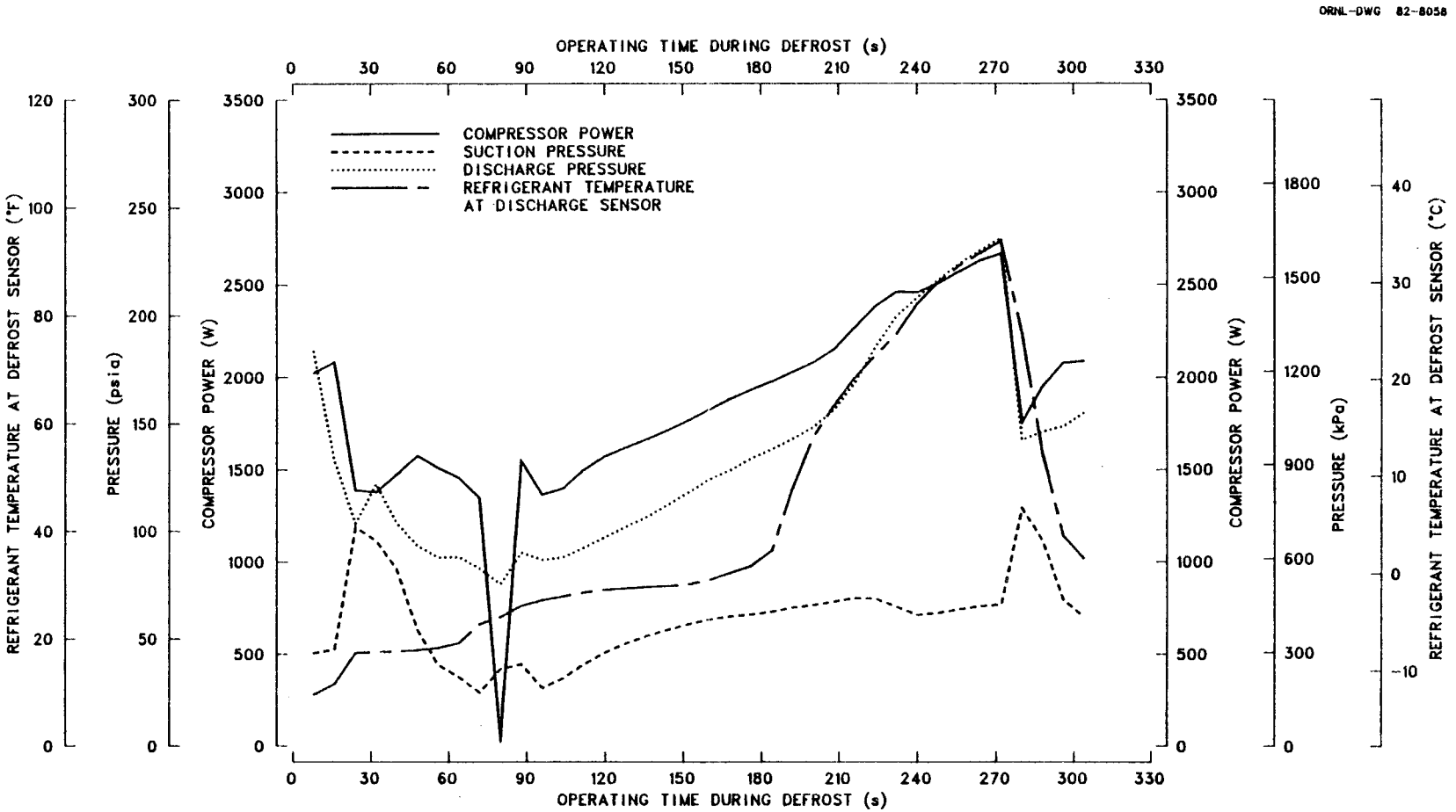

Fig. 39. Defrosting cycle observed after −1.1°C (30°F), 80% relative humidity test.

ORNL-DWG 82-8057

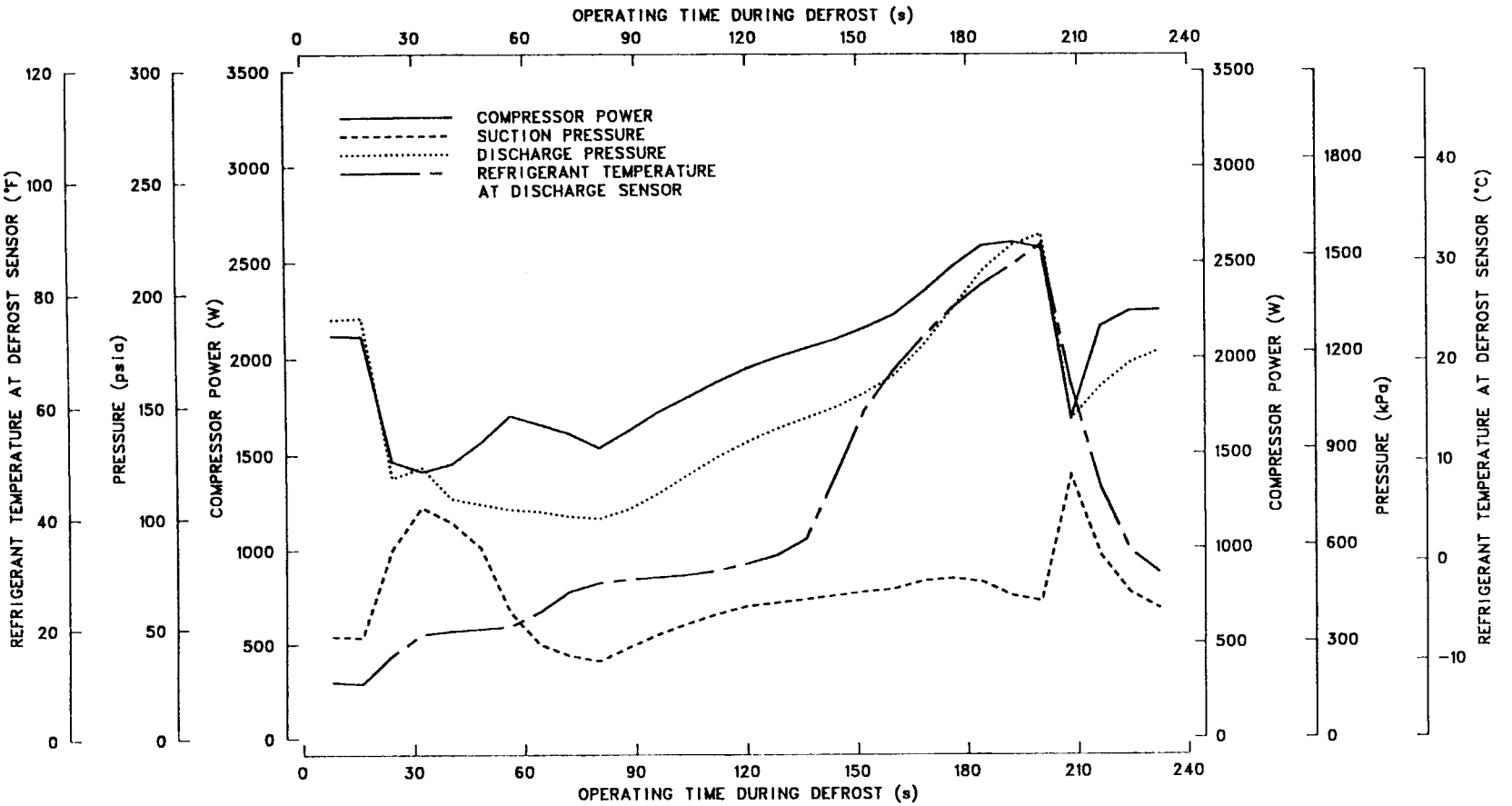

Fig. 40. Defrosting cycle observed after −1.1°C (30°F), 90% relative humidity test.

compressor power in Fig. 39 deviated from trends in compressor power plotted for the 70 and 90% humidity defrosting tests. An external high- and low-pressure cut-out disrupted the flow of power to the compressor because of a drop in suction pressure below 83.7 kPa (10 psig). The compressor was reenergized once the suction pressure became greater than 222 kPa (30 psig). This pressure cut-out switch was used to protect the compressor during the defrosting operation. Similar disruption of the compressor during the 90% humidity defrosting test was not observed.

9.2 Adequacy of Defrosting Termination

The time-and-temperature defrosting control for the heat pump tested terminates a defrosting cycle once the outlet refrigerant temperature from the outdoor heat exchanger exceeds 12.7°C (55°F). Observations of the outdoor heat exchanger during the defrosting cycle revealed the 12.7°C (55°F) termination temperature level to coincide well in time with the elimination of frost from the upper coil circuit of the outdoor heat exchanger. Under the severest of defrosting conditions [1.7°C (35°F), 90% relative humidity], the upper heat exchanger circuit was free of frost within 4 min of defrosting operation. Figures 38, 39, and 40 display the time required to adequately defrost the outdoor heat exchanger. However, the lower coil circuit usually had some frost remaining on the bottom helical windings of the coil even after the upper coil had completely defrosted. The remaining frost on the lower coil circuit occurred because the coldest refrigerant exits the bottom of each respective coil of the outdoor heat exchanger.

9.3 Energy Consumption of Defrosting Operation

Compressor power consumption, chilling of the indoor air, and use of auxiliary heat to temper the chilled air during defrosting operations all lower the COP of a heat pump. However, previous field studies by Groff and Reedy have shown these defrosting losses to be minimal.[8]

Experimental results reveal the loss in performance due to defrosting to be small for ambient temperatures of 4.4°C (40°F) or less and relative humidities less than 70%. The observed total losses in heating capacity and COP are listed in Table 11 for both frosting and defrosting. The losses in heating capacity and COP due to defrosting increased as relative humidity increased. However, as observed, the capacity losses due to frosting were larger than those losses due to chilling of the indoor air stream (Table 11). Increased relative humidity for a given temperature yields larger frosting and defrosting losses; frosting losses produce the predominant loss in capacity.

Defrosting produced a greater percentage reduction of COP than of heating capacity. An assumed 5 kW of auxiliary heat was included in the calculation of integrated COP. The additional power consumption, therefore, increased COP degradations over capacity degradations resulting from defrosting operations.

Table 11. Percentage drop in performance due to frosting/defrosting

Relative humidity (%)	Quasi steady state[a]		COP		ΔCOP[b]		ΔQH[b]	
	COP	QH (Btu/h)	fr[c]	fr/def[d]	fr (%)	def[e] (%)	fr (%)	def (%)
Temperature = 4.4°C (40°F)								
60	2.74	28,507	2.67	2.61	2.21	2.49	3.58	1.16
70	2.82	29,200	2.62	2.36	7.23	9.03	11.02	4.11
80	2.87	30,800	2.73	2.35	4.82	13.36	7.66	6.38
90	2.89	31,168	2.79	2.47	3.31	11.07	5.95	5.04
Temperature = 1.7°C (35°F)								
60	2.64	26,637	2.58	2.51	2.45	2.77	4.17	1.32
70	2.73	27,740	2.45	2.28	10.18	6.24	15.18	2.58
80	2.76	28,977	2.46	2.04	10.87	15.43	16.30	7.77
90	2.61	27,782	2.40	1.87	8.28	20.47	13.90	11.08
Temperature = −1.1°C (30°F)								
70	2.54	23,800	2.35	2.24	7.50	4.33	6.33	2.00
80	2.75	27,502	2.43	2.00	11.73	15.41	15.52	8.06
90	2.63	26,138	2.32	1.87	11.88	17.20	16.76	9.15
Temperature = −6.7°C (20°F)								
80	2.22	20,954	2.19	1.98	1.46	9.16	5.76	4.16
90	2.33	21,672	2.10	1.79	9.58	13.13	14.08	6.61

[a]quasi — Approximate (quasi-) steady-state COP and QH were extrapolated to the start of each frosting test and used as a base for the percentage breakdown of frosting and defrosting losses.

[b]Δ(COP,QH) — Percentage breakdown of frosting and defrosting based on quasi-steady-state COP and QH as determined from each temperature and relative humidity test run.

[c]fr — Performance measured over duration of respective test, not including defrosting operation.

[d]fr/def — Performance measured over duration of respective test, including defrosting operation.

[e]def — Performance during defrosting period including chilling of indoor air, 5-kW auxiliary heat, and defrosting power used by compressor and indoor fan.

10. ALTERNATIVE DEFROSTING LOGICS FOR AN OUTDOOR HEAT EXCHANGER OF SPINE FIN CONFIGURATION

10.1 Time and Temperature

A time-and-temperature defrosting control based on a 90-min cycle would not initiate a defrosting cycle soon enough to hinder heavy frost accumulations on the outdoor heat exchanger during extreme winter weather conditions. The results observed at ambient relative humidities of 80 and 90%, shown in Figs. 41 and 42, display the large reduction in COP due to the accumulation of frost at a time before defrosting would occur for the 90-min timed cycle. Tests conducted for both humidity levels with ambient temperatures of 1.7, −1.1, −6.7, and −8.3°C (35, 30, 20, and 17°F) showed 90% of the free-flow area of the outdoor heat exchanger blocked with frost prior to defrosting. In each case the frost had enveloped the spine fins and had formed a solid frost layer.

The above results reveal the need for a shorter time period between defrosting cycles for operating conditions having relative humidities greater than 80% in the frosting zone. A shorter cycle could easily reduce both frosting and defrosting losses; however, the shorter cycle would also increase the number of false, needless defrosting operations. Thus the shorter cycle could feasibly be more detrimental to efficient heat pump operation.

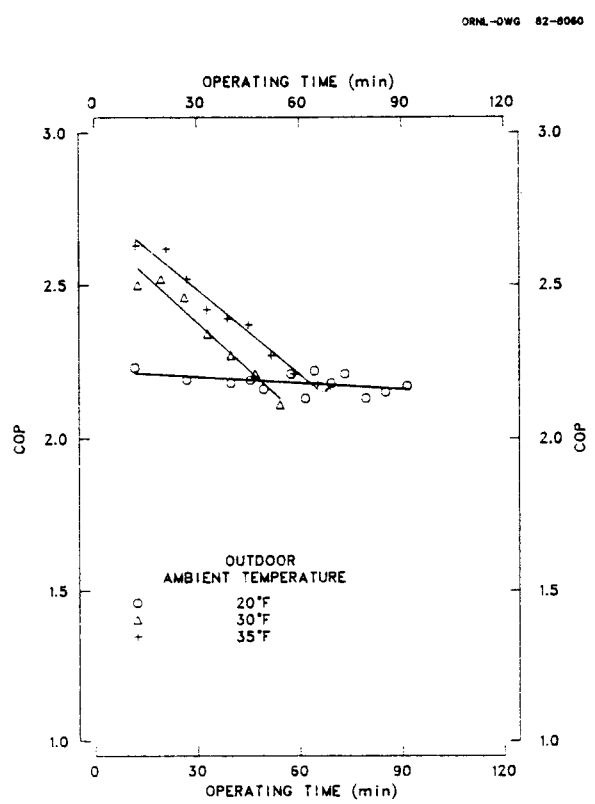

Fig. 41. COP observed at 80% relative humidity.

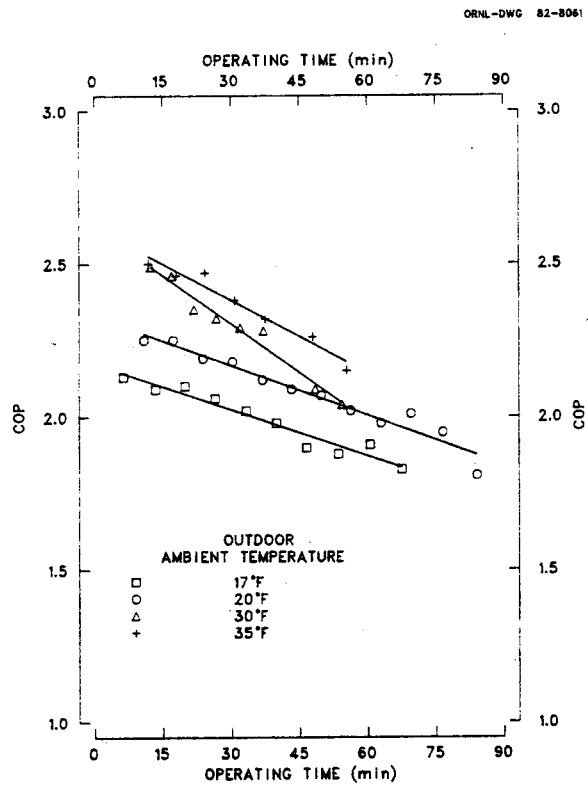

Fig. 42. COP observed at 90% relative humidity.

10.2 Demand Defrosting Sensors

A demand defrosting control would provide more timely initiation of the defrosting cycle and would reduce both frosting and defrosting losses. During extreme weather conditions conducive to heavy frost accumulations, the demand defrosting control would initiate the defrosting cycle prior to any extensive mixing of refrigerant and compressor oil, and would thus provide better protection for the compressor as compared to a time-and-temperature defrosting control.

10.2.1 Static Pressure Sensor

A defrosting sensor monitoring the static pressure drop across the outdoor heat exchanger would probably not be adaptable to this heat pump. A maximum pressure drop of 38 mm (0.15 in.) of water was observed across the air side of the one-row spine fin heat exchanger when it was almost totally blocked with frost. Under dry-coil conditions the pressure drop was approximately 1.3 mm (0.05 in.) of water. The low pressure drop across the coil would be too low for accurate sensing by currently available sensors.

10.2.2 Fan Power Consumption

Fan power consumption is a direct function of pressure drop across the outdoor coil. As frost accumulates on the outdoor heat exchanger, the increase in air pressure drop results in higher outdoor fan power consumption (Fig. 43).

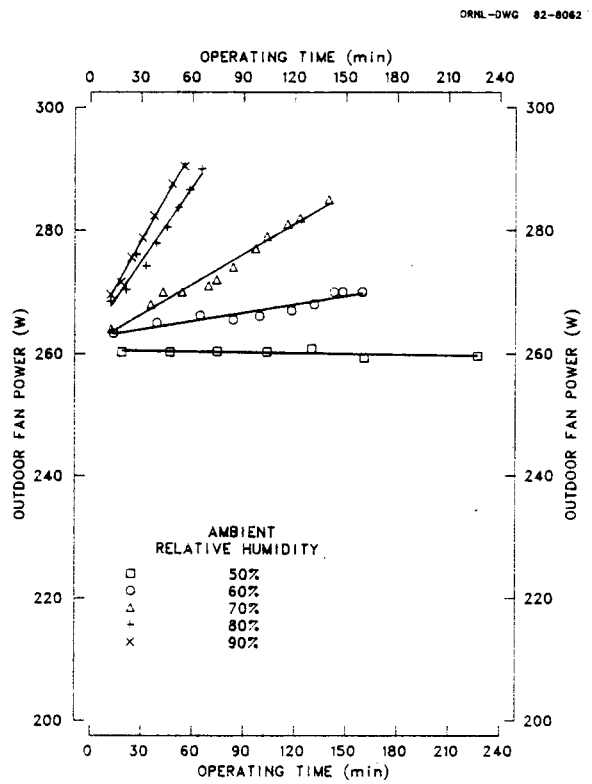

Fig. 43. Outdoor fan power measured at 1.7°C (35°F).

Steady-state outdoor fan power consumption was observed to be nominally 260 W. Under frosting conditions at an ambient temperature of 1.7°C (35°F), the power consumption was observed to increase by nominally 10% of steady-state consumption. The small percentage of change in power consumption, variations in residential line voltage, and the probable need for individual adjustment of a power defrosting sensor per heat pump would seem to hinder promotion of this defrosting scheme.

10.2.3 Temperature Difference across the Frost Layer

The temperature difference between the ambient air and the evaporator tube wall is currently used in some heat pump systems as a control signal for a defrosting initiation. Frost accumulations are sensed by the increase in the temperature difference between the ambient air and the evaporator tube wall, caused by the increase of air-side thermal resistance. Using a temperature difference of approximately 8.3 C° (15 F°), the time at which to initiate the defrosting operation would be sensed more accurately as compared to the time-and-temperature logic based on a 90-min cycle (Figs. 44 and 45). The temperature difference scheme might require an additional signal to safeguard against false defrosting operations. For instance, the refrigerant temperature at the inlet to the outdoor heat exchanger could be used as a second conditional requirement for initiation of the defrosting cycle.

The temperature gradient (Figs. 44 and 45) observed at 1.7 and −1.1°C (35 and 30°F) reveals the advantage of the 8.3 C° (15 F°) temperature gradient in predicting the proper initiation of a defrosting cycle.

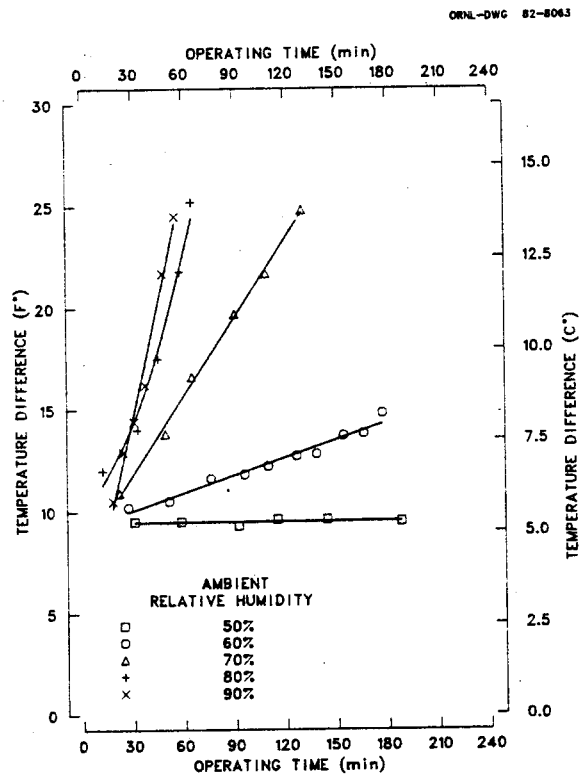

Fig. 44. Temperature difference between the ambient air and the evaporator tube wall observed at 1.7°C (35°F).

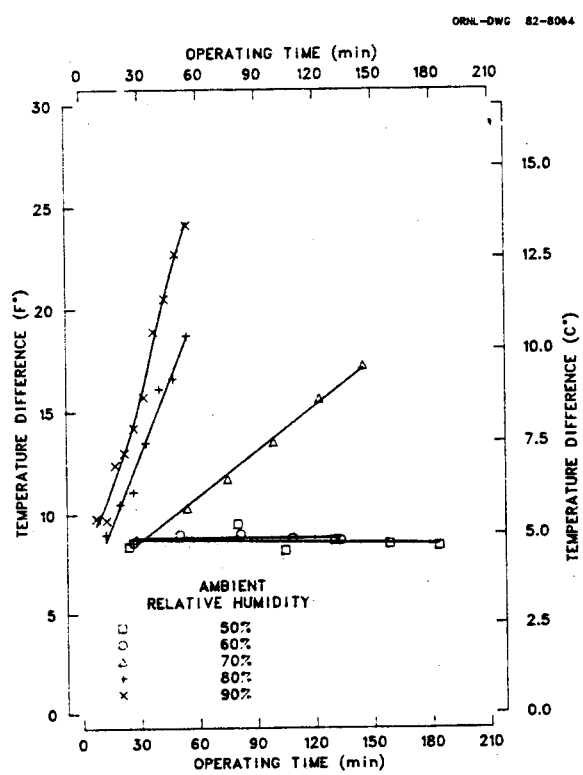

Fig. 45. Temperature difference between the ambient air and the evaporator tube wall observed at −1.1°C (30°F).

11. CHARGE SENSITIVITY TEST

Charging tests were performed to observe the sensitivity of the system to variations of refrigerant charge during heating-mode operation. The tests revealed an improvement in stability of the thermostatic expansion valve used during the heating mode for refrigerant charges greater than the nameplate charge. Stable operation of the valve was observed for a refrigerant charge of 5.24 kg (11 lb 9 oz), which is 0.51 kg (1 lb 2 oz) more than the nameplate charge. However, unstable control was again observed at the higher charge (Fig. 46) for ambient temperatures less than 8.3°C (47°F).

The charging test results show the compressor efficiency to be unaffected by the variation of refrigerant charge. The compressor efficiency at 8.3°C (47°F) was nominally 53.5% for charges ranging from 0.45 kg (1 lb) less than the design charge to 0.68 kg (1.5 lb) more than the design charge.

11.1 Performance as a Function of Refrigerant Charge

The addition of refrigerant charge caused a slight increase in the system COP from 2.84 to 2.92, a 2.8% increase from the COP at the minimum charge level (Fig. 47). The heating capacity

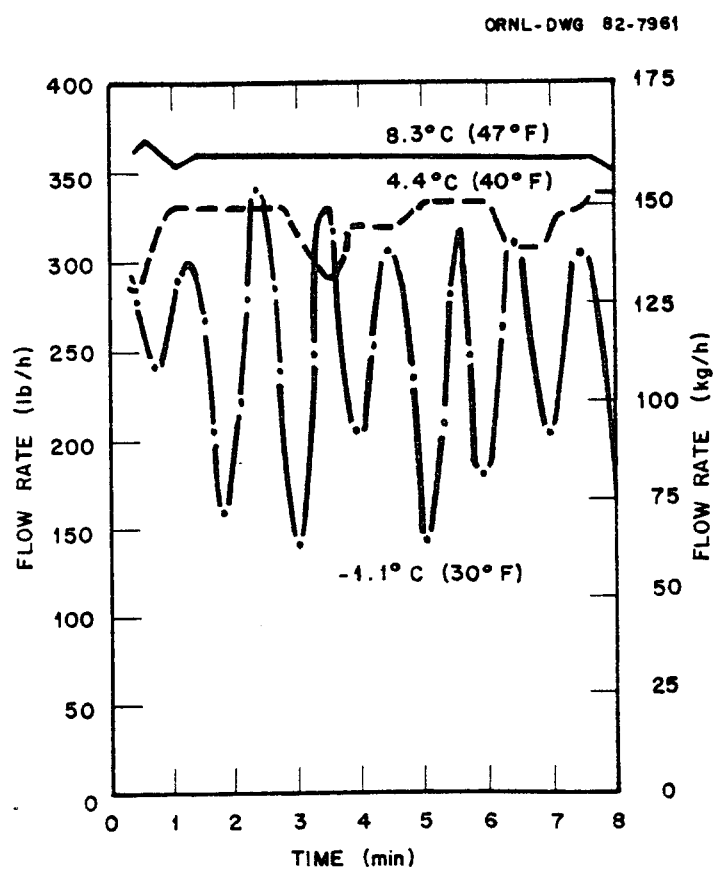

Fig. 46. Refrigerant flow rate at refrigerant charge of 5.24 kg (11 lb 9 oz).

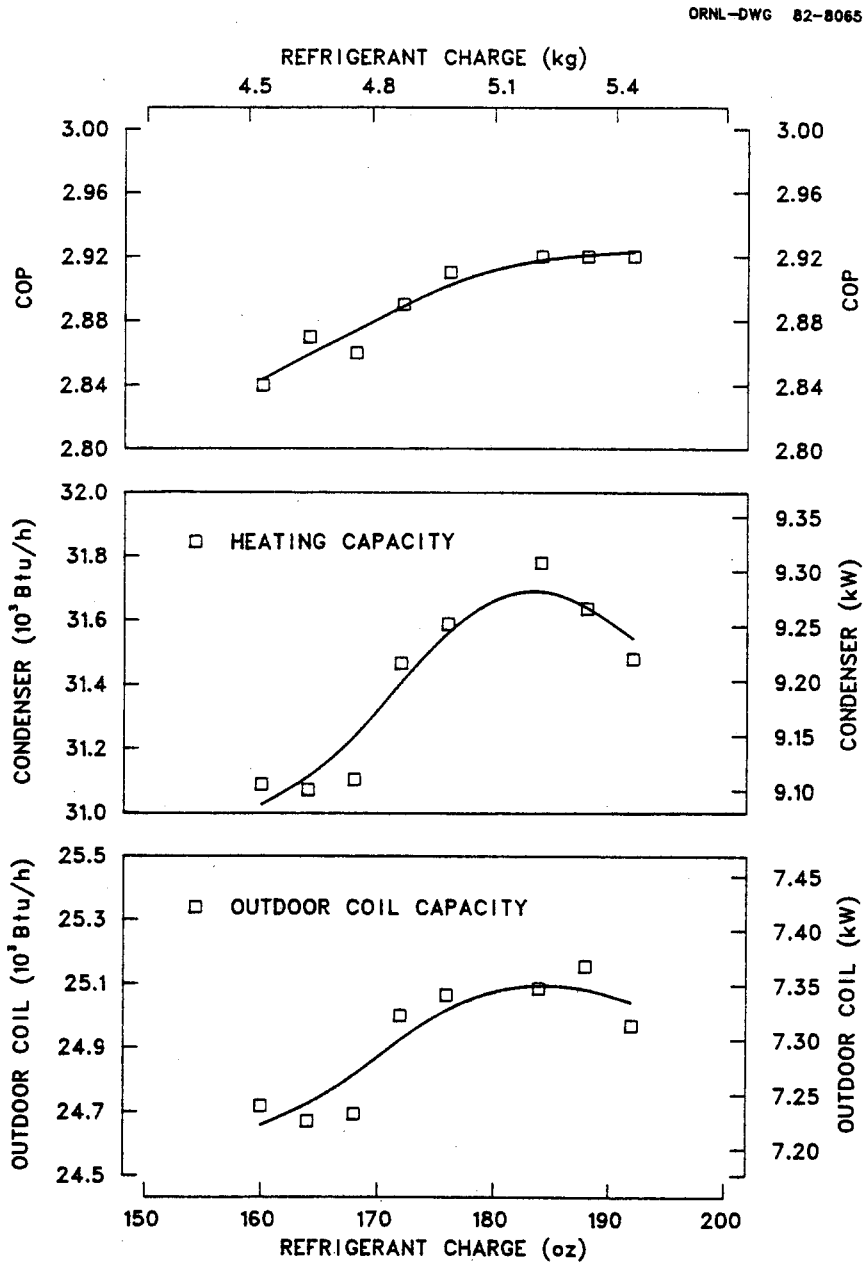

Fig. 47. Influence of refrigerant charge on system performance observed at an ambient temperature of 8.3°C (47°F).

and the outdoor heat exchanger capacity both increased slightly, up to a maximum level at a refrigerant charge of 5.21 kg (11.5 lb). Both condenser and outdoor heat exchanger capacity were 2% greater than the capacities observed at the design charge of 4.73 kg (10 lb 7 oz); see Fig. 47.

11.2 Sensitivity of System Pressures and Temperatures to Amount of Charge

The variation of refrigerant charge had little effect upon refrigerant temperatures and pressures throughout the system (Figs. 48 and 49). The high- and low-side pressures at the compressor were

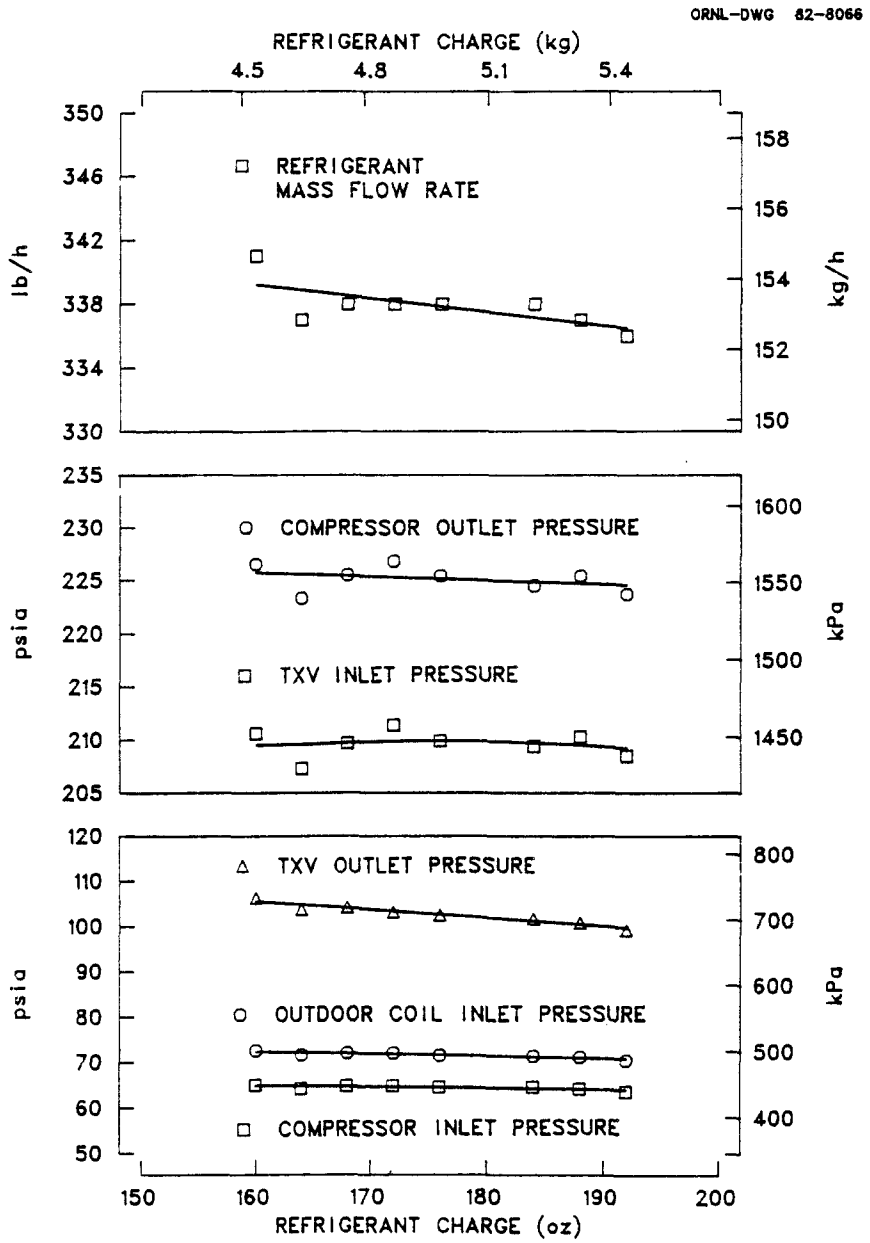

Fig. 48. Refrigerant pressures as influenced by charge variation observed at an ambient temperature of 8.3°C (47°F).

unaffected by variations of refrigerant charge ranging from 0.45 kg (1 lb) less than the design charge to 0.68 kg (1.5 lb) more than the design charge. However, the refrigerant temperature at the inlet to the expansion valve within the outdoor unit decreased as the refrigerant charge was increased, dropping from 31.6°C (89°F) at a charge of 4.3 kg (9.5 lb) to 26.1°C (79°F) at a charge of 5.44 kg (12 lb) (Fig. 49). This temperature drop and increased refrigerant subcooling within the liquid line is related to the backup of liquid refrigerant within the indoor heat exchanger. During heating-mode operation, the subcooling increases as the amount of refrigerant charge is

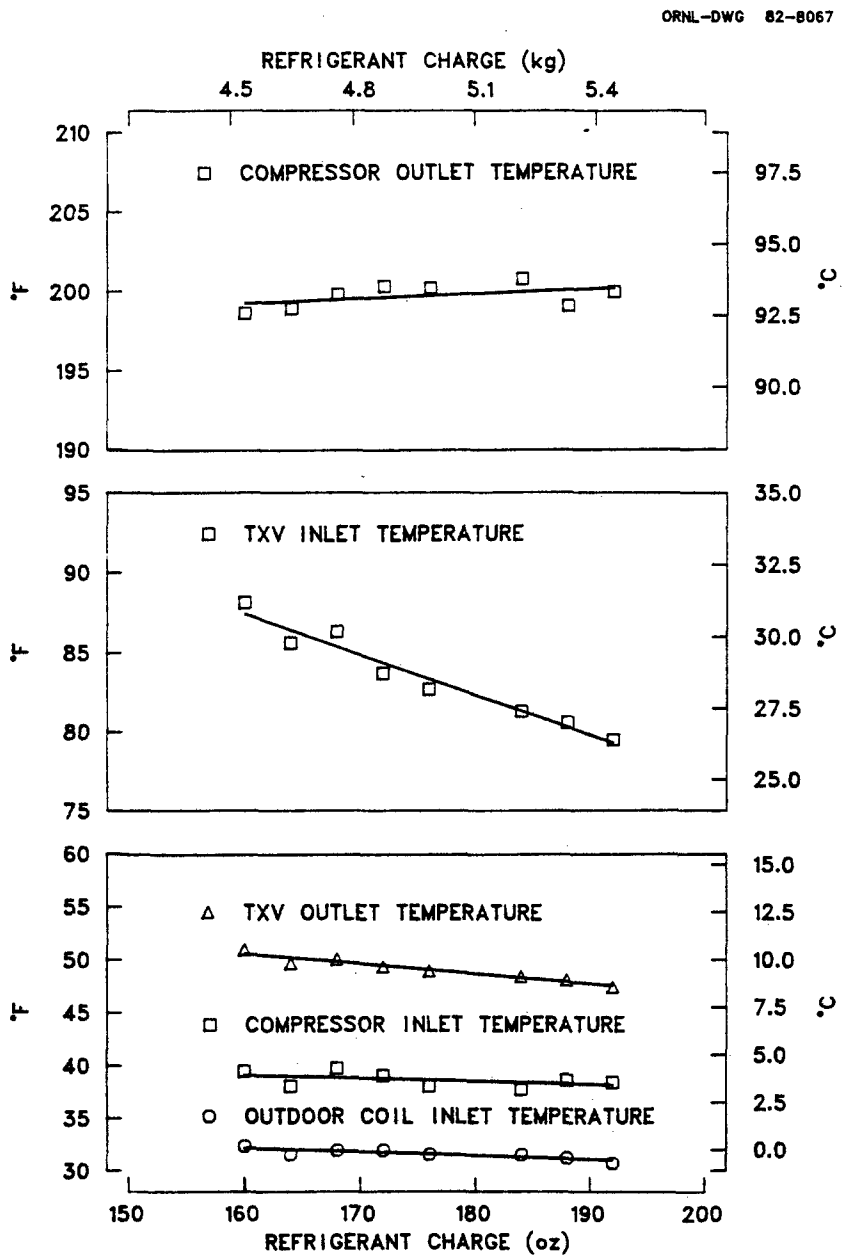

Fig. 49. Refrigerant temperatures as influenced by charge variation observed at an ambient temperature of 8.3°C (47°F).

increased. The backup of liquid refrigerant as refrigerant charge is increased produces large heat flows from refrigerant to air and thereby results in a lowering of refrigerant temperature at the condenser exit.

11.3 Thermostatic Expansion Valve Instability

Instantaneous values of refrigerant mass flow rate and compressor inlet superheat were also observed at each charge level. At the design charge of 4.73 kg (10 lb 7 oz), the refrigerant mass flow rate fluctuated from 99.7 to 174.6 kg/h (220 to 385 lb/h), and the compressor inlet superheat

varied from saturated vapor conditions to 10°C (18°F) of superheat (Fig. 50). The addition of 0.45 kg (1 lb) of refrigerant charge eliminated the hunting of the expansion valve, as typified by the constancy of the refrigerant mass flow rate illustrated in Fig. 50. Although the instantaneous superheat varied, the fluctuation of superheat is less pronounced than the superheat variation at the design charge of 4.73 kg (10 lb 7 oz). The elimination of the expansion valve hunting and compressor inlet superheat fluctuation is related to the matching of the expansion valve and outdoor heat exchanger capacity. As the refrigerant charge was increased to 0.45 kg (1 lb) greater than the design charge, the heat gained by the outdoor heat exchanger increased (Fig. 47). The increased outdoor heat exchanger capacity matched the capacity of the thermostatic expansion valve, thereby enabling the system to operate under a more stable condition. At the design charge level, the capacity of the outdoor heat exchanger was not matched to the capacity of the expansion valve, resulting in unstable or cyclic operation of the expansion valve. These results correlate well with the earlier charging test results in which the expansion valve hunting was eliminated at a refrigerant charge of 0.51 kg (1 lb 2 oz) over the design charge. They also agree well with the observations made by Huelle in his studies of thermostatic expansion valves.[9]

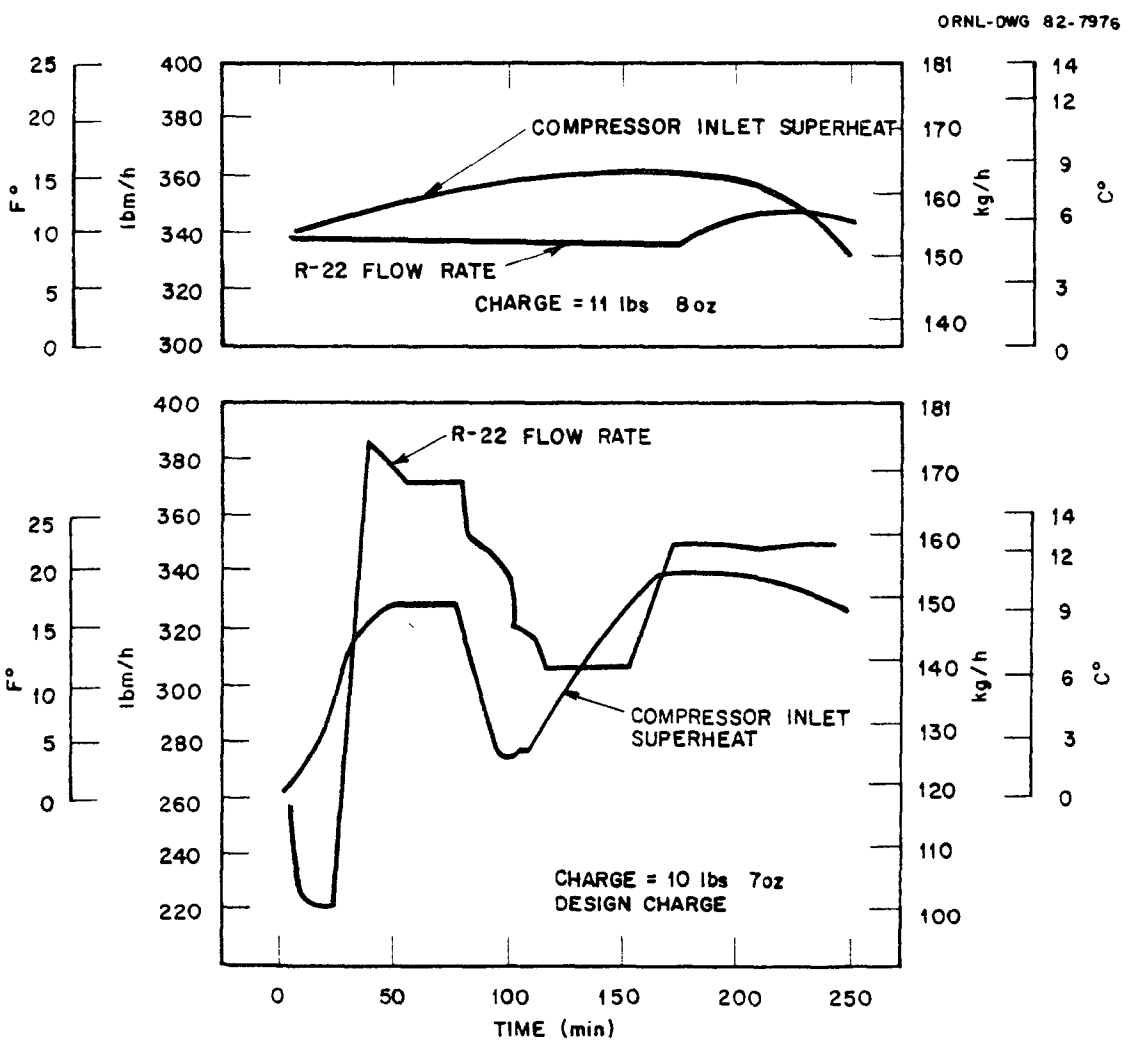

Fig. 50. Thermostatic expansion valve stability as influenced by charge variation observed at 8.3°C (47°F) and 55% relative humidity outdoor ambient conditions.

REFERENCES

1. A. A. Domingorena, *Performance Evaluation of a Low-First-Cost, Three-Ton, Air-to-Air Heat Pump in the Heating Mode*, ORNL/CON-18, Oak Ridge, Tenn. (October 1978).

2. A. A. Domingorena, *Performance Evaluation of a Selected Three-Ton Air-to-Air Heat Pump in the Heating Mode,* ORNL/CON-34, Oak Ridge, Tenn. (January 1980).

3. W. A. Miller, *The Influence of Ambient Temperature and Relative Humidity on the Heating Mode Performance of a High-Efficiency Air-to-Air Heat Pump,* M.S. thesis, Dept. of Mechanical Engineering, University of Tennessee, Knoxville, 1980.

4. C. F. Sepsy and W. O. Winchell, *A Study of Frost Removal from Extended Heat Exchangers,* Edison Electric Institute Report RP82 (1971).

5. F. C. McQuiston and J. D. Parker, *Heating, Ventilating, and Air Conditioning,* Wiley and Sons, New York, 1977.

6. N. Yamakawa, N. Takahashi, and S. Ohtani, "Forced Convection Heat and Mass Transfer under Frost Conditions," *Jpn. J. Heat Transfer* **4**(2) (1972).

7. W. H. Parken, R. W. Beausoliel, and G. E. Kelly, "Factors Affecting the Performance of a Residential Air-to-Air Heat Pump," *ASHRAE Trans.* **83**(1): 839–49 (1977).

8. G. C. Groff and W. R. Reedy, "Investigation of Heat Pump Performance in the Northern Climate through Field Monitoring and Computer Simulation," *ASHRAE Trans.* **84**(1) (1978).

9. Z. R. Huelle, "The MSS LINE — A New Approach to the Hunting Problem," *ASHRAE J.* **14**(10): 43–46 (1972).

APPENDIXES

APPENDIX A.
EXPERIMENTAL DATA

Tabulation of heating-mode performance data observed during steady-state nonfrosting conditions is presented in Table A.1. Frosting performance data observed for an outdoor ambient temperature of 1.7°C (35°F) is tabulated as a function of run time in Tables A.2 through A.5. The evaporator wall temperatures were monitored at times other than those listed in Tables A.2 through A.5, and the tabulated wall temperatures are interpolated values calculated from least squares fits of the data. The location of refrigerant temperature and pressure sensors is shown in Fig. 5 of the main text.

Table A.1. Performance data from steady-state dry-coil tests

DATE, 1979	RELATIVE HUMIDITY, %	AIR TEMPERATURES, F: OUTDOOR COIL IN	OUTDOOR COIL OUT	INDOOR COIL IN	INDOOR COIL OUT	REFRIGERANT TEMPERATURES, F: COMPRESSOR IN	COMPRESSOR OUT	REVERSING VALVE OUT	CONDENSER IN	CONDENSER OUT	OUTDOOR TXV IN	OUTDOOR TXV OUT	EVAPORATOR IN	EVAPORATOR OUT	AVERAGE EVAPORATOR WALL	REFRIGERANT PRESSURES, PSIA: COMPRESSOR IN	COMPRESSOR OUT	OUTDOOR TXV IN	OUTDOOR TXV OUT	EVAPORATOR IN	AIR FLOW RATES: OUTDOOR CFM	INDOOR LBM/HR	REFRIGERANT FLOW RATE, LBM/HR	OU
11/8	60.6	47.0	37.8	70.0	93.8	38.7	199.2	185.7	175.1	93.9	79.5	46.8	30.0	32.9	32.7	63.8	221.9	208.6	100.0	69.6	2516	5276	334.1	
12/9	49.9	38.5	31.4	70.9	91.9	32.5	201.5	186.4	173.7	90.7	76.6	41.3	25.2	23.7	28.5	57.9	213.1	200.6	89.7	63.7	2792	5380	291.9	
12/18	49.7	34.3	28.2	69.7	89.4	30.1	202.6	186.3	171.9	87.9	73.1	37.0	21.7	22.5	25.0	54.2	204.0	192.2	83.3	59.6	2795	5361	271.0	
12/19	48.4	30.5	25.3	69.9	88.6	27.3	204.6	187.1	171.3	87.4	71.3	33.7	18.9	19.8	22.0	51.4	199.4	188.5	79.0	56.5	2789	5381	251.4	
12/19	61.0	19.8	16.7	69.5	85.1	21.3	210.1	189.6	168.2	84.2	63.5	24.0	11.0	12.5	13.3	44.5	185.8	176.7	65.9	48.4	2720	5404	203.7	
12/20	61.7	17.1	14.7	70.3	84.5	19.6	212.4	190.8	167.3	84.2	61.3	21.4	8.8	10.2	11.3	42.7	183.6	175.3	62.9	46.3	2795	5437	191.5	

	POWER INPUT, W		HEATING CAPACITY, BTU/HR		COP		
DOOR AN	COMPRESSOR	TOTAL	REFRIG-ERANT METHOD	AIR METHOD	REFRIG-ERANT METHOD	AIR METHOD	COMPRESSOR ISENTROPIC EFFICIENCY
55	2564	3157	31253	30134	2.90	2.80	0.535
60	2416	3013	27750	27114	2.70	2.64	0.516
59	2322	2918	26069	25345	2.62	2.55	0.508
62	2258	2857	24317	24151	2.49	2.48	0.497
68	2053	2657	20094	20234	2.22	2.23	0.467
69	1996	2602	18941	18528	2.13	2.09	0.461

Table A.2. Test data observed for frosting ambient conditions of 1.7°C (35°F) and 60% relative humidity

RUN TIME, MIN	RELATIVE HUMIDITY, %	AIR TEMPERATURES, F: OUTDOOR COIL IN	OUTDOOR COIL OUT	INDOOR COIL IN	INDOOR COIL OUT	REFRIGERANT TEMPERATURES, F: COMPRESSOR IN	COMPRESSOR OUT	REVERSING VALVE OUT	CONDENSER IN	CONDENSER OUT	OUTDOOR TXV IN	OUTDOOR TXV OUT	EVAPORATOR IN	EVAPORATOR OUT	AVERAGE EVAPORATOR WALL	REFRIGERANT PRESSURES, PSIA: COMPRESSOR IN	COMPRESSOR OUT	OUTDOOR TXV IN	OUTDOOR TXV OUT	EVAPORATOR IN	AIR FLOW RATES: OUTDOOR CFM	INDOOR LBM/HR	REFRIGERANT FLOW RATE, LBM/HR
13.8	61.9	34.6	28.8	69.5	89.6	30.7	200.6	184.4	170.4	86.6	71.5	33.8	21.6	23.0	24.9	54.2	204.2	193.4	82.7	59.5	2762	5369	274.4
39.3	59.1	34.8	28.9	69.7	89.5	29.2	203.3	186.7	172.0	86.4	71.2	36.2	21.0	22.3	24.3	53.5	203.6	192.9	81.6	58.8	2691	5370	269.1
64.6	60.3	34.6	28.8	69.8	89.4	28.0	203.9	187.0	172.0	86.2	70.9	35.7	20.5	22.1	23.6	53.1	203.0	192.4	80.9	58.3	2607	5371	267.3
84.0	60.0	34.7	28.9	70.5	89.8	26.6	203.8	186.8	171.9	86.8	71.1	35.4	20.0	22.1	22.9	52.7	203.9	193.3	80.4	57.7	2413	5367	265.1
99.4	60.3	34.4	28.5	70.1	89.5	26.5	202.7	185.7	170.8	86.4	70.7	34.8	20.6	21.8	22.5	52.3	202.8	192.2	79.8	58.4	2381	5370	263.4
118.2	60.4	34.3	28.4	69.9	89.0	26.4	202.3	185.2	170.3	86.0	70.2	34.5	19.1	21.6	21.8	52.0	201.4	191.0	79.2	56.7	2319	5375	263.2
131.5	60.0	34.2	28.3	69.8	88.8	25.5	202.0	184.8	169.8	85.8	69.9	34.3	18.7	21.1	21.3	51.6	200.6	190.1	78.8	56.3	2274	5377	262.8
143.0	59.3	34.1	28.0	69.7	88.5	24.8	201.7	184.4	169.2	85.5	69.4	33.6	18.1	20.4	20.8	51.1	199.5	189.2	77.6	55.7	2193	5380	256.5
148.1	60.1	34.2	28.2	69.4	88.3	25.3	201.8	184.5	169.3	85.4	69.3	33.6	18.2	20.6	20.7	51.2	199.1	188.8	77.8	55.8	2193	5382	257.1
159.6	59.5	34.3	28.2	68.7	87.4	24.9	201.1	183.8	168.4	84.6	68.5	33.5	17.7	20.4	20.2	50.7	196.6	186.3	77.5	55.2	2154	5390	257.9
172.6	59.5	33.8	27.9	68.3	86.8	23.6	199.9	182.3	167.0	84.0	67.7	32.7	16.9	19.7	19.7	50.0	194.5	184.5	76.2	54.4	2095	5396	252.9
187.1	60.4	34.6	28.6	72.7	90.5	24.5	202.3	184.3	168.9	87.8	69.9	33.2	17.2	20.0	19.1	50.4	204.5	194.5	76.6	54.7	1957	5360	249.9

POWER INPUT, W			HEATING CAPACITY, BTU/HR		COP		
OUTDOOR FAN	COMPRESSOR	TOTAL	REFRIG-ERANT METHOD	AIR METHOD	REFRIG-ERANT METHOD	AIR METHOD	COMPRESSOR ISENTROPIC EFFICIENCY
263	2345	2945	26407	25899	2.63	2.58	0.510
265	2327	2929	26027	25517	2.60	2.55	0.506
266	2316	2920	25883	25264	2.60	2.54	0.506
266	2308	2911	25617	24860	2.58	2.50	0.507
266	2301	2904	25445	25002	2.57	2.52	0.509
267	2289	2893	25446	24638	2.58	2.50	0.509
268	2276	2881	25407	24518	2.58	2.49	0.510
270	2263	2870	24828	24273	2.54	2.48	0.503
270	2264	2871	24900	24411	2.54	2.49	0.505
270	2244	2851	25014	24192	2.57	2.49	0.509
270	2223	2830	24547	23960	2.54	2.48	0.503
269	2261	2867	23983	22898	2.45	2.34	0.507

Table A.3. Test data observed for frosting ambient conditions of 1.7°C (35°F) and 70%

		AIR TEMPERATURES, F				REFRIGERANT TEMPERATURES, F										REFRIGERANT PRESSURES, PSIA				
		OUTDOOR COIL		INDOOR COIL		COMPRESSOR		REVERSING VALVE	CONDENSER		OUTDOOR TXV		EVAPORATOR		AVERAGE EVAPORATOR	COMPRESSOR		OUTDOOR TXV		EVAPORATOR
RUN TIME, MIN	RELATIVE HUMIDITY, %	IN	OUT	IN	OUT	IN	OUT	OUT	IN	OUT	IN	OUT	IN	OUT	WALL	IN	OUT	IN	OUT	IN
12.3	69.6	34.9	29.3	66.9	87.3	31.1	199.3	183.8	169.8	86.4	71.9	37.3	21.9	23.5	25.1	54.7	198.2	187.5	84.8	59.9
35.6	69.8	35.2	29.4	65.8	85.5	30.0	199.5	183.4	168.7	84.3	69.4	35.5	20.0	22.1	22.8	53.1	193.0	182.7	81.9	57.7
42.8	69.1	35.4	29.7	68.7	87.1	27.5	201.4	184.4	169.0	86.0	69.6	34.5	18.4	22.0	22.1	51.8	197.0	187.1	80.2	56.0
54.0	69.8	35.5	30.0	69.4	87.4	25.2	202.4	185.0	169.3	86.6	69.5	33.8	17.1	21.3	20.9	50.8	196.9	187.1	78.8	54.6
58.7	69.9	35.7	30.1	69.4	87.2	24.4	202.3	184.5	168.8	86.4	69.1	33.0	16.4	20.8	20.4	50.2	196.1	186.5	77.4	53.9
69.6	70.2	36.1	30.3	69.5	86.7	23.4	201.8	183.7	167.7	86.1	68.6	32.0	15.0	19.9	19.1	48.8	194.2	184.7	75.7	52.4
74.3	69.6	35.7	30.1	69.3	86.3	22.6	201.0	182.7	166.6	85.7	68.0	31.2	14.3	19.1	18.6	48.1	192.7	183.4	74.5	51.7
84.0	70.4	35.9	30.2	70.4	86.7	22.2	200.1	181.4	165.2	86.1	67.6	30.5	13.7	18.5	17.4	47.6	194.0	184.8	72.9	51.1
97.0	70.6	36.0	30.4	70.0	86.0	21.7	199.8	180.7	163.9	85.5	67.5	29.9	12.5	17.8	15.7	46.6	191.4	182.3	71.8	49.9
103.7	69.6	36.0	30.4	69.6	85.5	21.1	199.4	180.2	163.2	85.0	66.7	29.2	11.6	17.1	14.8	45.7	189.5	180.3	70.7	49.0
115.8	69.2	36.2	30.6	72.2	87.1	19.8	199.3	179.5	162.3	86.6	66.9	28.1	10.5	15.7	13.2	44.8	193.6	185.0	68.6	47.9
123.0	70.3	36.0	30.6	69.3	84.7	19.0	198.9	179.0	161.3	84.5	66.0	27.4	9.5	15.2	12.3	44.0	186.5	177.9	67.3	47.0
139.8	69.2	36.0	30.5	68.9	83.2	17.0	196.2	175.7	157.4	82.8	64.2	24.8	6.9	13.5	9.8	41.9	182.0	173.8	64.2	44.6

relative humidity

R FLOW RATES			POWER INPUT, W			HEATING CAPACITY, BTU/HR		COP		
DOOR FM	INDOOR LBM/HR	REFRIG-ERANT FLOW RATE, LBM/HR	OUTDOOR FAN	COMPRESSOR	TOTAL	REFRIG-ERANT METHOD	AIR METHOD	REFRIG-ERANT METHOD	AIR METHOD	COMPRESSOR ISENTROPIC EFFICIENCY
611	5394	280.2	264	2332	2933	26985	26411	2.70	2.64	0.507
208	5412	270.9	268	2281	2886	26293	25589	2.67	2.60	0.503
095	5396	262.3	270	2271	2878	25337	23831	2.58	2.43	0.505
916	5393	252.1	270	2250	2857	24366	23300	2.50	2.39	0.496
865	5395	246.7	270	2231	2838	23866	23049	2.46	2.38	0.491
722	5400	243.2	271	2196	2804	23530	22293	2.46	2.33	0.500
653	5404	234.2	273	2177	2787	22693	22050	2.39	2.32	0.487
602	5400	229.3	275	2168	2780	22140	21126	2.33	2.23	0.485
592	5407	220.8	278	2139	2753	21367	20764	2.27	2.21	0.479
407	5412	222.5	279	2111	2727	21541	20653	2.31	2.22	0.492
394	5396	210.0	282	2102	2721	20224	19298	2.18	2.08	0.479
368	5420	205.4	282	2063	2682	19952	20033	2.18	2.19	0.472
103	5435	195.8	285	2005	2627	19058	18653	2.13	2.08	0.471

ta observed for frosting ambient conditions of 1.7°C (35°F) and 80% relative humidity

		REFRIGERANT PRESSURES, PSIA					AIR FLOW RATES			POWER INPUT, W			HEATING CAPACITY, BTU/HR		COP		
'ORATOR OUT	AVERAGE EVAPORATOR WALL	COMPRESSOR IN	COMPRESSOR OUT	OUTDOOR TXV IN	OUTDOOR TXV OUT	EVAPORATOR IN	OUTDOOR CFM	INDOOR LBM/HR	REFRIG-ERANT FLOW RATE, LBM/HR	OUTDOOR FAN	COMPRESSOR	TOTAL	REFRIG-ERANT METHOD	AIR METHOD	REFRIG-ERANT METHOD	AIR METHOD	COMPRESSOR ISENTROPIC EFFICIENCY
26.0	23.9	57.7	212.5	198.7	90.3	62.9	2034	5349	289.4	269	2433	3039	27322	26574	2.63	2.56	0.506
23.4	23.1	54.4	204.3	190.9	85.5	59.2	1781	5371	276.7	270	2339	2947	26370	25525	2.62	2.54	0.510
22.6	22.3	53.1	202.6	189.8	82.5	57.6	1649	5376	262.6	272	2309	2918	25106	24516	2.52	2.46	0.499
21.4	21.2	51.6	199.6	187.2	80.4	55.9	1514	5383	247.6	274	2269	2880	23756	23643	2.42	2.41	0.483
20.0	19.8	49.8	196.9	184.8	78.0	53.9	1438	5388	241.1	278	2222	2837	23149	22760	2.39	2.35	0.488
18.7	18.1	48.4	194.7	182.8	75.8	52.4	1305	5394	236.2	281	2185	2803	22711	22137	2.37	2.31	0.491
16.9	15.9	47.0	193.0	181.6	73.2	50.9	1305	5398	223.0	284	2150	2771	21461	21376	2.27	2.26	0.480
15.2	13.5	45.2	190.0	179.0	70.5	48.6	1112	5406	213.2	287	2104	2728	20546	20240	2.21	2.17	0.474
13.4	10.6	43.3	187.6	176.7	67.5	46.4	853	5413	207.3	290	2053	2680	19938	18967	2.18	2.07	0.485

Table A.4. Test d

RUN TIME, MIN	RELATIVE HUMIDITY, %	AIR TEMPERATURES, F: OUTDOOR COIL IN	AIR TEMPERATURES, F: OUTDOOR COIL OUT	AIR TEMPERATURES, F: INDOOR COIL IN	AIR TEMPERATURES, F: INDOOR COIL OUT	REFRIGERANT TEMPERATURES, F: COMPRESSOR IN	REFRIGERANT TEMPERATURES, F: COMPRESSOR OUT	REFRIGERANT TEMPERATURES, F: REVERSING VALVE OUT	REFRIGERANT TEMPERATURES, F: CONDENSER IN	REFRIGERANT TEMPERATURES, F: CONDENSER OUT	REFRIGERANT TEMPERATURES, F: OUTDOOR TXV IN	REFRIGERANT TEMPERATURES, F: OUTDOOR TXV OUT	REFRIGERANT TEMPERATURES, F: EVA IN
12.1	80.1	35.9	32.1	71.2	91.9	32.6	201.6	186.3	173.7	93.0	76.5	40.3	24.5
21.1	80.8	35.5	31.3	69.8	89.6	28.7	200.8	184.7	171.3	90.1	73.3	37.6	21.3
27.1	80.7	35.7	31.4	70.1	89.1	27.1	200.8	184.1	170.3	89.4	72.3	36.2	19.9
32.9	80.9	35.4	31.1	70.1	88.4	25.2	200.7	183.4	169.2	88.8	71.5	35.0	18.1
38.9	79.9	35.3	30.8	70.3	87.9	23.9	200.2	182.4	167.5	88.2	70.3	33.5	16.4
45.1	80.3	35.4	30.8	70.2	87.3	22.9	199.8	181.7	166.2	87.5	69.3	32.2	15.0
51.7	82.0	35.4	30.9	70.4	86.9	21.0	198.7	180.1	164.4	87.2	68.7	30.8	13.5
58.4	78.3	35.4	30.9	70.5	86.1	19.2	197.1	178.0	161.9	86.3	67.9	29.0	11.7
65.4	82.2	35.9	31.0	70.8	85.4	17.7	194.9	175.2	158.6	85.6	66.9	26.0	8.9

Table A.5. Test data observed for frosting ambient conditions of 1.7°C (35°F) and 90% relative humidity

		AIR TEMPERATURES, F				REFRIGERANT TEMPERATURES, F										REFRIGERANT PRESSURES, PSIA					AIR FLOW RATES		
RUN TIME, MIN	RELATIVE HUMIDITY, %	OUTDOOR COIL IN	OUTDOOR COIL OUT	INDOOR COIL IN	INDOOR COIL OUT	COMPRESSOR IN	COMPRESSOR OUT	REVERSING VALVE OUT	CONDENSER IN	CONDENSER OUT	OUTDOOR TXV IN	OUTDOOR TXV OUT	EVAPORATOR IN	EVAPORATOR OUT	AVERAGE EVAPORATOR WALL	COMPRESSOR IN	COMPRESSOR OUT	OUTDOOR TXV IN	OUTDOOR TXV OUT	EVAPORATOR IN	OUTDOOR CFM	INDOOR LBM/HR	RE E F R LB
11.9	92.4	34.8	32.2	76.2	96.6	30.3	206.6	190.3	177.8	97.4	77.8	39.9	24.1	25.2	25.1	57.4	224.5	211.1	87.1	62.4	1626	5320	2
18.0	89.8	34.2	31.6	73.0	93.3	26.4	204.1	187.3	174.6	94.0	75.6	37.4	21.1	23.0	23.6	54.4	213.0	200.0	82.2	59.0	1407	5352	2
24.3	88.9	34.6	31.4	71.4	90.4	25.4	200.4	183.3	170.1	90.4	72.3	35.7	19.2	21.9	21.8	52.4	204.6	192.1	79.0	56.8	1230	5380	2
30.8	90.2	34.3	31.1	71.7	89.9	23.5	198.1	180.5	166.9	89.8	71.0	33.9	17.4	20.1	19.8	50.5	202.4	190.5	76.7	54.9	1230	5385	2
37.5	85.3	34.1	31.0	71.8	89.2	21.9	196.5	178.6	164.6	89.2	70.1	32.4	15.7	18.2	17.5	48.7	199.7	188.0	74.3	53.1	1103	5392	2
48.0	91.7	35.0	31.6	72.0	88.3	18.9	193.9	175.3	160.9	88.3	69.3	29.7	12.5	15.2	13.4	46.0	195.8	184.5	70.5	49.9	980	5400	2
55.4	90.4	35.0	31.6	72.0	87.2	16.9	189.8	170.7	156.0	87.1	67.8	26.7	9.5	13.0	10.2	43.5	191.9	181.3	66.4	47.1	674	5411	2

FRIG-RANT LOW ATE, M/HR	POWER INPUT, W			HEATING CAPACITY, BTU/HR		COP		COMPRESSOR ISENTROPIC EFFICIENCY
	OUTDOOR FAN	COMPRESSOR	TOTAL	REFRIG-ERANT METHOD	AIR METHOD	REFRIG-ERANT METHOD	AIR METHOD	
80.3	270	2472	3079	26227	26046	2.50	2.48	0.506
54.4	272	2372	2981	25022	26073	2.46	2.56	0.493
57.9	276	2306	2919	24569	24532	2.47	2.46	0.496
45.6	279	2263	2879	23361	23520	2.38	2.39	0.490
36.4	282	2217	2836	22488	22515	2.32	2.33	0.491
24.3	288	2144	2769	21326	21126	2.26	2.24	0.495
09.1	290	2081	2709	19864	19740	2.15	2.14	0.487

APPENDIX B.
COMPUTER PROGRAM FOR THE DATA-ACQUISITION SYSTEM

The data acquisition system used in the experiments described in this report consisted principally of an analog-to-digital converter, a scanner, and a Digital Equipment Corporation PDP-8E minicomputer. The programs stored in the minicomputer were written in a modified version of the FOCAL language; they are presented here in flowchart form so that they may be readily understood.

At the introduction to each flowchart, the teletype (TTY) entries required to run that particular program are noted; for example, to run the heat balance and coefficient of performance program, one would enter "GO 3.1".

Initial Scan and Humidity Control

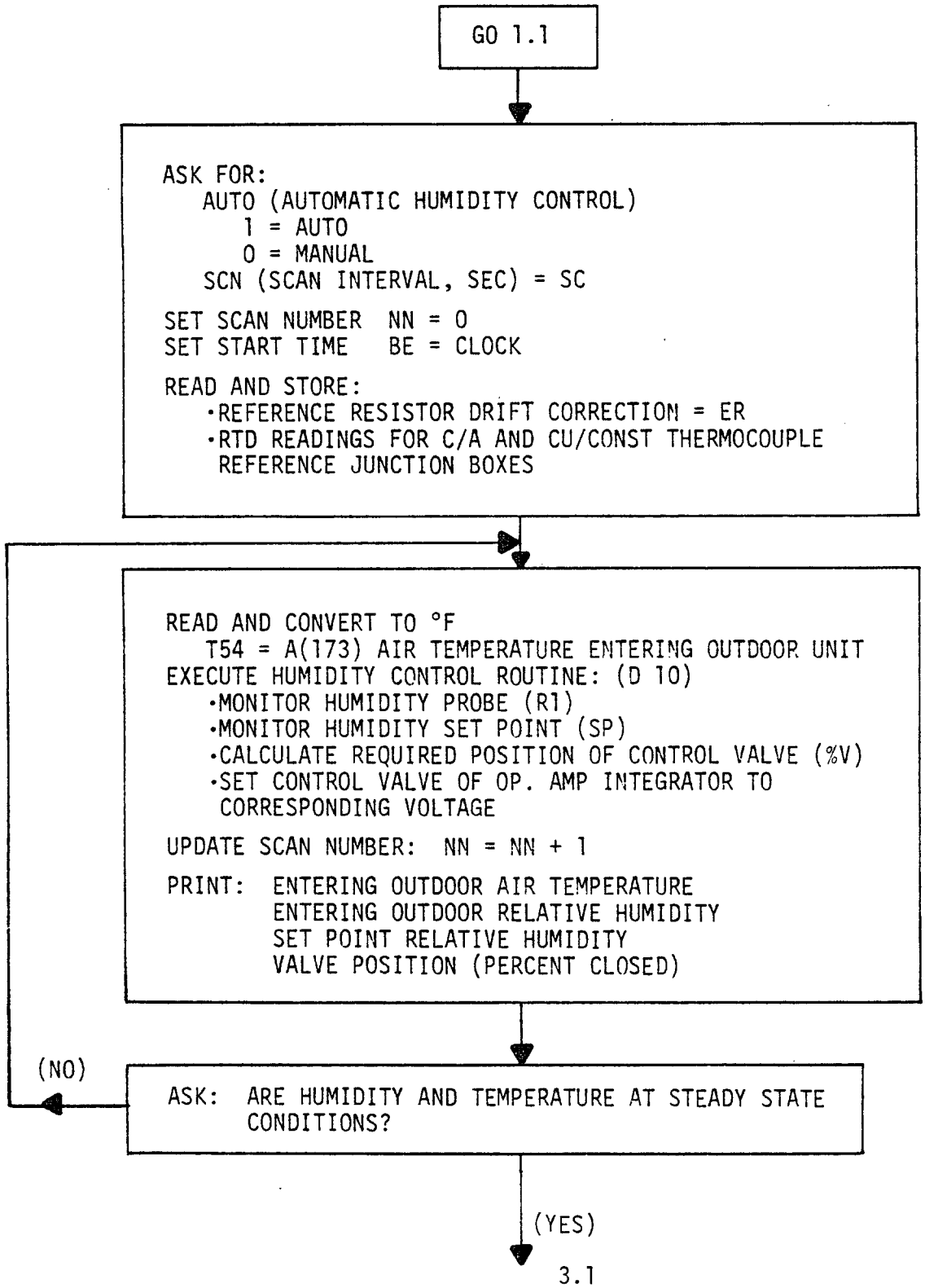

Scan and Heat Balance Program for Averaging over an Integral Number of R-22 Flow Rate Oscillation Cycles

```
GO 3.1
↓
ASK FOR:  DTR (TIME BETWEEN RUNS, SEC) = DT
          SCN (TIME BETWEEN DATA SCANS, SEC) = SC
          NACY (NUMBER OF CYCLES OF REFRIGERANT FLOW RATE
               OSCILLATION OVER WHICH MONITORED MEASUREMENTS
               ARE AVERAGED) = NA
          PWR (POWER INPUT TO CENTRIFUGAL FAN OF INDOOR
              UNIT, WATTS) = PW
          AUTO (AUTOMATIC HUMIDITY CONTROL) = AU
              AUTO = 1
              MANUAL = 0
          COIL (PRINT HEAT EXCHANGER COIL TEMPERATURES) = CO
              1 = YES
              0 = NO
          MFAN (MASS FLOW RATE OF AIR ACROSS INDOOR UNIT,
               LBM/HR) = MF

SET START TIME TO = CLOCK

SET FSTR INDEX VALUES FOR DATA SCAN
  LIST:  BS = BEGIN SCAN INDEX
         ES = END SCAN INDEX

FOR K = BS,ES:  SET A(FSTR(K)) = 0
        CLEARS STORAGE LOCATIONS FOR DATA INPUT AVERAGING
↓
3.25
```

Scan and Heat Balance Program - continued

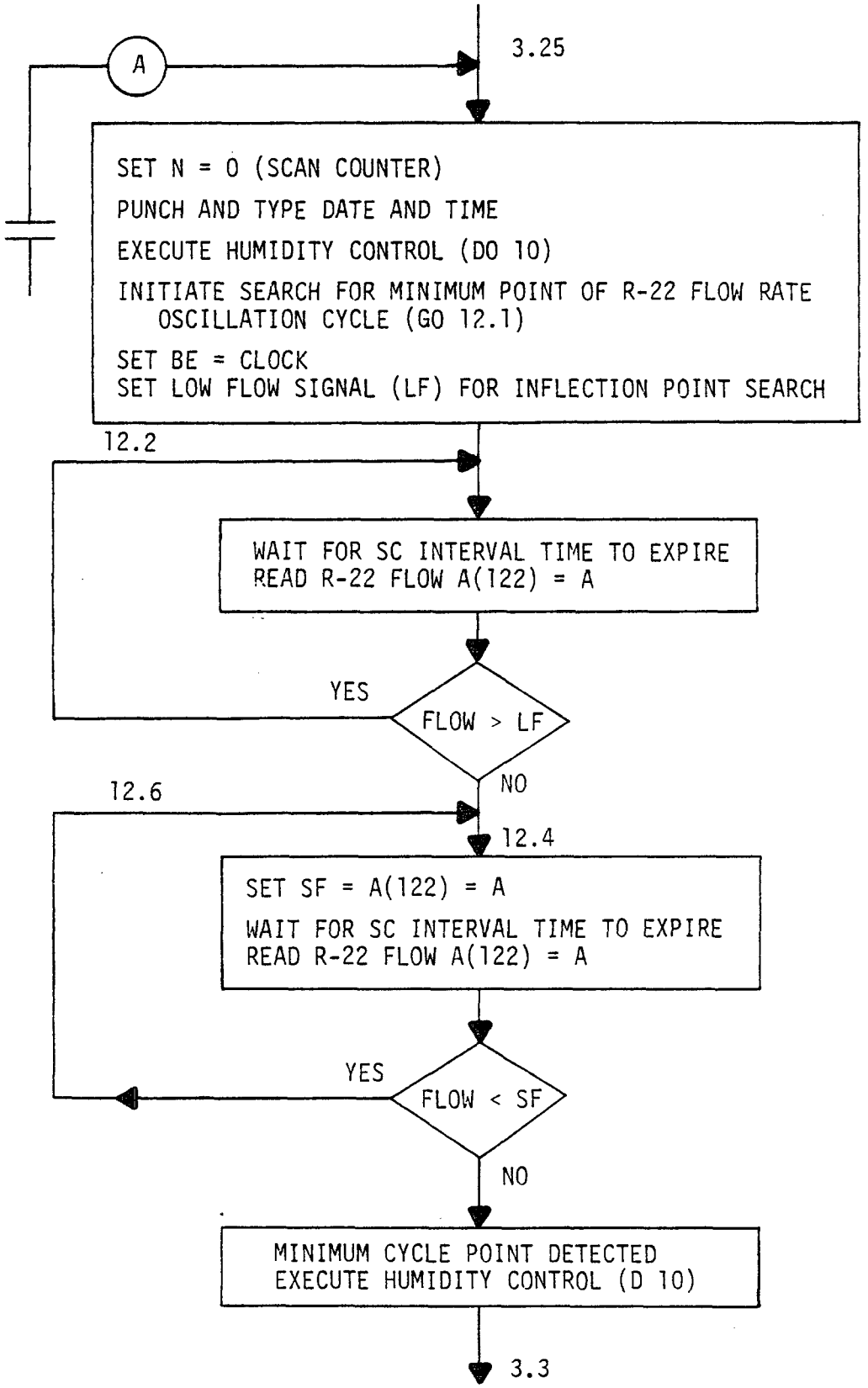

Scan and Heat Balance Program - continued

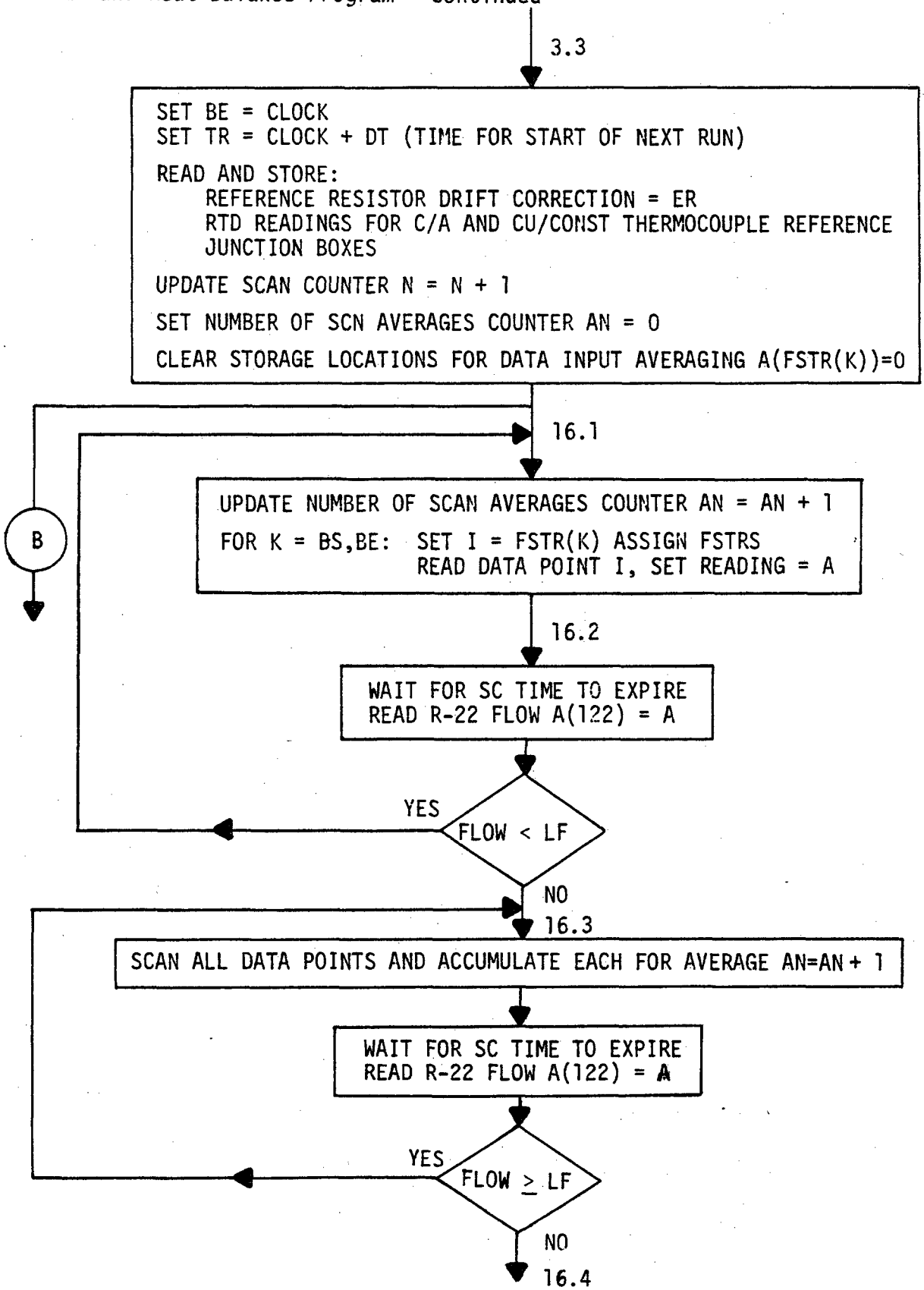

Scan and Heat Balance Program - continued

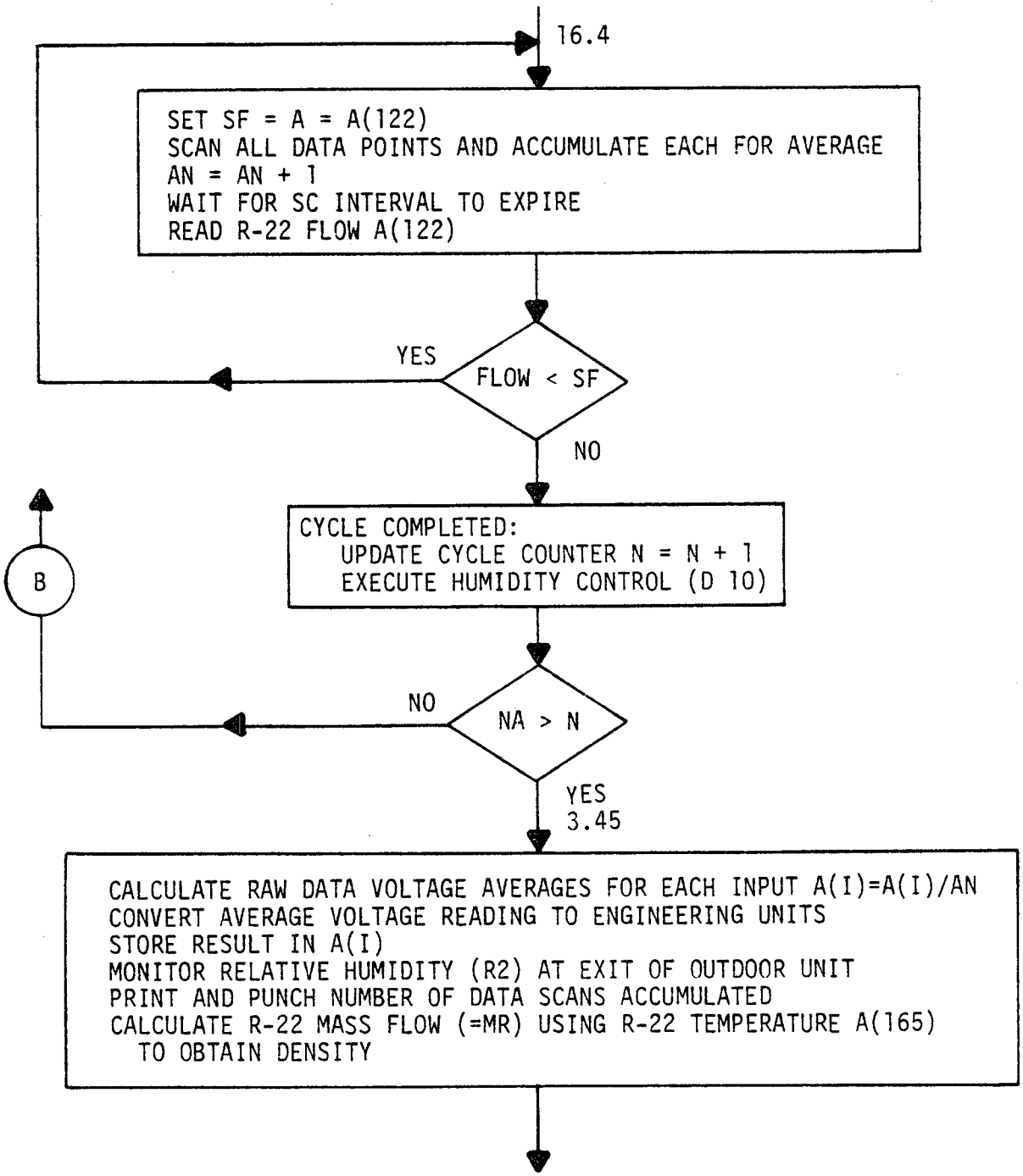

Scan and Heat Balance Program - continued

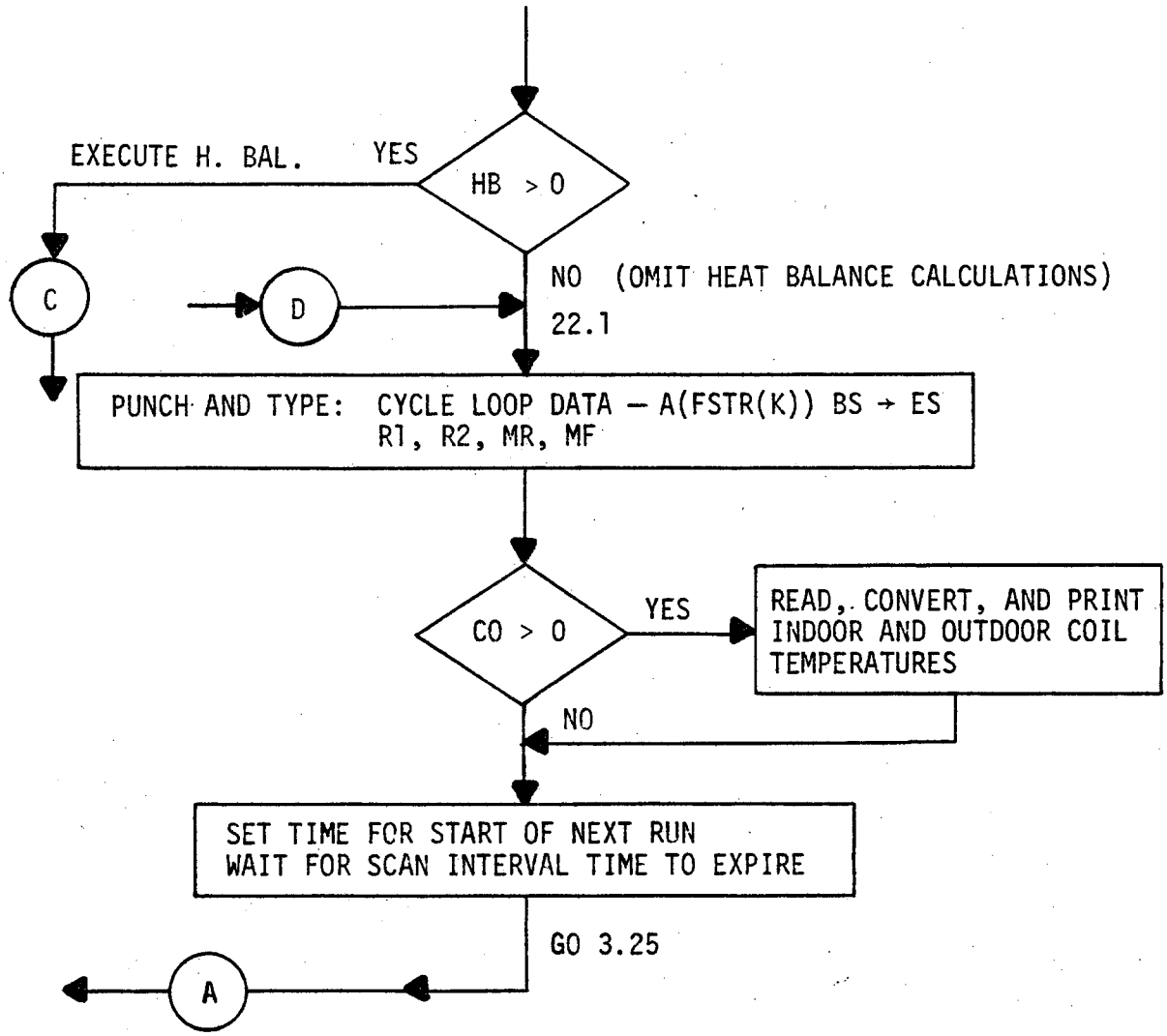

Scan and Heat Balance Program - continued

HEAT BALANCE

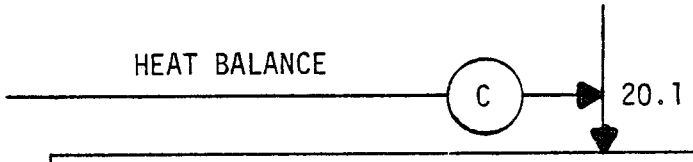

P = A(123) - 3 CONDENSER INLET PRESSUPE ESTIMATE, PSIA

CALCULATE:

- T_{SAT} (=TS) FROM P
- hg (=HG) FROM T_{SAT}
- SUPERHEAT SW = A(104) - TS
- $\delta h/\delta t$ (=HT) FROM P
- INDOOR COIL INLET ENTHALPY H5 = HG + HT * SW

P = P - A(120) INDOOR COIL EXIT PRESSURE

CALCULATE:

- T_{SAT} (=TS) FROM P
- hf (=HF) FROM T_{SAT}
- C_p (=CP) FROM T_{SAT}
- INDOOR COIL EXIT ENTHALPY H(26) = HF - C_p * (TS - A(165))

FROM T_{SAT} AT OUTDOOR COIL ENTRANCE A(168)

CALCULATE:

- P_{SAT} (=PU) FROM T_{SAT}
- OUTDOOR COIL EXIT PRESSURE P = PU - A(121)
- T_{SAT} FROM P
- Hg (=HG) FROM T_{SAT}
- SUPERHEAT SH = A(170) - TS
- $\delta H/\delta T$ (=HT) FROM P
- OUTDOOR COIL EXIT ENTHALPY H(51) = HG + HT * SH

IF SH IS NEGATIVE, ASSUME SATURATED MIXTURE AND SET H(51) = HG

Scan and Heat Balance Program - continued

```
P = A(127)  COMPRESSOR SUCTION PRESSURE, PSIA
CALCULATE:
     TS, HG, HT FROM P
     SUPERHEAT SR = A(100) - TS

CALCULATE INLET COMP. ENTHALPY  H1 = HG + HT * SR
     IF SR IS NEGATIVE, SET H1 = HG

P = A(123)  COMPRESSOR DISCHARGE PRESSURE, PSIA
CALCULATE:
     TS, HG, HT FROM P
     SUPERHEAT SW = A(102) - TS
     DISCHARGE ENTHALPY H2 = HG + HT * SW

PERFORM HEAT BALANCES
     COMPRESSOR SHELL HEAT LOSS (=QS)
        QS = MS * (H2 - H1) - A(128) * BW
     OUTDOOR COIL CAPACITY
        QO = MR * (H(51) - H(27))
     HEAT PUMP POWER CONSUMPTION (CD)
        CD = PW + A(128) + A(129)
     INDOOR COIL CAPACITY
        AIR SIDE:  QA = MF * 0.24 * (A(176) - A(175))
        R-22 SIDE: QH = MR * (H5 - H(26)) + PW * BW
     COP-R QH/(CD * BW)
     COP-A QA/(CD * BW)

     WHERE:  MR - R-22 MASS FLOW RATE, LBM/HR
             MF - INDOOR AIR MASS FLOW RATE, LBM/HR
             A(128) - COMP. POWER, WATTS
             A(129) - OUTDOOR FAN POWER, WATTS
             PW - INDOOR FAN POWER, WATTS
             BW - CONVERSION 3.413 BTU/WATT-HR
```

Humidity Control Routine - DO 10 (See Fig. 8)

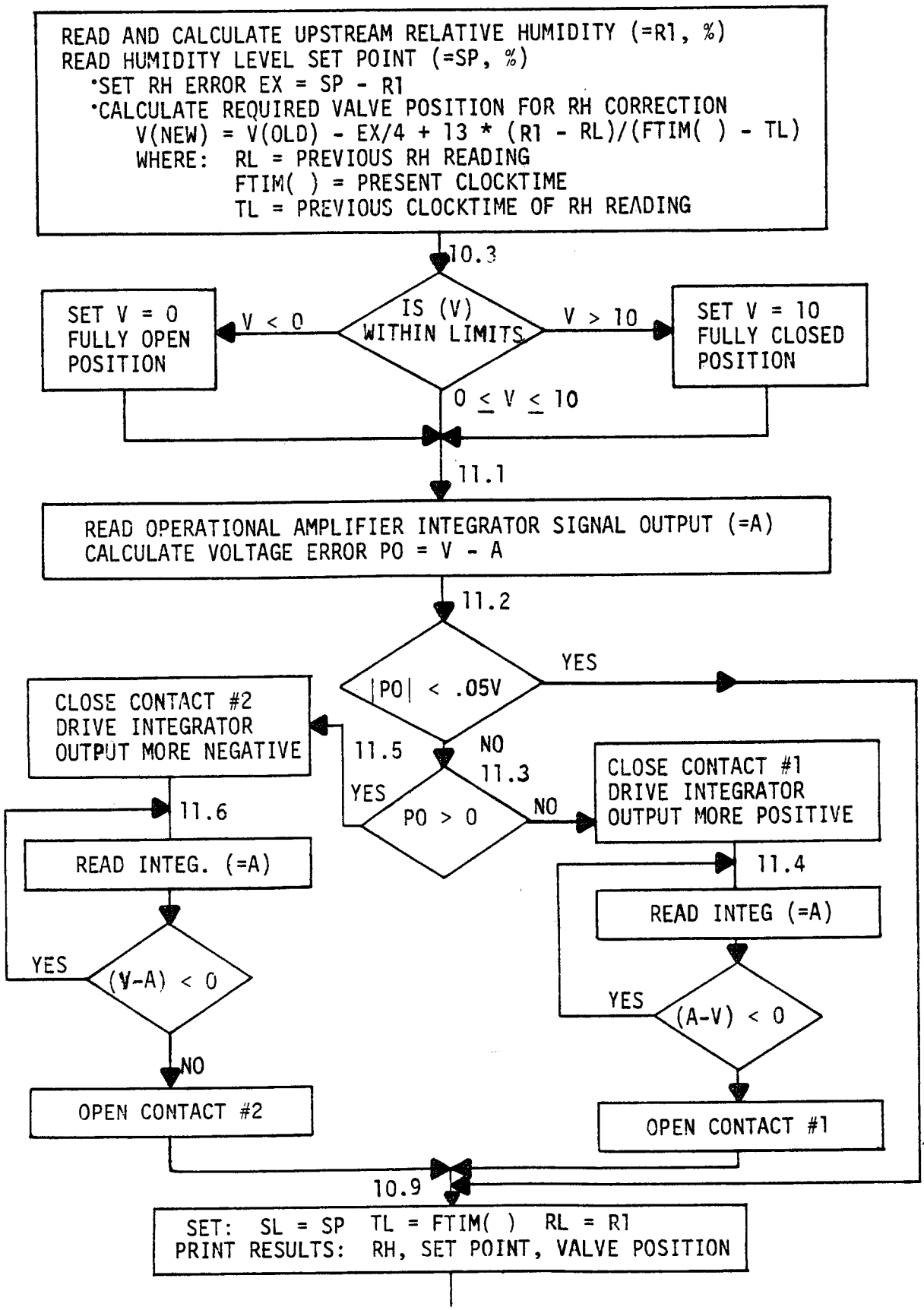

Humidity Conversion Routine (Part I)
Measure Humidity Probe Output, Convert to Equivalent "Dial Reading"

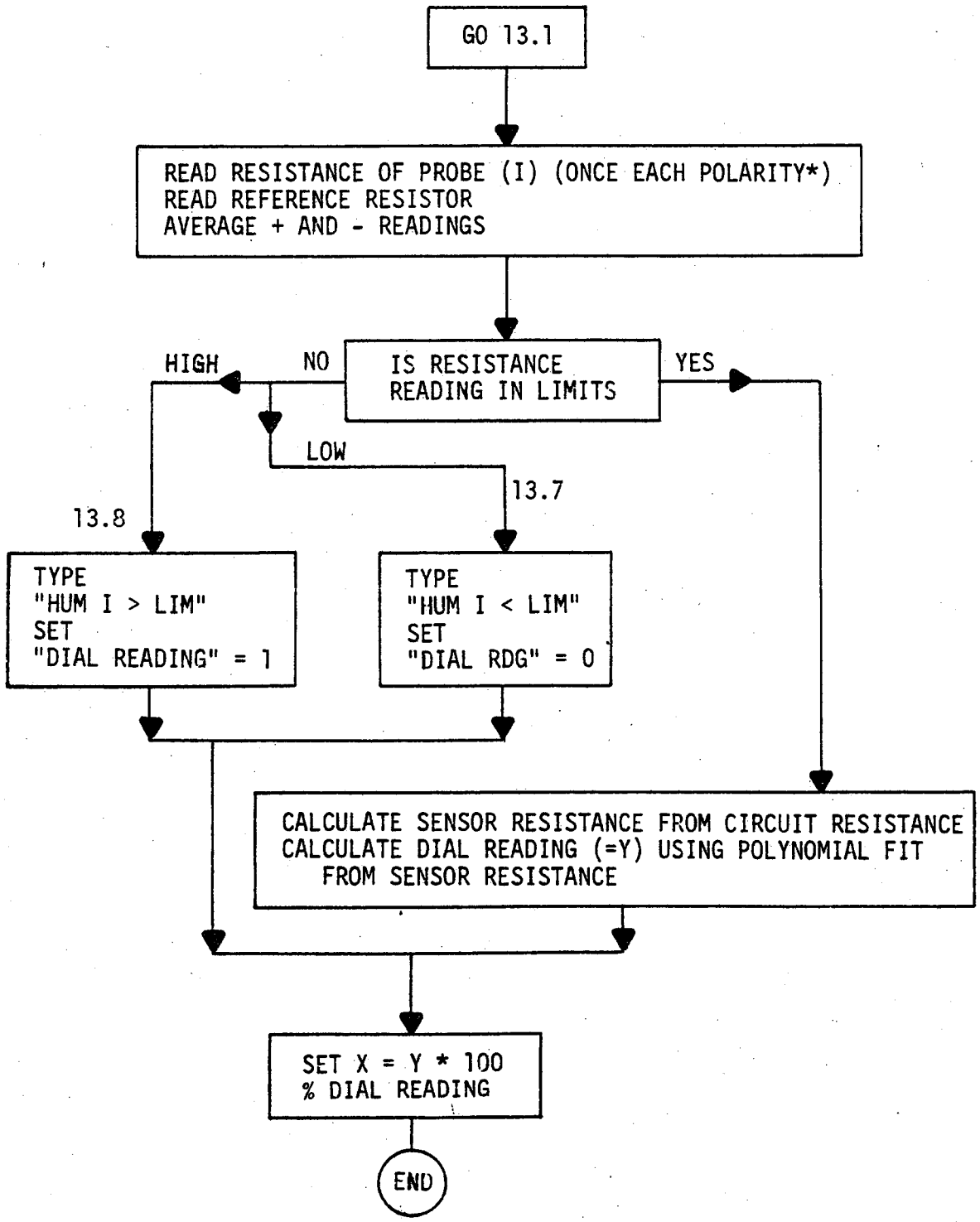

*Dunmore-type lithium-chloride hygrosensors are polarity sensitive and normally require a-c excitation. Reading the reference resistor after reading the probe is done only to remove the current excitation from the probe.

Humidity Conversion Routine (Part II)
Calculate % RH from Equivalent Dial Reading (EDR) = x% (DO 13)
and Temperature at Probe (=T, °F): A(173) for R1
A(174) for R2

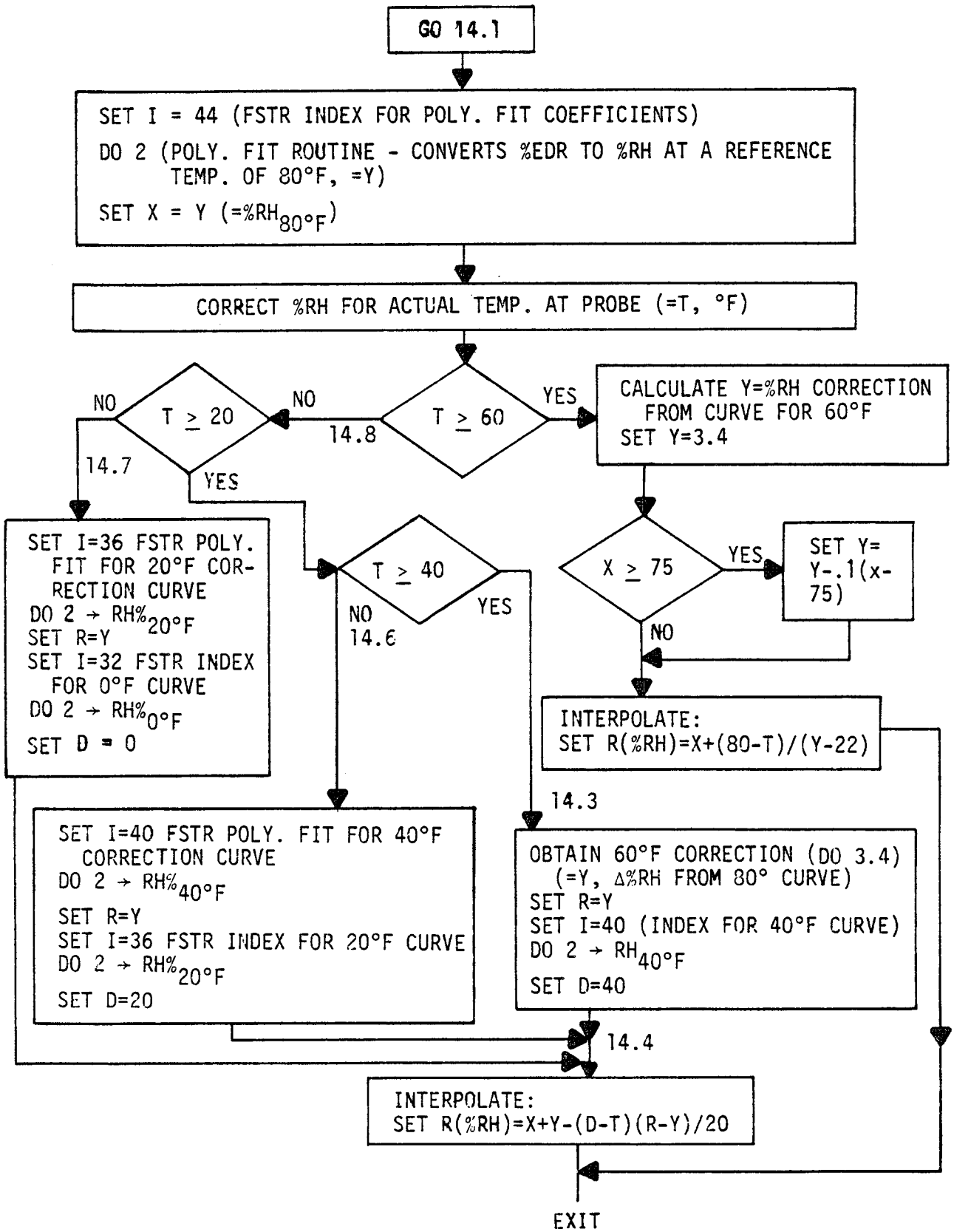

APPENDIX C.
PERFORMANCE AT −8.3°C (17°F)

The frosting results observed at −8.3°C (17°F) are similar to those discussed in Sect. 7.1.3 for tests at −6.7°C (20°F). Acute frosting was observed during the 90% humidity test run, and 90% of the free-flow area of the outdoor heat exchanger was blocked with frost at termination of the test. Light frosting occurred during the 70% humidity test run, with no appreciable accumulation at the end of the test. At completion of the 90% humidity run, 2.93 kg (6.45 lb) of frost was collected. The performances of the heat pump and the outdoor airflow are shown in Figs. C.1 through C.5. Comments and discussion of the results at −6.67°C (20°F) are applicable to the data in this appendix.

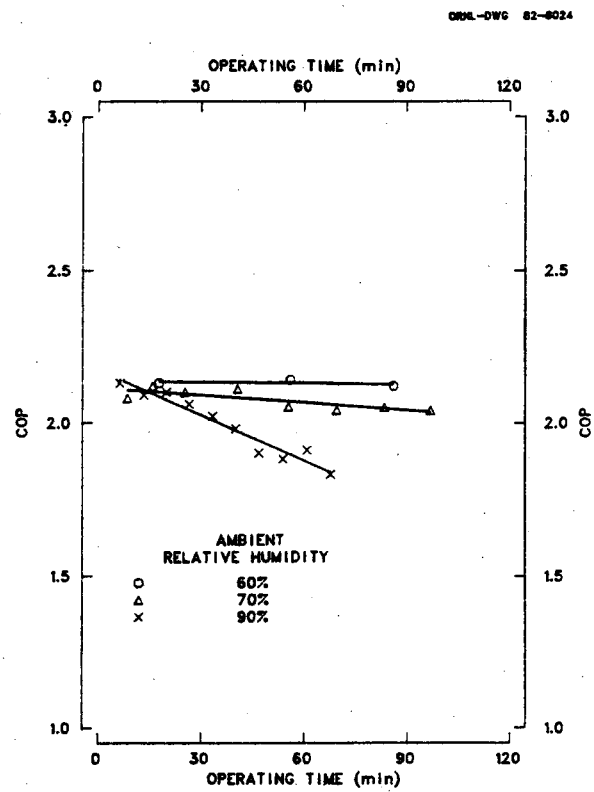

Fig. C.1. COP measured at −8.3°C (17°F).

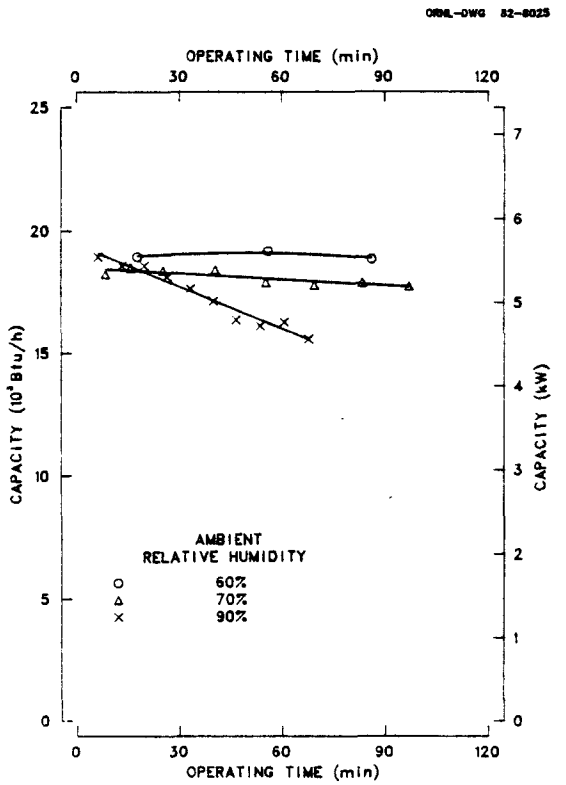

Fig. C.2. Heating capacity measured for an ambient temperature of −8.3°C (17°F).

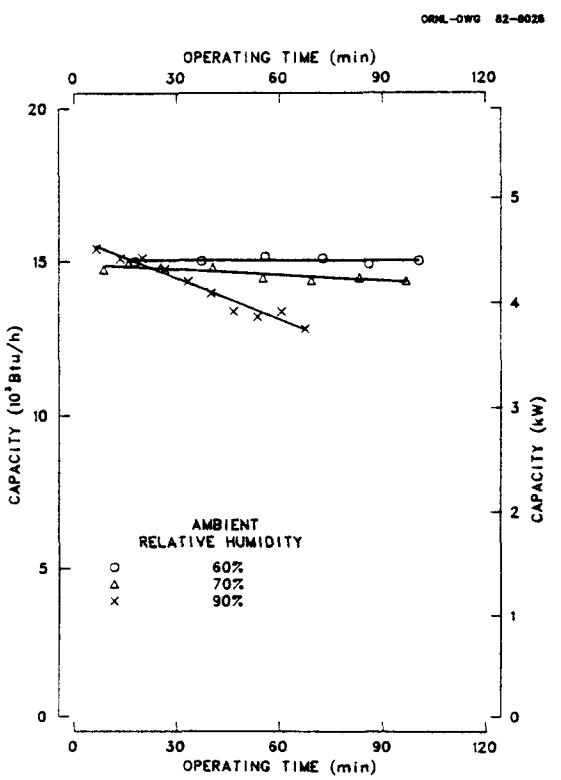

Fig. C.3. Outdoor heat exchanger capacity measured for an ambient temperature of −8.3°C (17°F).

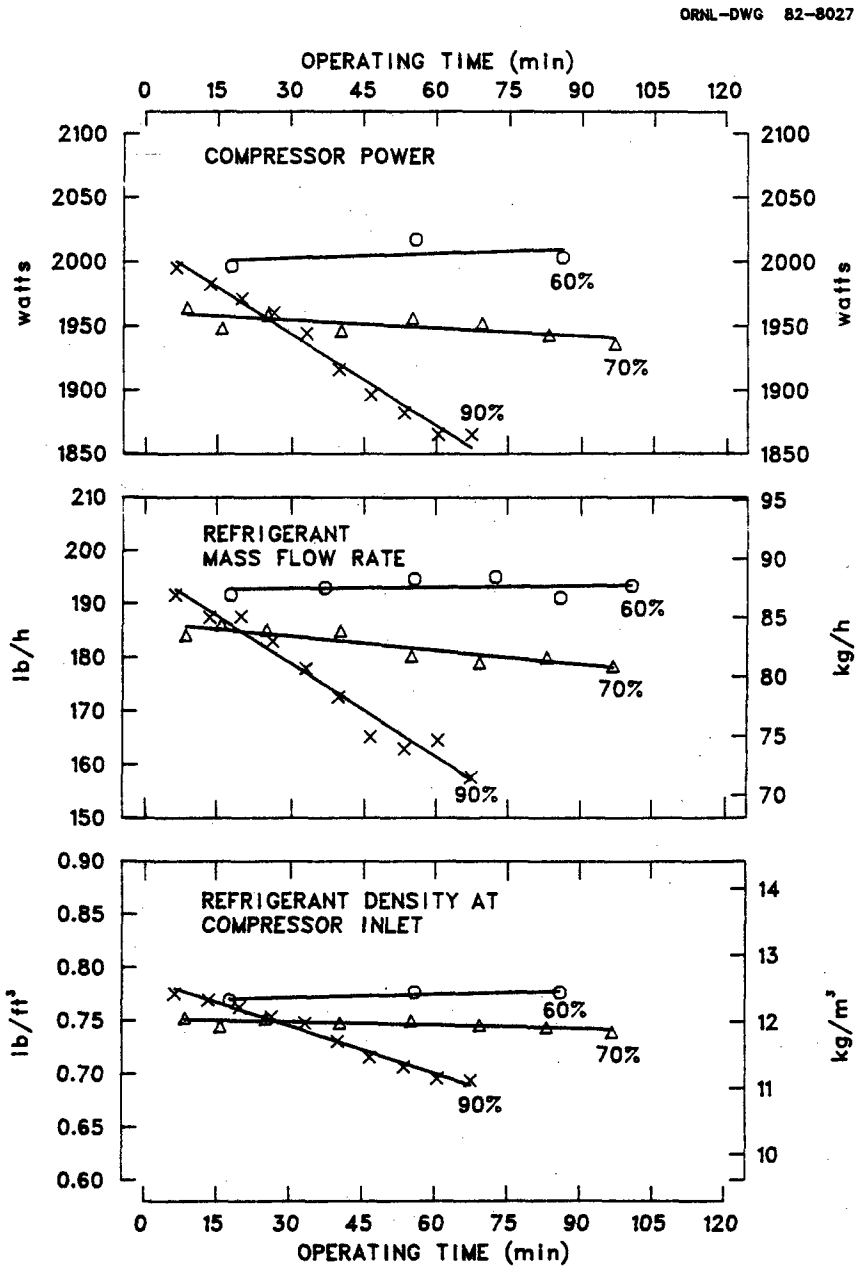

Fig. C.4. Parametric study of heat pump performance traits observed at various outdoor relative humidity levels for an ambient temperature of −8.3°C (17°F).

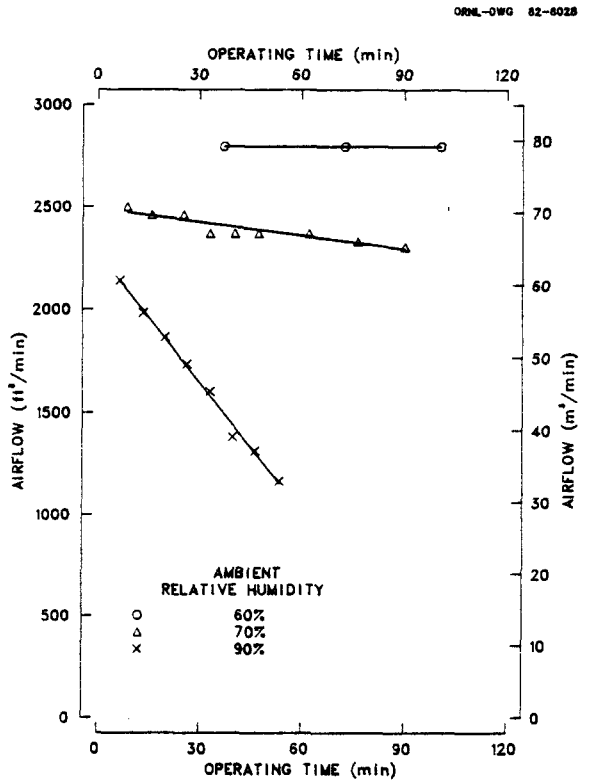

Fig. C.5. Outdoor airflow measured while the heat pump operated at −8.3°C (17°F).

Do not microfilm

INTERNAL DISTRIBUTION

1. R. K. Adams
2. S. J. Ball
3. V. D. Baxter
4. R. S. Carlsmith
5. F. C. Chen
6. R. C. DeVault
7. R. D. Ellison
8. P. D. Fairchild
9. S. K. Fischer
10. W. Fulkerson
11. K. S. Gaddis
12. C. A. Gallagher
13. C. Gilmore
14. R. E. Goodson, Consultant
15. G. R. Hadder
16. D. M. Hamblin
17. V. O. Haynes
18. K. E. Heidereich
19. D. E. Holt
20. L. Jung
21. T. R. LaPorte, Consultant
22. W. P. Levins
23. H. A. McLain
24. V. C. Mei
25. J. W. Michel
26. D. R. Miller
27. G. N. Miller
28. W. A. Miller
29. R. E. Minturn
30. W. R. Mixon
31. L. I. Moss, Consultant
32. J. C. Moyers
33. E . A. Nephew
34. H. Perez-Blanco
35. J. Reed
35. C. K. Rice
36. R. C. Robertson
37. C. S. Robinson
38. M. Russell, Consultant
39. G. Samuels
40. I. A. Tag
41. L. F. Truett
42. E. A. Vineyard
43. T. J. Wilbanks
44. W. H. Williams, Consultant

45-46. Central Research Library
47. Document Reference Section
48. Energy Research Library
49. Laboratory Records - RC

50-52. Laboratory Records Dept.
53. ORNL Patent Office

EXTERNAL DISTRIBUTION

54. Roy Abbott, Advance Technology Operations, General Electric Company, AP6, Appliance Park, Louisville, KY 40225
55. John Adams, Whirlpool Corporation, Research & Engineering Center, Monte Road, Benton Harbor, MI 49022
56. Richard Alben, General Electric Company, Corporate R&D Center, Bldg. K-1, Rm 5B37, P.O. Box 8, Schenectady, NY 12301
57. C. A. Allen, Energy Information Administration, EI-60, Federal Building, 1200 Pennsylvania Avenue N.W., Washington, DC 20461
58. Lawrence Ambs, Department of Mechanical Engineering, University of Massachusetts, Amherst, MA 01003
59. Kent Anderson, The Trane Company, 2020 14th Street, Arlington, VA 22101
60. John Andrews, Solar Technology Group, Building 701, Brookhaven National Laboratory, Upton, NY 11973
61. B. Backstrom, Chalmers University of Technology, S-41296, Goteborg, Sweden
62. James Bard, Executive Vice-President, Bard Manufacturing Co., Inc., P.O. Box 607, Bryan, OH 43506

63. E. K. Bastress, Energy Conversion & Utilization Technology Div., CS-142, Forrestal Building, Department of Energy, Washington, DC 20585
64. William Beale, Sunpower, Inc., 6 Byard Road, Athens, OH 45701
65. Warren Beeton, Vice-President-Engineering, Bristol Corporation, 649 Industrial Park, Bristol, VA 24201
66. J. Berghmans, Universitiet Leuven, Instituut Mechanica, Celestynen Laan 300A, B3030 Heverlee, Belgium
67. Morton Blatt, 1200 Prospect Street, P.O. Box 2351, LaJolla, CA 92038
68. Peter Bodett, Duo-Therm Division, Motor Wheel Corporation, LaGrange, IN 46761
69. Ulrich Bonne, Honeywell Incorporated, 10701 Lyndale Avenue South, Corporate-Technology Center, Materials & Processes Dept., Bloomington, MN 55420
70. J. E. Bose, Director, School of Technology, Oklahoma State University, Stillwater, OK 74078
71. T. Bostrom, Swedish Council for Building Research, St. Goransgatan 66, S-11233 Stockholm, Sweden
72. Joseph Braymer, Mechanical & Aerospace Eng. Dept., Case Western Reserve, University Circle, Cleveland, OH 44106
73. James Brisee, North Carolina Energy Institute, Department of Commerce, P.O. Box 12235, Research Triangle Pk., NC 27709
74. Jim Calm, Energy Management & Utilization Div., Electric Power Research Inst., Heat Pump Development, P.O. Box 10412, Palo Alto, CA 94303
75. Joe Canal, General Electric Company, Troup Highway, Tyler, TX 75711
76. C. Gerald Carrington, Birmingham, England
77. Roger Chesebro, Westinghouse Electric Corporation, Research & Development Center, 1310 Beulah Road, Pittsburg, PA 15235
78. Raymond Cohen, Ray W. Herrich Laboratories, Purdue University, West Lafayette, IN 47907
79. W. R. Coleman, Residential & Commercial Services, American Elec. Power Services, 100 E. Broad, Columbus, OH 43201
80. V. I. Conley, Virginia Polytechnic Inst. & State Univ., Dept. of Mechanical Eng., Blacksburg, VA 24061
81. Ken Cooper, York Division, Borg-Warner Corporation, P.O. Box 1592, York, PA 17405
82. Gerard Coyne, General Electric Company, Central Air Conditioning Dept., Troup Highway, Tyler, TX 75711
83. James Crawford, Manager, Advanced Systems, General Electric Company, 6200 Troup Highway, Tyler, TX 75711
84. Kenneth Cuccinelli, Division of Marketing Services, American Gas Association, 1515 Wilson Blvd., Arlington, VA 22209
85. J. J. Cuttica, Manager, Fuel Cell Energy Systems, Gas Research Institute, 8600 W. Bryn Mawr Avenue, Chicago, IL 60631
86. Nicholas D'Aleandro, Vice-President, A/C Engineering, Fedders Corporation, Woodbridge Avenue, Edison, NJ 08817
87. Ali Dabiri, Science Applications, Inc., 1200 Prospect Street, P.O. Box 2351, LaJolla, CA 92038
88. Jerry Dapper, BDP Company, Div. of Carrier Corporation, 7310 W. Morris Street, Indianapolis, IN 46231
89. Douglas DeWerth, Project Manager, Utilization Technology, Research & Development, 8501 East Pleasant Valley Road, Cleveland, OH 44131
90. Thomas Dean, University of Kansas, Lawrence, KS 66045
91. R. J. Denny, Air-Conditioning & Refrigeration Institute, 1815 N. Fort Meyer Drive, Arlington, VA 22209
92. Irvin Derks, Manager Engineering Development, Bard Manufacturing Co., Bryan, OH 43506
93. David Didion, Mechanical Systems Section, Building Environment Division, National Bureau of Standards, Bldg. 226, Room B126, Washington DC 20234

94. Albert Domingorena, Carrier Corporation, Building TR-4, Carrier Parkway, Post Office Box 4808, Syracuse, NY 13221
95. Richard Dougall, University of Pittsburg, Dept. of Mechanical Eng., Pittsburg, PA 15261
96. Alan Drucker, Consumer Products Division, Carrier Corporation, Syracuse, NY 13221
97. G. D. Duffy, Air Conditioning News, P.O. Box 2600, Troy, MI 48084
98. Amir Ecker, Northrup, Inc., 302 Nichols Drive, Hutchins, TX 75141
99. Thomas Edwards, The Rovac Corporation, 100 Rovac Parkway, Rockledge, FL 32955
100. A. H. Elmahdy, Energy and Services Section, National Research Council, Division of Building Research, Ottawa, Canada
101. Richard English, Energy Systems Division, Carrier Corporation, Carrier Parkway, P.O. Box 4895, Syracuse, NY 13221
102. Richard Erth, York Division, Borg-Warner, P.O. Box 1592, York, PA 17405
103. V. A. Eustace, IRD Co. Ltd., Fossway, Newcastle upon Tyne, Great Britain
104. J. N. Eustis, Department of Energy, Office of Industrial Programs, CE-121.1, 1000 Independence Avenue, S.W., Washington, DC 20585
105. Scott Farley, The Coleman Company, Inc., Special Products Group, 250 North St. Francis, Wichita, KS 67201
106. Arthur Fellerman, McQuay Group, 13600 Ind. Park Boulevard, Minneapolis, MN 55440
107. Robert Fischer, Battelle-Columbus Laboratory, 505 King Avenue, Columbus, OH 43201
108. R. J. Fiskum, Energy Conversion Equipment Branch, CE-113.2, Department of Energy, 1000 Independence Avenue S.W., Washington, DC 20585
109. G. W. Gatecliff, Research Laboratory, Tecumseh Products Company, Ann Arbor, MI 48105
110. J. H. Gibbons, Office of Technology Assessment, U.S. Congress, 600 Pennsylvania Avenue S.E., Washington, DC 20510
111. P. V. Gilli, Graz University of Technology, Kopernikusgasse 24, A-8010, Graz, Austria
112. A. C. Giurlando, P.E., Fedders Corporation, Edison, NJ 08817
113. Paul Glamm, The Trane Company, 3600 Dammel Creek Road, LaCrosse, WI 54601
114. L. R. Glicksman, Massachusetts Institute of Technology, 77 Massachusetts Avenue, Bldg. 3-137, Cambridge, MA 02139
115. Alan Glover, School of Engineering, Mechanical Engineering Dept., University of Auckland, Auckland, New Zealand
116. Victor Goldschmidt, Purdue University, Ray W. Herrick Laboratories, West Lafayette, IN 47907
117. Sheldon Goldstein, Carteret, NJ 07008
118. R. Eugene Goodson, Hoover Universal, Inc., P.O. Box 1003, 825 Victors Way, Ann Arbor, MI 48106
119. Peter Gorike, Abt. Anwendungstechnik, Rheinish-Westfakuscges, Krupstrasse 5, 4300 Essen 1, Federal Republic of Germany
120. D. E. Grether, International Environmental Corp., 5000 7th Street, SW, Oklahoma City, OK 73125
121. Russ Griffith, Copeland Corporation, Campbell Road, Sidney, OH 45365
122. G. C. Groff, Research Division, Carrier Corporation, Syracuse, NY 13201
123. Marvin Gunn, Energy Conversion & Utilization Technology Div., CS-142, Forrestal Building, Department of Energy, Washington, DC 20585
124. John Hackstedde, Tecumseh Products Company, Tecumseh, MI 49236
125. R. Hanski, Studsvik Energiteknik AB, S-611 82 Nykoping, Sweden
126. James Harnish, Chief Engineer, Advanced Products, Unitary Products Engineering, York Division, Borg-Warner Corporation, York, PA 17405
127. D. J. Harrje, Princeton University, Energy & Environment, Von Neuman Building, Princeton, NJ 08544
128. Gordon Hart, Owens-Corning Fiberglass Technical Center, Granville, OH 43023
129. Floyd Hayes, Thermal Systems, The Trane Company, 3600 Pammell Creek Road, LaCrosse, WI 54601

130. Wayne Helmer, Southern Illinois University at Carbondale, School of Eng. & Tech., Dept. of Thermal & Env. Eng., Carbondale, IL 62901
131. R. J. Hemphill, Gas Research Institute, 8600 Bryn Mawr Avenue, Residential & Commercial Util., Chicago, IL 60631
132. Robert Hemphill, Deputy Manager of Power, 546 Chestnut Street Tower II, Tennessee Valley Authority, Chattanooga, TN 37401
133. Arlo Hendrickson, General Electric Company, Troup Highway, Tyler, TX 75711
134. James Hill, Thermal Solar Program, National Bureau of Standards, Washington DC 20234
135. C. C. Hiller, Sandia Laboratories, Livermore, CA 94550
136. Ralph Hise, Consolidated Natural Gas Service Company, 11001 Cedar Avenue, Cleveland, OH 44106
137. Larry Hobart, American Public Power Association, 2000 Virginia Avenue N.W., Washington, DC 20037
138. Tina Hobson, Building Equipment Division, CE-113.2, Department of Energy, 1000 Independence Avenue S.W., Washington, DC 20585
139. Allen Holman, Mechanical Data, 215 Center Park Drive, Suite 100, Knoxville, TN 37922
140. Robert Holtz, Program Manager, Closed Cycle Systems, Argonne National Laboratory, 9700 S. Cass Avenue, Argonne, IL 60439
141. Fred Honnold, Consumer Products Division, Carrier Corporation, Syracuse, NY 13201
142. John Hughes, Commonwealth Edison Company, P.O. Box 767, Chicago, IL 60690
143. Michael Hughes, Friedrich Air Conditioning & Refrigeration, 2000 W. Commercial Boulevard, Fort Lauderdale, FL 22209
144. Bao Hwang, David Taylor Naval Ship R&D Center, Mail Code 2722, U. S. Naval Academy, Annapolis, MD 21402
145. Howard Izawa, InterNorth, Inc., Northern Gas Company, 4840 F Street, Omaha, NB 68117
146. S. R. Jackbsen, Danish Ministry of Energy, Energy R&D Secretariat, Strandgage 29 DK 1401, Copenhagen, Denmark
147. Richard Jacobson, Honewell Inc., 10701 Lyndale Avenue South, Bloomington, MN 55420
148. T. Jacoby, Tecumseh Products Company, Tecumseh, MI 49286
149. H. Jaster, General Electric Corporate Research & Development, General Electric Company, P.O. Box 43, Schenectady, NY 13201
150. P. L. Johnson, Oak Ridge Associated Universities, Executive Office, Administration Building, Oak Ridge, TN 37830
151. F. R. Kalhammer, Energy Management and Utilization Division, Electric Power Research Inst., 3412 Hillview Avenue, P.O. Box 10412, Palo Alto, CA 94303
152. F. Kalivoda, Copeland Corporation, Sydney, OH 45365
153. Mark Kalman, E-Tech Incorporated, 3570 American Drive, Atlanta, GA 30341
154. Herbert Kaufman, Empire State Electric Energy Research Corp., 1271 Avenue of the Americas, New York, NY 10002
155. George Kelly, Building Environment Division, IAT, National Bureau of Standards, Building 226, Washington, DC 20234
156. Rube Kelto, Tecumseh Products Company, Tecumseh, MI 49286
157. R. W. King, Manager, Advanced Engineering, Copeland Corporation, Sydney, OH 45365
158. Sanford Klein, University of Wisconsin, Mechanical Engineering, Madison, WI 53706
159. Milton Kosfeld, Vice-President, Engineering Compressors, Fedders Corporation, Woodbridge Avenue, Edison, NJ 08817
160. H. Kruse, University Hannover, Welfengarten 1 A Hannover, West Germany
161. P. Kuppers, Kernforschungsanlage/Ple, Postfache 1913, D-5170, Julich 1, Germany
162. Todd LaPorte, Institute of Government Studies, University of California, Berkeley, CA 94720
163. Gary Laden, Deputy Assistant Director, Div. of Energy & Product Inf., Bureau of Consumer Protection, Federal Trade Commission, Washington, DC 20580
164. M. Yves Langhame, Quebec, Canada

165. J. Langmead, Director of Technical Services, Gas Appliance Man. Assoc., 1901 N. Ft. Meyer Drive, P.O. Box 9245, Arlington, VA 22209
166. Arvo Lannus, Residential & Commercial Applications, Electric Power Research Inst., 3412 Hillview Avenue, P.O. Box 10412, Palo Alto, CA 94303
167. Dr. Y. N. Lee, Roy C. Ingersoll Research Center, Wolf & Algonquin Roads, Borg-Warner Corporation, Des Plaines, IL 60018
168. W. David Lee, Arthur D. Little, Inc., Acorn Park, Cambridge, MA 02140
169. A. W. Liles, EXXON Enterprises Inc., P.O. Box 192, Florham Park, NJ 07932
170. D. C. Lim, Energy Conversion Equipment Branch, CE-113.2, Department of Energy, 1000 Independence Avenue S.W., Washington, DC 20585
171. Nance Lovvorn, Alabama Power Company, 15 South 20th Street, P.O. Box 2641, Birmingham, AL 35291
172. R. A. Lucheta, Westinghouse Electric Corporation, Research & Development Center, 1310 Beulah Road, Pittsburg, PA 15235
173. H. P. Luckett, Editor in Chief, *Popular Science*, 380 Madison Avenue, New York, NY 10017
174. Ward MacArthur, Honeywell Inc., 2600 Ridgeway Parkway, Minneapolis, MN 55413
175. J. F. T. MacLaren, University of Strathclyde, Glasgow, Scotland
176. J. C. Major, Swiss Federal Institut for Reactor Research, CH-5303 Wurenlingen, Switzerland
177. Robert Mauro, Energy Management & Utilization Div., Electric Power Research Inst., 3412 Hillview Avenue, P.O. Box 10412, Palo Alto, CA 94304
178. Jim McCallum, Executive Editor, Air Cond. & Refrig. Bus., 614 Superior Avenue W., Cleveland, OH 44113
179. E. A. McPherson, SED Systems Ltd., P.O. Box 1464, Saskatoon, Saskatchewan, Canada S7K3P7
180. F. C. McQuiston, Oklahoma State University, 301 Engineering North, Stillwater, OK 74074
181. Richard H. Merrick, Arkla Industries Inc., P.O. Box 534, Evansville, IN 47704
182. Philip Metz, Brookhaven National Laboratory, Upton, NY 11973
183. Alessio Mezzina, Solar Technology Group, Brookhaven National Laboratory, Building 701, Upton, NY 11973
184. Mark Middleton, Columbus Products Co., 300 Phillipi Road, Columbus, OH 43228
185. R. Scott Miller, General Electric Company, CRD-River Road, Building #37-615, Schenectady, NY 12345
186. J. P. Millhone, Office of Buildings Energy Research & Development, CE-11, Department of Energy, 1000 Independence Avenue S.W., Washington, DC 20585
187. F. H. Morse, Office of Solar Heat Technologies, CE-31, Department of Energy, 1000 Independence Avenue S.W., Washington, DC 20585
188. Robert Morse, Tecumseh Products Company, Tecumseh, MI 49286
189. Larry Moss, P.O. Box 1496, Estes Park, CO 80517
190. T. Mukai, Permanent Delegation-Japan, 7, Avenue Hoche, 75008, Paris, France
191. W. E. Murphy, Department of Mechanical Engineering, Texas Engineering Exp. Sta., Texas A&M University, College Station, TX 77843
192. Neno Nenov, Linde Division, Union Carbide Corporation, Tonawanda, NY 14150
193. R. W. Newell, Vice President, Research & Development, City Investing Company, 5600 Old Greenwood Road, Fort Smith, AR 72903
194. Van-Thanh Nguyen, Mitre Corporation, Metreck Division, 1820 Dolley Madison Blvd., McLean, VA 22102
195. Dennis O'Neal, 400 N. River Road, Apartment 603, West Lafayette, IN 47906
196. Jerald Parker, School of Mechanical & Aerospace Eng., Oklahoma State University, 218 Engineer North, Stillwater, OK 74074
197. A. Patani, Honeywell Inc., 10701 Lyndale Avenue South, Bloomington, MN 55420
198. Michael Perlsweig, Division of Conservation Research and Technology, Department of Energy, 20 Massachusetts Avenue N.W., Washington DC 20545

199. Lawrence Peterson, 1671 S.W. Fairhill, Roseburg, OR 97470
200. Joe Pietsch, Northrup, Inc., 302 Nichols Drive, Hutchins, TX 75141
201. B. J. Pleiss, A. O. Smith Corporation, 531 North 4th Street, Tipp City, OH 45371
202. Lee Preston, A. O. Smith Corporation, 531 North 4th Street, Tipp City, OH 45371
203. T. Ratchford, Committee on Science and Technology, Subcommittee on Energy R&D, House of Representatives, Washington, DC 20515
204. V. Recchi, National Research Council, % O. T. B. Zona Industriale, Contrada del Parco, Bari, Italy
205. Robert Reid, Department of Mechanical & Aerospace Eng., Environment & Resource Center, University of Tennessee, 329 South Stadium Hall, Knoxville, TN 37916
206. Gordon Reistad, Oregon State University, Department of Mechanical Eng., Corvallis, OR 97331
207. Patrick Reynolds, Mechanical Technology Inc., 968 Albany-Shaker Road, Latham, NY 12110
208. Hal Rhea, Director of Engineering, Lennox Industries, Inc., P.O. Box 877, 1600 Metro Drive, Carrollton, TX 75006
209. Steve Riedel, General Electric Company, Fort Wayne, IN
210. Bill Riley, Advance Development, Heil Quaker Corporation, 647 Thompson Lane, P.O. Box 40566, Nashville, TN 37204
211. J. Rizzuto, New York State Energy Research & Development Auth., Agency Building No. 2, Empire State Plaza, Albany, NY 12223
212. Arthur Rosenfeld, Lawrence Berkeley Laboratory, Building 90, Room 3058, 1 Cyclotron Road, University of California, Berkeley, CA 94720
213. J. H. Rothenburg, Utilities Systems, Dept. of Housing & Urban Dev., 451 Seventh Street S.W., Washington, DC 20410
214. William Rudoy, University of Pittsburg, Dept. of Mechanical Eng., Pittsburg, PA 15261
215. J. D. Ryan, Energy Conversion Equipment Branch, CE-113.2, Department of Energy, 1000 Independence Avenue S.W., Washington, DC 20585
216. L. A. Sarkes, American Gas Association, 1515 Wilson Boulevard, Arlington, VA 22209
217. M. L. Savitz, Deputy Assistant Secretary for Conservation, CE-10, Department of Energy, 1000 Independence Avenue S.W., Washington, DC 20585
218. D. E. Scherpereel, Director, Mechanical Systems Research, Elisha Gray II – Research & Engineering Center, Monte Road, Benton Harbor, MI 49022
219. Carl Schmittle, York Division, Borg-Warner, York, PA 17405
220. Robert Schoenhals, Department of Mechanical Engineering, Purdue University, West Lafayette, IN 47907
221. Mark Schuetz, AMTI, 141 California Street, Newton, MA 02158
222. James Schultze, Technology Program Manager, General Electric Company, Appliance Park, Building 6, Room 208, Louisville, KY 40225
223. J. L. Schulze, General Electric Company, Appliance Park, Louisville, KY 40225
224. T. C. Scott, Dept. of Mechanical & Aerospace Eng., University of Virginia, Charlottesville, VA 22901
225. Musoke Sendanla, Tennessee Valley Authority, Electrical Systems, 1150 Chestnut Street Tower II, Chattanooga, TN 37401
226. Takao Senshu, Mechanical Engineering Research Laboratory, Hitachi, Ltd., 390 Muramatsu, Shimizu-shi, Shizuoka-ken, Japan
227. Charles Sepsy, Ohio State University, Dept. of Mechanical Eng., Room 2075 - Robinson Lab, 206 West 18th Avenue, Columbus, OH 43210
228. Michael Sexton, Dept. of Mechanical & Aerospace Eng., University of Virginia, Charlottesville, VA 22901
229. Ramesh Shah, Harrison Radiator Division, General Motors Corporation, Lockport, NY 14094
230. James Shaw, Public Service Company of Oklahoma, P.O. Box 201, Tulsa, OK 74102
231. Duncan Sheldon, Lincoln Laboratory, P.O. Box 73, Lexington, MA 02173

232. Samuel Shelton, School of Mechanical Engineering, Georgia Instute of Technology, Atlanta, GA 30332
233. Neil Sher, Technology Strategy Center, Honeywell Control Systems, 1700 West Highway 36, St. Paul, MN 55113
234. D. E. Sherpereel, Research and Engineering Center, Whirlpool Corporation, Benton Harbor, MI 49022
235. Tony Sigmon, Research Triangle Institute, Energy & Environmental Res., P.O. Box 12194, Research Triangle, NC 27709
236. J. A. Smith, Test and Evaluation Branch, CE-113.2, Department of Energy, 1000 Independence Avenue S.W., Washington, DC 20585
237. Mason Somerville, Department of Mechanical Engineering, University of Arkansas, Fayetteville, AR 72701
238. Dr. Yates Sorrell, N. C. Alternative Energy Corporation, P. O. Box 12699, Research Triangle Pk., NC 27709
239. E. W. Spannhake, White Consolidated Industries, Inc., 11770 Berea Road, Cleveland, OH 44111
240. Ing. F. Steimle, Angewandte Thermodynamik & Kimatechnik, Fachbereich 13, Universitatsstr. 15, 4300 Essen 1, West Germany
241. Don Stephenson, National Research Council, Division of Buildings Res., Montreal Road, Ottawa, Canada KIA 0R6
242. John Stephenson, University of Auckland, Auckland, New Zealand
243. W. F. Stoecker, University of Illinois Urbana-Champaign, Dept. of Mech. & Indus. Eng., 144 Mechanical Eng. Bldg., Urbana, IL 61801
244. Robert Stricker, The Rovac Corporation, 100 Rovac Parkway, Rockledge, FL 32955
245. Shiv Sud, Strategic Planning and Analysis Group, Ministry of Energy, 56 Wellesley Street West, Queen's Park, Toronto, Canada
246. P. F. Swenson, Consolidated Natural Gas Service Company, 11001 Cedar Avenue, Cleveland, OH 44106
247. C. J. Swet, 7040 Woodville Road, Mt. Airy, MD 21771
248. W. D. Syniuta, Advanced Mechanical Technology, Inc., 141 California Street, Newton, MA 02158
249. C. C. Thiel, Jr., Division of Advanced Technology Applications, National Science Foundation, 1800 G Street N.W., Washington, DC 20550
250. W. H. Thielbahr, Energy Conservation Branch, Department of Energy, Idaho Operations Office, 550 Second Street, Idaho Falls, ID 83401
251. W. C. Thomas, Virginia Polytechnic Inst. & State Univ., Blacksburg, VA 24061
252. Tommy Thompson, Vice-President, Engineering, BDP Company, Div. of Carrier Corporation, 7310 W. Morris Street, Indianapolis, IN 46231
253. William Toscano, Foster-Miller Associates, 135 Second Avenue, Waltham, MA 02154
254. E. L. Tramel, Residential Technical Applications, Conservation & Energy Mgmt., Chattanooga Power Service Cnt., Chattanooga, TN 37401
255. D. Tree, Ray Herrick Laboratory, Purdue University, West Lafayette, IN 47907
256. Dutch Uselton, Northrup Incorporation, 302 Nichols Drive, Hutchins, TX 75141
257. Himanshu Vakil, General Electric Corporate R&D, P.O. Box 8, Schenectady, NY 12301
258. Hendrik Van Der Ree, TNO, Heat Pump Section, Laan Van Westenenk 501, Apeldoorn, The Netherlands
259. S. E. Veyo, Westinghouse Electric Corporation, Research & Development Center, 1310 Beulah Road, Pittsburg, PA 15235
260. Michael Wahlig, Lawrence Berkeley Laboratory, Building 90, Room 2024, 1 Cyclotron Road, University of California, Berkeley, CA 94720
261. D. J. Walukas, Foster-Miller Associates, Inc., 795 Oak Ridge Turnpike, Oak Ridge, TN 37830

262. Andy Wan, Room EM204, US Department of Commerce, National Bureau of Standards, Washington DC 20234
263. Bernie Warning, Friedrich A. C. & R., 4200 N. Pan Am Expressway, P.O. Box 1540, San Antonio, TX 78295
264. Ralph Webb, Department of Mechanical Engineering, Pennsylvania State Univ., 208 Mechanical Eng. Bldg., University Park, PA 16802
265. David Wensky, Copeland Corporation, 250 East Wilson Bridge Rd., Suite 255, Worthington, OH 43085
266. Eugene West, Sr. Vice President, Engineering, Amana Refrigeration, Inc., Amana, IA 52204
267. G. W. Wiener, Manager, Materials Science Division, Westinghouse R&D Center, 1310 Beulah Road, Pittsburg, PA 15235
268. M. Wilden, University of New Mexico, Albuquerque, NM 87115
269. J. C. Wilson, Carlyle Compressor Company, 4803, Syracuse, NY 13221
270. Lawrence Woodworth, Brookhaven National Laboratory, Building 120, Upton, NY 11973
271. Les Wright, Project Manager, Residential Space Cond. Sys., 8600 W. Bryn Mawr Avenue, 10 West 35th Street, Chicago, IL 60631
272. Hiromu Yasuda, Mechanical Engineering Research Lab., Hitachi, Ltd., 390 Muramatsu, Shimizu-shi, Shizuoka-ken, Japan
273. T. Yoshii, Mitsubishi Heavy Industries America, Inc., Suite 2101 John Hancock Center, 875 North Michigan Avenue, Chicago, IL 60611
274. David Young, Ontario Hydro, Research Division, 800 Kipling Avenue, Toronto, Canada M8Z 5S4
275. P. Zegers, Commission of the European Communities, 200 Rue de la Loi, Brussels 1049, Belgium
276. Ronald Zerkle, University of Cincinnati, Cincinnati, OH
277. R. V. Zigler, General Electric Company, 570 E. 16th, Holland, MI 49423
278. Alan Zimmerman, Special Products Group, The Coleman Company, Wichita, KS 67201
279. Congressional Information Service, Research Building 83, Kodak Park, Rochester, NY 14050
280. Edison Electric Institute, 8th Floor, 1111 19th Street N.W., Washington DC 20036
281. Office of the Assistant Manager for Energy R&D, U.S. Department of Energy, Oak Ridge Operations, Oak Ridge, TN 37830
282. National Energy Information Center, Library, Room 1404, 12th & Pennsylvania Ave. N.W., Washington DC 20461

283-309. Technical Information Center, Department of Energy, P.O. Box 62, Oak Ridge, TN 37830

310-359. External Energy Conservation Distribution, Oak Ridge National Laboratory, Building 9102-2, Rm. 112, Oak Ridge, TN 37830

☆U.S. GOVERNMENT PRINTING OFFICE: 1982-646-055/230